

**Bio – Matrices Interaction**  
–  
**from Microstructured Hydrogel Volumes  
and Hydrogel Surfaces**

**Dissertation**

zur Erlangung des akademischen Grades  
Doktor der Ingenieurwissenschaften  
(Dr.- Ing.)  
der Technischen Fakultät  
der Christian-Albrechts Universität zu Kiel

vorgelegt von

**Katharina Siemsen**

Kiel 2020

**Reviewers:**

Prof.Dr. Christine Selhuber-Unkel

Prof. Dr. Regine Willumeit-Römer

Date of the oral examen: 29.10.2020





## DECLARATION

---

I, Katharina Siemsen, hereby declare that I wrote this dissertation entirely by myself without improper external assistance besides the advice of my supervisor and to the best of my knowledge and belief.

I furthermore declare that my thesis was not yet presented fully or in parts in any other examination procedures besides in the course of this corresponding procedure.

Finally, I declare that I have identified all quotations of other authors and used none but the indicated sources to keep the rules of good scientific practice defined by the German Research Society (DFG).

Katharina Siemsen

Faculty of Engineering

Institute for Materials Science

Christian-Albrechts University of Kiel

Kiel,

---

Signature

## ABSTRACT

---

*In vivo* cellular behavior is highly relevant to understand for various diseases and future tissue engineering but challenging to study using traditional *in vitro* cell growth methods: Many cellular mechanism functions differently when cells are grown in three-dimensional (3D) conditions similar to *in vivo* conditions as in traditional 2D culture techniques. As it is known for some time that 2D cell cultures and their mechanical properties influence the cellular behavior, this is also true for the 3D environment. Especially for the stability of the nucleus, the subcellular compartment responsible for storing the main part of our DNA, the 3D environment, and the mechanical and structural properties of it are highly valuable. Considering an implant inside the body's soft tissue, the mechanical and structural properties will mediate the cell-matrix interaction. Recent advances in biomaterial research have enabled both cell growth in 3D and increased control of the cell-matrix interaction on an artificial substrate, e.g., as with structured PDMS channels. Despite these advances, there remain challenges in this field. An essential challenge until now is the creation of 3D structured samples that display the properties of the extracellular matrix in a controllable manner. These properties are hydration for the diffusive exchange of nutrition, controllable variability of the mechanical properties, and highly controllable biofunctionalization in 3D.

In this thesis, novel means of growing cells in 3D environments with defined mechanical properties, creating new bio-crosslinker and investigating substance release from hydrated matrices showing the power of biomaterial-cell interactions for life sciences and biomedical research are presented

In the first part of this work, the 3D cell-matrix interactions are discussed using fibrosarcoma cells grown in 3D-microstructured hydrogel matrices with a range of controlled mechanical properties. With the tuning of the matrix stiffness, cell behavior was affected, creating a preference for specific positions within the structured environment. Interestingly, the mechanical properties of the matrix were also found to impact the nucleus, affecting the stability of the nuclear envelope, and the intracellular position of the nucleus during cell migration.

The second part of this thesis focuses on two different approaches for cell-matrix interactions in two dimensions (2D). In the first approach, the focus is on the compliance of miniaturized biosensors to primary endothelial cells. In the second approach, a chemically engineered bio-crosslinker is presented for enhanced biofunctionalization and cell adhesion. For studying the new bio-crosslinker (BCL) effectiveness, cells were grown on pHEMA, a protein-inert hydrogel. Once inserted inside the

pHEMA precursor mixture, the pHEMA hydrogels included free reactive groups and can be biofunctionalized with fibronectin instantly to support cell adhesion.

In the final part of this thesis, I present a study of hydrogel matrices, which release different drugs. I demonstrate the influence of the drug solution on hydrogel swelling and its release for an anti-seizure drug. The possibility of matrix degradation within the incubation time is also investigated. Initial studies have shown that the substances were released over several days, attesting to the high suitability for indirect drug administration. In the second approach, an anti-inflammatory drug release from swollen hydrogel matrices is investigated. The aim here was to create an anti-inflammatory soft substratum for future tissue cuts.

The results of the investigations presented in this work have also highlighted three essential features of biomaterials: matrix structural size, matrix topography or architecture, and dimensionality. Each element played a key role in the studies presented in this work, clearly demonstrating the importance of each when designing, and working with biomaterials.

## ZUSAMMENFASSUNG

---

Das Wissen und Verständnis über das Zellverhalten für *in vivo* Konditionen ist ein wichtiges Unterfangen für die Erforschung verschiedenster Krankheiten und die zukünftige Entwicklung künstlicher Gewebe. Dies erfordert Veränderungen in der *in vitro* Zellkultur, da klassische Methoden nicht ausschließlich allen Anforderungen gerecht und *in vivo* Konditionen nicht vollständig abgebildet werden können: Einige Mechanismen innerhalb einer Zelle reagieren unterschiedlich, wenn die Kultivierung in drei-dimensionalen Bedingungen, ähnlich zu *in vivo* Konditionen, statt in zwei-dimensionalen Bedingungen stattfindet. Die klassischen 2D Zellkulturen können schwerlich die Bedingungen bieten, wie sie Zellen natürlicherweise in den weichen und beengten Verhältnissen im Gewebe vorfinden.

Ein weiterer wichtiger Punkt in der Zellkultur, den es zu beachten gilt, ist der Einfluss der mechanischen und topographischen Eigenschaften, die von den genutzten Substraten auf die Zellen einwirken. Diese verändern nachweislich das Verhalten der Zellen während 2D *in vitro* Anwendungen als auch in ersten 3D Anwendungen. Insbesondere die Stabilität des Zellkerns, Träger der DNA, kann von den Eigenschaften der Proben in 3D beeinflusst werden. Dies ist insbesondere wichtig für Implantate in weichen Geweben, wie zum Beispiel dem Gehirn. Fortschritte in der Biomaterial-Forschung konnten die Zellkultivierung in 3D und damit eine gesteigerte Kontrolle der Zell-Matrix Interaktion ermöglichen. Hierzu werden z.B. 3D Kanäle aus PDMS für die 3D Zell-Matrix Interaktion genutzt. Trotz der großen Fortschritte liegt eine weitere Herausforderung bis heute in der Herstellung von 3D Proben, die der extrazellulären Matrix (EZM) gleich oder zumindest nahe-kommt. Folgende wichtige Eigenschaften der EZM sollten beachtet werden: Der hoher Wasser Anteil des Gewebes, der es den Zellen ermöglicht Diffusion an Nährstoffe zu gelangen; Die mechanische Adaption der Substrate an das jeweilige Gewebe; Die Möglichkeit der kontrollierten Biofunktionalisierung für die Adhäsion von Zellen.

In der vorliegenden Arbeit werden neue Ansätze für das Wachstum von Zellen in mechanisch adaptierten und 3D strukturierten Proben vorgestellt, sowie ein neues Molekül für die verbesserte Biofunktionalisierung von 3D Proben. Zusätzlich wird die Freisetzung von Substanzen aus mechanisch adaptierten Hydrogelen für den zukünftigen *in vivo* Einsatz präsentiert. Diese Themen zeigen den Einfluss der Biomaterial-Forschung auf die Life Sciences und biomedizinische Forschung.

Im ersten Teil der Arbeit werden die Untersuchungen der 3D Zell-Matrix Interaktionen vorgestellt. Fibrosarcoma Zellen wurden dazu in 3D strukturierten Proben untersucht, die eine Spannweite an



unterschiedlichen mechanischen Eigenschaften besaßen. Mit den veränderten mechanischen Eigenschaften wurde die Stabilität des Zellkerns beeinflusst und verändert. Interessanterweise zeigten sich auch Veränderungen im Zellverhalten, die den bevorzugten Ort innerhalb der Proben und auch die Lokalisierung des Zellkerns innerhalb der Zelle beeinflussten.

Im zweiten Teil meiner Arbeit fokussiere ich mich auf die Zell-Matrix Interaktion auf 2D Proben. Hierzu zeige ich zwei unterschiedliche Ansätze. In einem Ansatz untersuchte ich die Vereinbarung von Biosensoren und deren Biokompatibilität auf empfindliche Endothelzellen. Im zweiten Teil wird ein neu designtes Molekül, ein Bio-Crosslinker (BCL), präsentiert, das die Biofunktionalisierung von 3D strukturierten Proben verbessern wird. Für die Untersuchung der Effektivität wurde ein inertes Hydrogel genutzt, pHEMA, und der Einfluss des BCL auf die Zelladhäsion beobachtet. Es konnte festgestellt werden, dass der BCL erfolgreich eingebaut und mit Fibronectin funktionalisiert werden konnte.

Im finalen Part meiner Arbeit präsentiere ich Untersuchungen der Medikamenten-Freisetzung aus geschwollenen Hydrogelen. Im ersten Ansatz wurde ein Medikament gegen epileptische Anfälle in ein degradierbares Hydrogel infiltriert und eine langsame Freisetzung beobachtet. Die Infiltrationsmenge des Medikamentes als auch die Abgabe wurde durch die Konzentration der Lösungen beeinflusst. Im zweiten Teil wurde die Freisetzung einer anti-entzündlichen Substanz aus einem Hydrogel untersucht. Das Ziel war der Erhalt einer weichen anti-entzündlichen Unterlage für die Kultivierung von Gewebeschnitten.

Alle Ergebnisse, die in dieser Arbeit präsentiert werden, weisen auf drei höchst wichtige Eigenschaften von Biomaterialien hin: Die Größe der Strukturen in den Matrixen, den Einfluss der Topografie oder der Architektur und vor allem die Dimensionalität. Jede Eigenschaft spielt eine wichtige Rolle in dieser Arbeit und demonstriert ihren Einfluss, wenn es darum geht Biomaterialien zu konzeptionieren.

## ABBREVIATIONS

---

<b>AAm</b>	Acrylamide solution 40%
<b>AAD</b>	Adipic acid dihydrazide
<b><i>A.castellanii</i></b>	<i>Acanthamoeba castellanii</i>
<b>aliquor</b>	Artificial brain liquor
<b>APS</b>	Ammonium persulfate
<b>A-NHS</b>	Acrylic acid N-hydroxysuccimide ester
<b>BIS</b>	N,N'- Methylenebisacrylamide
<b>BCL</b>	Bio-crosslinker (Linker between material and adhesion protein)
<b>bi.dest. water</b>	Bidistilled water
<b>CL</b>	Crosslinker (Linker in between the monomer chains)
<b>DCC</b>	Dicyclohexylcarbodiimide
<b>DMEM</b>	Dulbecco's modified eagle medium
<b>DMF</b>	Dimethylformamide
<b>DMSO</b>	Demethylsulfoxid
<b>EDC</b>	1-ethyl-3-(3-dimethylaminopropyl) carbodiimide hydrochloride
<b>EGDMA</b>	Ethylenglycoledimetharcylate
<b>EtOH</b>	Etanol
<b>FAC</b>	Focal adhesion cluster
<b>FBS</b>	Fetal bovine serum
<b>FITC-Dextran</b>	Fluorescein isothiocyanate – Dextran 500.000 – Conjugate
<b>FluoroBrite</b>	FluoroBrite™ DMEM
<b>FN</b>	Fibronectin
<b>HEMA</b>	Hydroxyethylmethacrylate
<b>HEPES</b>	2-(4-(2-Hydroxyethyl)-1-piperazinyl)-ethansulfonic acid
<b>HCL</b>	Hydrochloric acid 37%
<b>HUVEC</b>	Primary Human Umbilical Vein Endothelial Cells
<b>HT1080</b>	Fibrosarcoma cells
<b>MES</b>	2-(N-morpholino)ethanesulfonic acid
<b>MOPS</b>	(3-(N-morpholino)propanesulfonic acid)
<b>MTT</b>	3-(4,5-dimethylthiazol-2-yl)-2,5-diphenyltetrazolium chloride
<b>NiTi</b>	Nickel titanium
<b>pAAm</b>	Polyacrylamide
<b>PBS</b>	Phosphate buffered saline
<b>Penstrep</b>	Penicillin Streptomycin
<b>PDMS</b>	polydimethylsiloxane
<b>pHEMA</b>	Poly(2-hydroxyethyl methacrylate)

<b>PEG</b>	Poly ethyleneglycol
<b>p-TSA</b>	p-Tolousulfonic acid
<b>PYG medium</b>	peptone yeast glucose 712 medium
<b>Ref 52 wt</b>	Rat embryonic fibroblasts 52 wild type
<b>sulfo-NHS</b>	N-Hydroxysulfosuccinimid
<b>Sulfo-SANPAH</b>	Sulfosuccinimidyl-6-(40-azido-20-nitro phenylamino) hexanoate
<b>TEMED</b>	N,N,N',N'-Tetramethylenediamine
<b>trans wells</b>	Millicell® Cell culture Inserts
<b>t-ZnO</b>	Tetrapodal zinc oxide
<b>UV</b>	Ultraviolet
<b>Vis</b>	Visible

# CONTENTS

---

Declaration .....	v
Abstract .....	vi
Zusammenfassung.....	viii
Abbreviations .....	x
1 Introduction and theoretical background .....	1
1.1 Introduction to the principles of cell-matrix interactions .....	1
1.1.1 The cell and its compartments .....	1
1.1.2 The cell within the extracellular matrix.....	3
1.1.3 Adhesion and migration on 2D surfaces and in 3D environments.....	3
1.1.4 Engineering the cell-matrix interaction.....	5
1.2 Introduction to the Matrix materials .....	10
1.2.1 Hydrogels as matrices for (bio)interactions and the hydrogel preparations .....	10
1.2.2 Hydrogel synthesis.....	10
1.2.3 Physical crosslinks.....	11
1.2.4 Covalent crosslinks .....	12
1.2.5 Hydrogel biofunctionalization procedures with different chemical components .....	14
1.3 Introduction to the brain as a potential matrix environment.....	15
1.4 Introduction to the Mechanical matrix characterization .....	17
1.4.1 Stiffness, strains and their slopes.....	17
1.4.2 Young's modulus and the different models for indentation methods.....	18
1.4.3 Determination of the Young's modulus .....	19
1.4.4 Determining the polymeric mesh size via mechanical measurements.....	20
1.5 Introduction to the Interaction between matrix material and Molecules.....	22
1.5.1 Molecule release from matrix materials .....	22
1.5.2 Sink conditions for in vitro experiments .....	23
1.5.3 Release mechanism and kinetics:.....	24
1.5.4 Methods for quantifying released substance concentration .....	26

1.6	Introduction to quantifying methods for the biocompatibility of matrices and the cell-matrices interaction for 2D and 3D .....	27
1.6.1	Adhesion assay .....	27
1.6.2	Morphology of cells .....	27
1.6.3	Cytotoxicity .....	28
2	3D cell-matrix interaction .....	31
2.1	Introduction .....	31
2.2	Results and discussion for 3D cell-matrix interaction .....	33
2.2.1	Improving the 3D experimental parameter .....	35
2.2.2	3D cell-matrix interaction with mammalian cells .....	42
2.3	Conclusion .....	59
2.4	Procedure details for 3D cell-matrix interaction .....	59
2.4.1	Cells and cell culture: .....	59
2.4.2	Sacrificial templates .....	60
2.4.3	Preparation of 3D microstructured pAAm matrices .....	61
2.4.4	Biofunctionalization: .....	61
2.4.5	Imaging and analysis of 3D experiments with fibrosarcoma cells .....	62
3	2D cell matrix interaction .....	63
3.1	Results, discussion, and conclusion for primary cells on biosensors .....	65
3.2	Results and discussion for 'Engineering of a new bio-crosslinker for enhanced cell adhesion'	67
3.3	Conclusion and Perspectives for 2D cell matrix interaction .....	73
3.4	Bio-crosslinker synthesis and sample preparation .....	74
3.4.1	Creating and incorporating the bio-crosslinker .....	74
3.4.2	Synthesizing pHEMA with the new bio-crosslinker .....	75
3.4.3	Biocompatibility, biofunctionalization and cell adhesion on BCL containing pHEMA ..	76
4	Swollen Hydrogel matrices as drug-release reservoirs .....	79
4.1	Introduction .....	79
4.2	Results and discussion for alginate-based hydrogel drug release .....	80

4.2.1	Conclusion .....	91
4.3	Results and discussion for free curcumin release from pAAm matrices.....	92
4.3.1	Conclusion .....	94
4.4	Methods for degradable alginates for drug release.....	95
4.4.1	Sample preparation and characterization of degradable alginate matrices.....	95
4.4.2	Drug infiltration into hydrogel samples.....	96
4.5	pAAm as hydrogel matrix for molecule release .....	97
4.5.1	Sample preparation and characterization.....	97
5	Conclusion and prospects of the presented work.....	99
6	Appendix.....	II
6.1	Lists of chemicals and devices.....	II
6.2	General cell culture methods .....	VI
6.2.1	Rat embryonic fibroblasts and fibrosarcoma cells .....	VI
6.2.2	Human umbilical vein endothelial cells (HUVEC) .....	VI
6.2.3	<i>Acanthamoeba castellanii</i> (AC) .....	VI
6.2.4	Cell adhesion assay.....	VII
6.2.5	Cytotoxicity assay .....	VII
6.3	Imaging the cell-matrix interaction .....	VIII
6.3.1	Experiments conducted at Cornell University in the Lammerding Lab:.....	IX
6.4	Hydrogel fixation on glass slides .....	X
6.5	Infiltration of fluorescent solutions into microstructures hydrogels and imaging .....	XII
6.6	The routine of the alginate hydrogel preparation .....	XII
6.7	Degradation of covalently crosslinked alginate .....	XIII
6.8	Delayed substance release from alginate matrices obtained with pHEMA layer .....	XIII
6.9	Artificial brain liquor for release experiments .....	XV
6.10	Calibration of the cantilever .....	XV
	List of Publications:.....	XVII
	Bibliography.....	XVIII

Acknowledgments/ Danksagung.....XL





# 1 INTRODUCTION AND THEORETICAL BACKGROUND

---

The presented work is segmented in several sections. Firstly, the overall topics and theoretical background are introduced within this particular section. These topics provide an overview of the following presentation of the investigations. The investigations are collected in chapters 2, “3D cell-matrix interaction”, chapter 3, “2D cell matrix interaction”, and chapter 4, “Swollen Hydrogel matrices as drug-release reservoirs” according to their content. Specific methods are mentioned in the scientific chapters. Supporting information to general procedures are placed in the appendix.

## 1.1 INTRODUCTION TO THE PRINCIPLES OF CELL-MATRIX INTERACTIONS

Cell adhesion and migration can be regulated by their interaction with the matrix materials. These can be distinguished in various topics such as the type of material itself, its stiffness, and in particular, in their dimensionality. In this chapter, I will discuss how cells interact with different known matrices: the extracellular matrix (ECM) and synthetic 2D as well as 3D matrices. Furthermore, I will describe the potentials of engineering the cell-matrix interaction by using topographical and mechanical discrepancies. When not declared otherwise, all explanations and descriptions are for anchor-dependent cells, cells that need to adhere to the matrix to proliferate and migrate.

### 1.1.1 The cell and its compartments

During cell adhesion and migration, the whole cell body with its compartments is involved. Here, a short introduction of the essential cell components is given.

The nucleus of a cell contains the main part of the DNA. Its core element consists of a nucleolus and chromatin. The chromatin part is a complex from nucleosomes and can vary in size and hierarchical structure in dependence from the animal. [1], [2] Two kinds of structures are present in the chromatin and should be defined: the euchromatin and the heterochromatin. While euchromatin is in a more open and accessible form and is actively transcribed, the latter is more compact and less transcribed. Both have because of the packaging different stiffness and define with the ratio present between euchromatin and heterochromatin the stiffness of the chromatin. [3] It has been found that the ratios vary by mechanotransduction following conversion from one structure to the other. With this, the stiffness of the chromatin is changed actively, and it determines the endurance of the nucleus towards deformation. [3]–[12] These inner structures, as mentioned above, are surrounded by the nuclear lamina, which is constituted from different types of lamins such as lamin A, lamin B, or lamin C. It is found to be responsible for providing an outer structural component towards the chromatin part. It gives in dependence on the displayed lamins a resistance against deformation. [9]

Mutated, Lamin A or C, are part of several diseases, e.g., cardiomyopathies. [9]–[11] The lamina is connected to the chromatin via SUN domains and to the inner membrane of the nuclear envelope, one of the two lipid bilayer that protects the nucleus. [1]

Further, at the other direction of the SUN domains, the SUN domains bind towards domains of nesprin proteins. These nesprin proteins are located through the outer membrane of the nuclear envelope. Both protein domains, the SUN and the nesprins form the LINK complexes. The stability of the nuclear envelope is directed through lamin A and C as they are the connection in the lamina towards the LINK complexes (linker of nucleoskeleton and cytoskeleton). The LINK complexes are directly connected to the perinuclear actin caps. Via the perinuclear actin caps, the LINK complexes are connected to the cytoskeleton, and thus all forces and strains are subjected to the nucleus. The cytoskeleton mediates the force sensing and signaling to and from the nucleus and controls the nucleus position within the cell body. [1], [3], [11], [13]–[15] In addition, the cytoskeleton is a structural component of the cell and is responsible for cell shape as well as cell migration and division. The cytoskeleton consists of different kinds of filaments. These filaments are microfilaments, intermediate filaments, and microtubules. The intermediate filaments form the stiff structural components of the cell. The microtubule is responsible for the internal cell trafficking of cell compartments in the cytoplasm, movement, and division of the cell. For cell movement, the positioning of the microtubules connected to the centromere in respect to the nucleus is essential. [16]–[18]

The microfilaments contain actin- and perinuclear actin filaments. These filaments mediate the stress and deformation from the surrounding matrix towards the cell. At the same time, cells exert stress towards the matrix using these actin filaments to gain information about the mechanical properties of the matrix. [15], [19] Both the microtubules and the actin fibers are needed for the positioning of the nucleus during migration, which facilitates the overall motility. Also, the positioning of the nucleus is highly important for the cells to function as it contains the main part of the DNA. Positioning the nucleus in an adverse place during migration in, e.g., a confined 3D environment could lead towards unnecessary damages of the nucleus and further towards the DNA. [3], [14], [15], [20]–[22] The cell membrane is the outer cell layer where cell adhesion complexes are located. These adhesion complexes are composed of the integrins and adhesion clusters. The adhesion clusters are inside the cytoplasm, and their composition and size depend on the matrix stiffness. They also depend on the matrix dimensionality and bind the actin filaments to the integrins and the cell membrane. [23]–[26] Because of the mentioned interconnections inside the cell, the cell-matrix interaction is not just organized by the adhesion complexes from the cell but from the whole diverse compartment of the cell, which interacts as a whole. [27]–[29]

### 1.1.2 The cell within the extracellular matrix

In their natural environment, cells are attached to the extracellular matrix (ECM). The ECM forms a fibrous network in between the cells and mediates cellular processes such as migration and differentiation. Basic components are adhesive glycoproteins and glycosaminoglycans such as hyaluronic acid, which is responsible for taking high compression loads as well as the healing in tissues. [30], [31] The adhesive glycoproteins can bind to cell membranes as well as to glycosaminoglycans and collagen fibers. Depending on the tissue, these adhesive glycoproteins are specified for the cell types. [32]–[34] The structure of the ECM is preserved by collagen and elastin fibers. Collagen is secreted from the cells that can appear in various assemblies like collagen type I with its fibrillar structure. Elastin grants the contractile behavior to the expanding tissue, e.g., muscles and blood vessels. The actual adhesion of cells to the surrounding ECM is mediated by fibronectin and laminin, which binds the collagen fibers directly to the cell membrane via focal adhesion complexes (FAC). These FACs can contain proteins such as FAK, p130CAS, vinculin, talin, or zyxin, as well as integrins. [25], [30], [33] The structural and mechanical cues of the ECM are determined from the density and stiffness of the fibrous structures. These govern the migration and proliferation behavior of the cells. Furthermore, cells can reorder their environment by protease reaction to adapt the motility. [30], [32], [35]–[37]

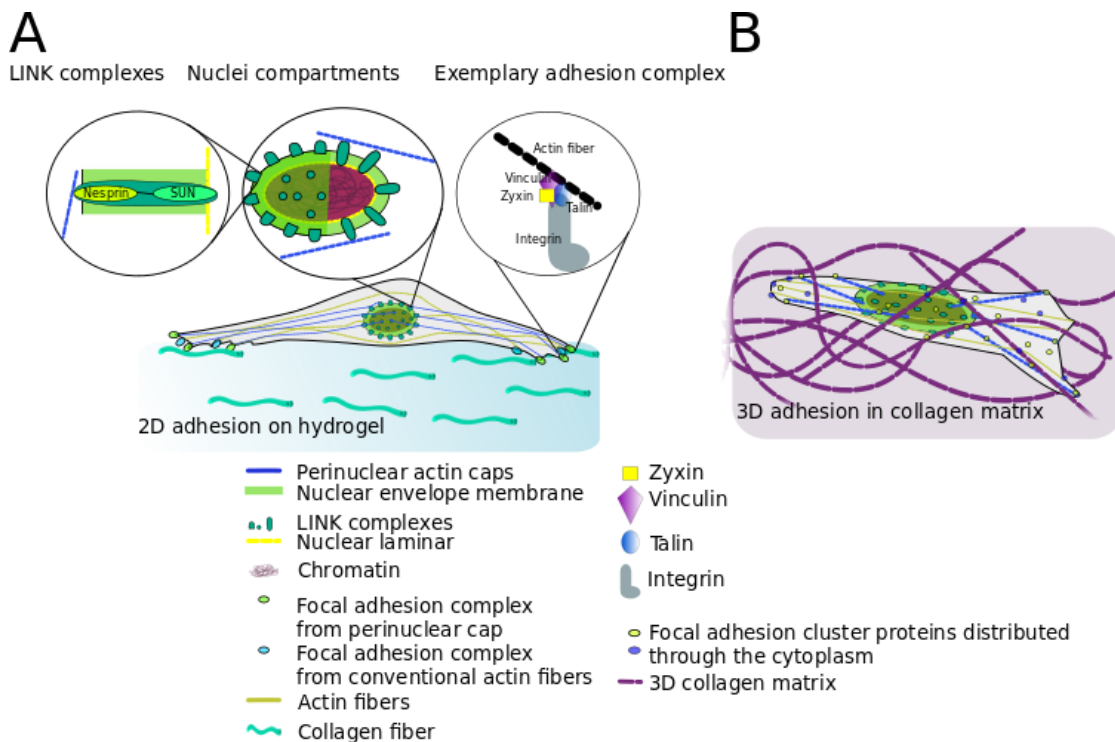
### 1.1.3 Adhesion and migration on 2D surfaces and in 3D environments

The cell behavior inside the natural ECM is mediated by structure and stiffness, as described above. Mediation by structure and stiffness will also be true for any new material synthesized. Because of this, any new material needs to be tested. The results of the cell-matrix interactions *in vitro* will lead us to predictions towards the *in vivo* usage of these materials, such as implant devices.

#### 1.1.3.1 Cell interaction with 2D matrix surfaces

The interaction between synthetic matrix and cell in 2D takes place on the cell's basal side. Here, the cell is in contact with the material and forms FAC with it. In Figure 1A, a cell adheres to a hydrogel surface, which includes collagen. The exemplary FAC in Figure 1 contains Integrin, Vinculin, and Zyxin. The cell adheres with Integrin to the collagen fibers. The FAC themselves are directly connected to the cytoskeleton via actin fibers. The actin fibers are directly attached to the cell nucleus via LINK complexes. This attachment enables a direct translation of forces from and to the matrix to and from the nucleus. In the assumption of an ideal distribution of adhesive proteins, cells do not only adhere but migrate on the surface.

The cell spreading on the 2D surface is influenced by these adhesion molecules but also by the stiffness of the material. The spreading of the FACs is regulated from the matrix stiffness and the possibility to adhere to the material. [38], [39] With increasing matrix stiffness, the number, and size of the cells FAC rise. At the same time, the speed of the cell increases with the size of the FACs up to a point when the size of the FACs exhibit such a strong adhesion, that the cell migration is inhibited. [40] Cellular motility on 2D surfaces can be described in two different modes, lamellipodia and amoeboid migration. The lamellipodia migration is based on the movement of filopodia. The cell is attached at the end, and filopodia are created at first by actin polymerization until the adhesion is created. The end of the cells the FACs are then depolymerized. For the amoeboid migration, the primary attachment is at the cell front. Pseudopodia are created towards the front, followed by blebs to form the next pseudopodia, while the last is depolymerized. The nucleus and the cell body are moved behind. The general nucleus is positioned behind the centromere and the microtubules. [41]



*Figure 1 Exemplary sketches for eukaryotic cellular adhesion on 2D hydrogel surfaces and in a 3D collagen matrix. A) the 2D adhesion on hydrogel shows the nuclei compartments involved in adhesion and migration as well as an exemplary adhesion complex. The adhesion complexes are clustered basal to the hydrogel surface to attach to the bio-functionalized hydrogel surface. B) The 3D adhesion in the collagen matrix is depicted with a cell inside the matrix structure. Here, the cell does not form focal adhesion complexes, but the adhesion proteins are distributed through the whole cytoplasm of the cell.*

### 1.1.3.2 Cell interaction with 3D environments

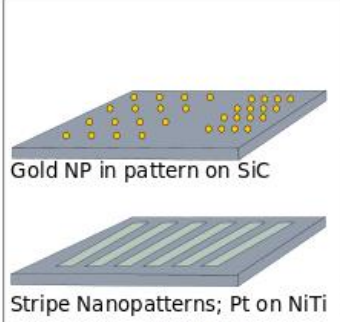
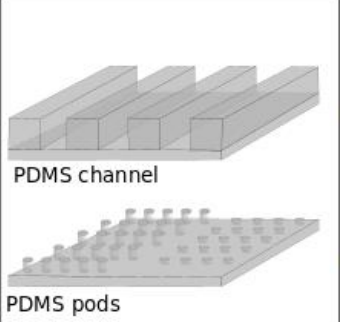
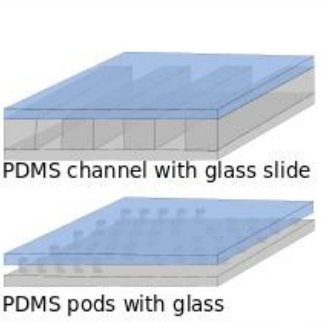
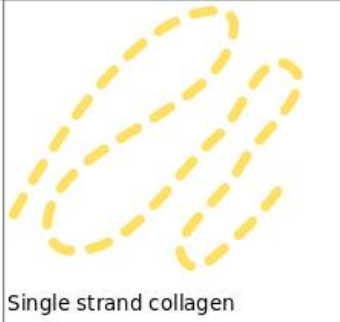
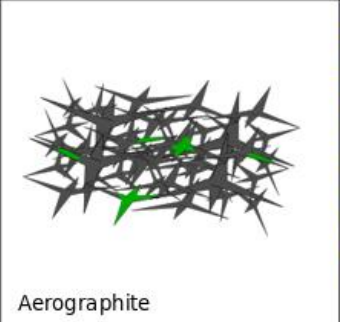

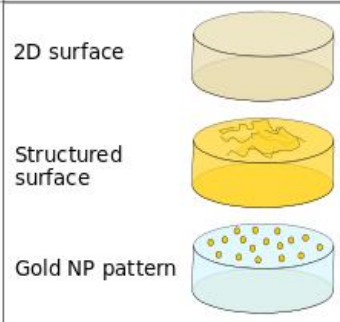
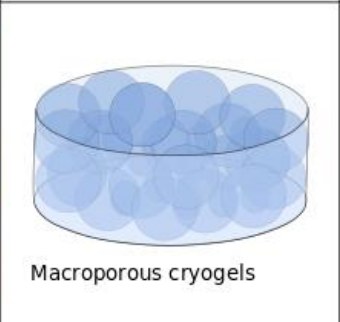

The cell's interactions with a synthetic 3D environment are the closest form to gain insight into the processes involved when the cells attach to their natural *in vivo* environment. The artificial 3D environments can be composed of different materials. These materials used for 3D environments vary (see Figure 2) and can be formed, e.g., from collagen networks or PDMS channels. [42]–[45] In contrast to 2D *in vitro* cell tests, cells in 3D environments are exposed with their whole body towards the surrounding material, see Figure 1B. Cells on 2D surfaces show distinct FAC located at their basal side. In contrast, the cells in 3D have no distinct FAC areas, but the proteins are distributed through the whole cytoplasm. These proteins have shown variation in number and type with the mechanical properties of the matrices. As an example, vinculin, which is agglomerated by traction forces, is depleted in soft hydrogels.  $\beta$ 1 integrins and also zyxin, an adhesion protein that exerts traction forces to the environment, can be found in such soft hydrogels. Adhesion and migration inside the matrix depend on the mechanical properties of the material and architecture as the space for cell proliferation and migration is essential. [46]–[49] Several modes of amoeboid and mesenchymal modes have been found, such as prominent protrusions and sub protrusions formed hierarchically, nuclear pistons, migration via blebbing myosin contraction at the cell front to name a few. [13], [23], [39], [40], [50]–[54] The cell nucleus, an organelle that influences the proper cellular function, is vital during 3D migration as it represents the stiffest component inside the cell. The positioning and motion of the nucleus inside the cell are orchestrated during the cytoskeleton. The microtubules and the perinuclear actin cap reorient the nucleus and push and pull it through constrictions by applying traction forces. [14], [22] The same is observed to test and indent the matrix materials as a first step to invade foreign tissue, e.g., transendothelial migration. [3], [41]

### 1.1.4 Engineering the cell-matrix interaction

#### 1.1.4.1 Topographical influences on adhesion and migration of cells

The interaction of cells towards a matrix is driven by the mechanical properties of the material, the materials chemistry, and surface charge and by the dimensionality and the architecture, in 2D the topography of those materials. [38], [39], [55], [56] These interactions are found in the ECM, where different structural features exist, from aligned collagen fibers to fibers, which are homogeneously clustered in scar tissue and result in different phenotypes of cells of one type. [57] The influence and importance of architectural features *in vivo* are so significant that even in different biological classes, the architecture of comparable structures can be located. [58] This is because cells are surrounded naturally by structured 3D architectures, which assist the proper function of cells. The architecture/topography surrounding the cell helps and influences the alignment of intracellular

compartments such as the cytoskeleton, which then also aligns the nucleus. The topography/architecture then affects the morphology and direction of migration as well as the generated forces towards the matrix, which increases with higher dimensionality in 2D to 2.5D. [59]–[61] Here, the term 2.5D is used for samples, that display a topography that encloses the cells in a not yet completely. In this dimensionality, 2.5D, single cells are not entirely surrounded from the

	2D surfaces	half enclosed	3D enclosed
Plane materials	 <p>Gold NP in pattern on SiC</p> <p>Stripe Nanopatterns; Pt on NiTi</p>	 <p>PDMS channel</p> <p>PDMS pods</p>	 <p>PDMS channel with glass slide</p> <p>PDMS pods with glass</p>
Fibrous materials	 <p>Single strand collagen</p>	 <p>Aerographite</p>	 <p>Collagen matrix</p>
Hydrogels	 <p>2D surface</p> <p>Structured surface</p> <p>Gold NP pattern</p>	 <p>Macroporous cryogels</p>	 <p>Microstructured hydrogels with interconnected channels</p>

matrix.

*Figure 2 Exemplary topographically and architectural in vitro environments. The examples are separated according to their dimensionality 2D, half-enclosed (2.5D), and 3D environments. They are further parted, according to their material parameters. These are bulk materials (mostly stiff without hydration and from one batch) such as glass or PDMS (A-C); there are fibrous materials (D-F) and hydrogels (G-I). Examples from the literature can be found in the supporting Table 1.*

3D architecture has been shown to highly support cell proliferation and cell alignment and migration in preferred directions. [62], [63] In Figure 2, different dimensionalities and architectures are shown.

The dimensionalities are parted in 2D surfaces, half-enclosed set-ups, and 3D enclosed environments. A table supports figure 2 with examples of the sketched dimensionalities and architecture. Table 1 does not claim to be complete, although it will provide exemplary *in vitro* environments for cell experiments. In this work, topography and architecture are meant to be used interchangeably in context to dimensionality. A topography of PDMS grooves is a surface-based half-enclosed structure, and this is meant to be used in 2D. In a 3D matrix, a channel would be an architectural feature as it surrounds the whole object which is subjected to the matrix.

#### ***1.1.4.2 Mechanical influence on adhesion and migration of cells***

As discussed in section 1.1.3.1, cells adhere to materials by forming FAC towards the 2D matrix at the basal side. In 3D, the focal adhesion proteins are distributed within the whole cytoplasm. On 2D surfaces, the FAC enhance its size and number with the increase of the Young's modulus of the material. [40] In fact, for cells in 3D matrices, the focal adhesion proteins vary in their occurrence according to the mechanical properties of the matrix and are distributed throughout the cytoplasm. Compared to the FACs on 2D surfaces, the appearing adhesion proteins in 3D environments were found to be more stable than on 2D surfaces. Doyle et al. found that the stable occurrence of the focal adhesion proteins has a reduced fluctuation in 3D and form a stationary connection between the integrins and the cytoskeleton. Both, the quantity and the distribution of the focal adhesion proteins, result from the forces generated between the matrix substrate and the cell-integrin receptors. [25], [46], [64], [65] With stiff substrates, the attached cells form stress fibers between the adhesion points. The attached integrins can then recruit additional adhesion proteins. On soft matrices, cells apply forces towards the substrate (traction forces). [20], [38] The Young's modulus describes the stress on the material applied and the resulting strain. The stress-strain curve and its slope give the actual material stiffness value. [66]–[68] The Young's modulus is a material-dependent parameter. In this work, the main focus is on the matrix material hydrogel.

Table 1 Support table for Figure 2. Exemplary in vitro environments for cell experiments, part 1.

Sketch	Architecture/ Topography	Material	Stiffness	Spacing	BCL and BF	Cells	Speed	Staining	Morphology and Migration	Examples
<b>A</b>	Surface pattern with gold NP	Bulk SiC coated with Mg	-	Pattern; 63nm-84nm; quasi-hexagonal	No	Ref-52- YFP-paxillin	-	Yes; Stained actin filaments with phalloidin after fixation;	Normal shape; No migration;	[69][4]
<b>B</b>	Micropillar	Bulk PDMS	Sylgard 184	W: 0.6-15 $\mu$ m D: 1-5.6 $\mu$ m; H:1,3,6,8 $\mu$ m	11-(triethoxysilyl)undecanal coating; Fn	Human endothelial cells (ECFCs) and HUVEC	-	Yes; live/dead staining; Mouse anti-vascular endothelial cadherin (VE-CAD) or mouse anti-fibronectin, FITC-conjugated phalloidin	Enhanced elongation and alignment; No migration;	[70]
<b>C</b>	Channels with glass cover	Bulk PDMS	Sylgard 184	W:3 $\mu$ m-10 $\mu$ m H: 11 $\mu$ m L: 150 $\mu$ m	Plasma active-tion; Collagen;	MDA-MB-231, BT 549, and HS578T	Faster in smaller channel; 0.3-0.7 $\mu$ m/m in	SiR-Actin for live cell imaging; F-actin and focal adhesions to align parallel to the channel direction	Mesenchymal to amoeboid phenotype change while migration; strong blebbing, loss of actin, $\beta$ 1 integrin found in 10 $\mu$ m and 3 $\mu$ m channel;	[42]
<b>C</b>	Micropillars with glass cover	Bulk PDMS with glass	-	W: 5,3 and 2 $\mu$ m H: 10 $\mu$ m OR: H:15 $\mu$ m and 5 $\mu$ m	Collagen	NIH 3T3 fibroblast	-	Modified nucleus with mCherry–Histone-4 and GFP-LifeAc; Changed Lmna amount;	Nuclei deformation depends on constriction size and Lmna occurrence; Protrusion smaller with Lmn1-/-; Wild type cells slower in constrictions	[43]
<b>E</b>	Fibrous half enclosed structure	Aerograp hite	-	Pores: 10 $\mu$ m-100 $\mu$ m Filament diameter: 0.5-3 $\mu$ m	-	Ref 52 wt; Ref-YFP-paxillin; YFP-fluorescence	-	YFP-fluorescence; RFP and Hoechst	Assembled actin fibers, visible FAC for Ref-YFP-paxillin cells; typical morphology;No migration	[71]



Sketch	Architecture/ Topography	Material	Stiffness	Spacing	BCL and BF	Cells	Speed	Staining	Morphology and Migration	Examples
F	Fibrous 3D	Collagen matrix	4 to 60 Pa	Pore size: 4 $\mu$ m <sup>2</sup> to 1 $\mu$ m <sup>2</sup>	- -	MT1-MMP–transduced HT1080	Pore size dependent	Yes; Alexa fluor-594 phalloidin, propidium iodide, and anti-vinculin antibodies	Increased migration; Form dendritic spreading to flat polarized in dependence of the location inside the matrix;	[72]
G	Plane hydrogel	Hydrogel poly-acrylamide (PA)	0.1-12kPa	70 $\mu$ m thin gel	sulfo-SANPAH; Collagen I	Contractile myocyte, C2C12	-	Rhodamine-phalloidin, Hoechst 33342; Immunofluorescent antibodies to myosin or vinculin	Elongated cells; Formation needed longer time on softer gels; Alignment towards other cells; No migration;	[67]
G	Grooved surface	Hydrogel ; PEG-based	91kPa - 2600kPa	Grooves with different width; 10 $\mu$ m worked best	-	NIH L929; fibroblasts	-	tetramethylrhodamine isothiocyanate (TRITC)-conjugated phalloidin; 4'6-diamidino-2-phenylindole; primary antibody anti-bovine VN from mouse; secondary antibodies ;	Cells aligned with the grooves; grew best with softer hydrogels;	[73]
G	Gold-NP pattern	Hydrogel ; Polyethylene glycol diacrylate based		15-200nm	Gold NP	3T3 fibroblasts	-	-	Normal cell behaviour, but at distances larger than 100nm difficulties to attach and spread	[74]
H	Microporous hydrogel	Alginate		pores up to 230 $\mu$ m	Gold NP	Dendritic cells	-	-	Volume fraction of pores lead to more cells, effective with 50%; Porous system do not induce maturation	[75]
I	Microstructured hydrogel	pAAm	18kPa	Range up to 20 $\mu$ diameter,	-	<i>A. castellanii</i>	100-400 nm/sec	-	Normal; Amoeboid squeezing,	[45]

### 1.1.4.3 Biofunctionalization of the material matrix

Material matrices of a different kind, as shown in Figure 2 and Table 1, are used to investigate cellular behavior according to stiffness and architecture, also see chapters 2 and 3. Some of the materials require the coupling of the adhesion proteins to the matrix in order to create a bioactive surface and adapt the surface chemistry and charge according to the cells. [76] The bioactive surface is important, e.g., with hydrogels, as they have a hydrophilic surface or are mostly inert towards protein absorption. A bioactive surface is modified chemically with adhesion proteins specified to the cell type used. The adhesion proteins can be of various types: collagen, fibronectin, or RGD (arginine-glycine-aspartic acid), all commonly used to promote cell adhesion. Cell adhesion will ensure proper cell functions in cell viability, migration, and proliferation. Besides the chemical modification also topographically structures can feature the unspecific adhesion of cells towards the surface. [57], [77]

## 1.2 INTRODUCTION TO THE MATRIX MATERIALS

### 1.2.1 Hydrogels as matrices for (bio)interactions and the hydrogel preparations

The focus in this section is on hydrogels, their preparation, and their characterization. Hydrogels are the material of choice for various applications within medical applications, filters, or materials used in cell investigations due to their exceptional performance in all fields by providing a porous three-dimensional network of polymeric crosslinked chains. [78], [79] This polymeric network is hydrophilic and absorbs water and will swell until equilibrium is reached. It offers the possibility for the diffusion of nutrition, proteins, and chemical signal molecules from and towards the cells. Herewith, hydrogels are the closest materials to mimicking synthetically *in vivo* conditions. [80] Their mechanical properties confine the range of use in applications, but these can be adjusted over the structural composite designs. The mechanical properties dependent on the hydrogels polymeric structure, the charges of the polymeric chains, and the swelling behavior. Obviously, the basis of these is the size of the meshes created from the crosslinked polymer chains. The mesh size is associated with the crosslinking density and the Young's modulus, which is itself related to the polymer fraction as well as to the hydraulic permeability. [80]–[82]

### 1.2.2 Hydrogel synthesis

Different kinds of hydrogels can be found in nature or are artificially built. Natural hydrogels are, for example, collagen fibers or hyaluronic acid, which are components inside the ECM, but also alginate is a natural hydrogel. Synthetic hydrogels for example are polyacrylamide, Poly(*N*-isopropylacrylamide) (pNIPAM) or Poly(2-hydroxyethyl methacrylate) (pHEMA). All of them can be synthesized in various forms, for instance, as fibers, as plane bulk samples, or structured with different topographies or internal architecture which will determine the cell behavior. [83] In this

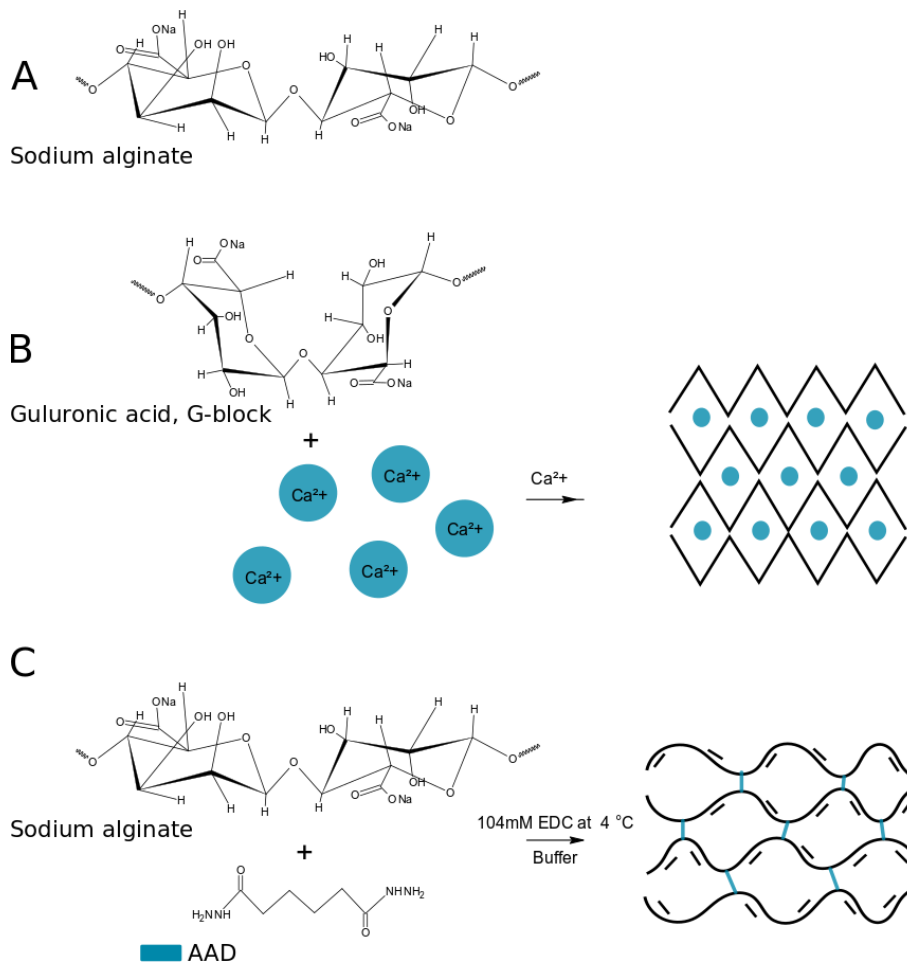
work, I will concentrate on three different kinds of hydrogels: alginate, pHEMA, and pAAm as the basis of this work to investigate cell-matrix interactions. In hydrogels, the hydrophilic polymeric chains are crosslinked using different types of crosslinking methods. These will influence the performance of the hydrogel not just because of the concentrations, but by the charges incorporated into the mesh structure of the hydrogel. We can distinguish between two types of polymerizations in hydrogels: Firstly, the physical crosslinks that work due to physical forces such as van der Waals forces, entanglements of polymer chains, temperature-dependent physical attachment or by forming chelate complexes with ions. [80], [84] The second type is using chemical covalent bonds. These bonds are, for most cases, stable and insoluble unless the crosslinker used has special properties such as a highly susceptible to hydrolysis [78]. Dissolvable covalent hydrogels are such as diamines, which are susceptible to hydrolyses. Non-degradable crosslinker, N,N'-Methylenebisacrylamide as an example, will be co-polymerized to the backbone of the resulting hydrogel. Just very harsh conditions such as high mechanical forces could divide those crosslinks without any recovery. Interestingly, this type of recovery after brute mechanical forces can be observed in hydrogels crosslinked via a physical ion linkage. [79]

### 1.2.3 Physical crosslinks

#### 1.2.3.1 Alginate:

A formidable example of physical crosslinking is alginate. Used in various biomedical applications due to its biocompatibility, the sodium salt of the alginate is crosslinked using  $\text{Ca}^{2+}$  ions. The structural polysaccharide of the brown algae is an isomeric bloc-co-polymer of two variations. One of the variation, the  $\alpha$ -L. guluronic acid (G-blocks) will interact to the so called 'Egg'box' structures while forming chelate complexes with the calcium ions using the charges of the carboxyl and oxygen atoms (Figure 3B). The crosslinking density here depends on the concentration of the respective building blocks used for the crosslinking. Considerable is the amount of G- and  $\beta$ -D-mannuronic acid (M-blocks) blocks, which influences the brittleness of the hydrogel. The block-co-polymers of MM, GM and MG conformation are flexible in their glycosidic bonds to each other and can rotate around these bonds. [84]–[87] Furthermore, the storage conditions of prepared alginate hydrogel samples are essential. Chelate complexes are formed by electrostatic interaction between the carboxylate and oxygen groups from the alginate G-Blocks with the divalent calcium ions. Stored in solvents with different chemical potentials or applying an osmotic pressure can lead to an exchange of ions or loss of ions to the environment, thus to a loss of junction zones a degradation of the alginate sample. [88], [89] The degradability of matrices is a powerful feature to adjust, for example, the growth of tissue and the destruction of supporting matrix, e.g., seaming from damaged tissue without additional operation to remove the threads. [90] Additionally, it comes with high importance of

compliance between the matrix, its degradation product and the surrounding tissue. Assuming an implant inserted into the brain where calcium ions are responsible for the guidance of signals between the neurons, an increase in calcium ions could be led to additional signaling between the neurons. [91], [92] This requires the usage of other methods to prepare a polymerized alginate. Therefore, other functional groups present inside the molecule structure needs to be used, such as carboxylic groups, which can be addressed for covalent crosslinking (Figure 3C). [78], [89], [93]



*Figure 3 Structure of sodium alginate and possible crosslinking procedures. A) depicts the structure of sodium alginate with its two building blocks 1 → 4) linked  $\beta$ -D-mannuronic acid (M-blocks) and  $\alpha$ -L-guluronic acid (G-blocks). B) shows the physical crosslinking of alginate via divalent ions and the formation of the ‘Egg-box’ model. C) presents the covalent crosslinking of alginate using a diamine linker adipic acid dihydrazide (AAD) and EDC forming a mesh with free carboxylate groups.*

## 1.2.4 Covalent crosslinks

### 1.2.4.1 EDC and AAD coupling

Functional groups such as carboxylic acids ( $-\text{COOH}$ ) can be conjugated with primary amines ( $-\text{NH}_2$ ) by using 1-ethyl-3-(3-dimethylaminopropyl) carbodiimide hydrochloride (EDC). [78] The EDC activates the carboxylate groups and reacts directly with the amine groups present. With this, an amide bond is formed. [94] A buffered, slightly acidic environment is favorable to stabilize the reaction. For this,

the buffer MES or MOPS can be used. The carboxyl groups are susceptible to nucleophilic compartments of molecules such as the amine groups of the adipic acid dihydrazide (AAD). The adipic acid dihydrazide can act as a degradable crosslinker due to the hydrazide bond formation, which can be hydrolyzed. [78] Figure 3C presents an exemplary synthesis via EDC and AAD.

#### *1.2.4.2 Free radical polymerization*

The free radical polymerization is used in mainly for the polymerization of synthetic hydrogels. Within three steps, the free radical polymerization occurs and creates covalently crosslinked polymeric structures. At the first step, the initiation, a free radical is formed by, e.g., UV-light, temperature, or redox initiators. A propagation follows as second step; one monomer by one is connected to a chain by transferring the radical. In the last step, the termination of the polymerization occurs with the lack of further monomers to be activated as well as with a radical combination. The radical polymerization can occur for each monomer with vinyl or with methacrylate groups. Polyacrylamide (pAAm) hydrogels, as an example, consist of the monomer acrylamide and the bifunctional crosslinker bisacrylamide. Using the vinyl groups of the monomers and the polymerization is initiated by N,N,N',N'-Tetramethylethylenediamine (TEMED) and ammonium persulfate (APS). [95] Figure 4 shows the reaction schemes of pAAm and pHEMA synthesis via radical polymerization using APS and TEMED.

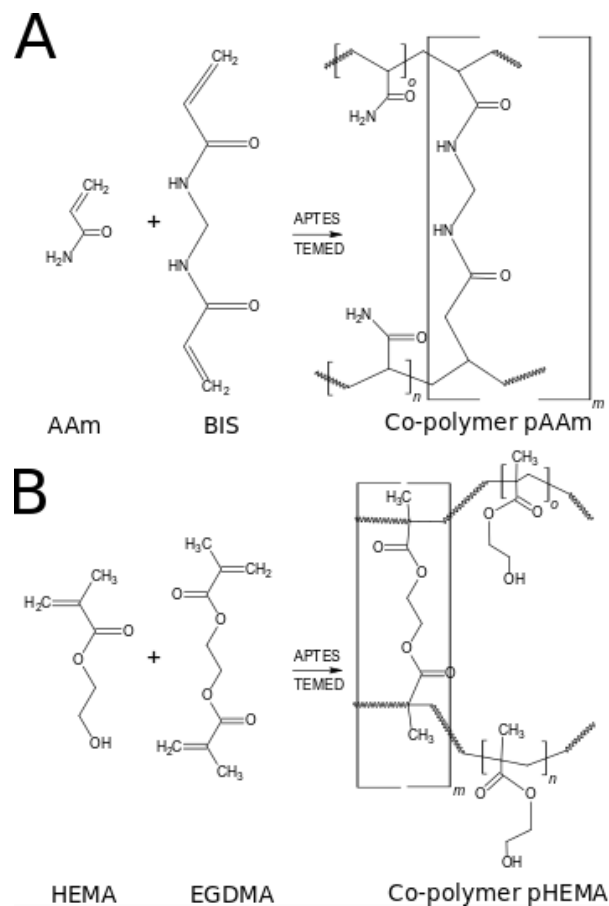


Figure 4 Scheme for the radical polymerization. A) Acrylamide (AAm) reacts with *N,N'*-methylene-bis-acrylamide (BIS) to the co-polymer pAAm. B) Hydroxyethylenemethacrylate (HEMA) and ethyleneglycoldimethacrylate (EGDMA) react to the co-polymer pHEMA. In both reactions, APS and TEMED as initiators are used.

### 1.2.5 Hydrogel biofunctionalization procedures with different chemical components

The biofunctionalization of hydrogels is required for most hydrogels since most hydrogels have no initial adhesion molecules available for cells or are inert toward protein absorption. These hydrogels can be from natural source such as alginate or from synthetic source such as Poly(2-hydroxyethyl methacrylate) (pHEMA) or polyacrylamide (pAAm) as mentioned before. Without proteins the adhesion of cells towards unmodified hydrogel surfaces is highly limited. Three possibilities for the biofunctionalization of hydrogels are discussed below.

#### 1.2.5.1 1-ethyl-3-(3-dimethylaminopropyl) carbodiimide hydrochloride (EDC)

The coupling via EDC is similar to the covalent crosslinking of the hydrogel. The EDC is used to activate a free carboxylate group and binds the adhesion protein to the matrix already prepared, e.g., RGD, Collagen, or fibronectin. Another opportunity is the crosslinking of RGD to alginate molecule chains via EDC with the support of N-Hydroxysulfosuccinimid (sulfo-NHS). Sulfo-NHS will stabilize the EDC reaction and can prevent the direct hydrolysis of the amide bond between the amine and the carboxyl group during the functionalization. This process for the biofunctionalization takes place at

the surface and closes to the surface, as the EDC molecules and adhesion proteins have to diffuse inside the sample. A 3D matrix biofunctionalization is here restricted to the depth of diffusion of all reactants. [78], [89], [96]

#### *1.2.5.2 Sulfosuccinimidyl-6-(40-azido-20-nitro phenylamino) hexanoate (Sulfo-SANPAH)*

The biofunctionalization of hydrogel surfaces can also be conducted with sulfo-SANPAH. Sulfo-SANPAH includes a photo reactive group, that reacts with available groups on the matrix surface such as carboxyl groups. Placed on the matrix and with UV-light is applied the sulfo-SANPAH is bound to the hydrogel. The sulfosuccinimidyl group can react with amine-containing molecules to bind adhesion proteins covalently to the hydrogel surface. This procedure is well established and practical for 2D cell-matrix *in vivo* investigations as the UV light can activate the sulfo-SANPAH at the surface. However, the depth necessary of diffusion of the sulfo-SANPAH and the reach of the UV light challenge this attempt for a 3D matrix biofunctionalization. [19], [97]–[99]

#### *1.2.5.3 Acrylic acid N-hydroxysuccimide ester (Acrylic-NHS)*

In contrast to EDC, sulfo-NHS, or sulfo-SANPAH application, the use of A-NHS is versatile in its use for different architectures, 2D as well as 3D. The NHS group is bound to an acrylate group with the advantage of being polymerizable into the overall polymeric matrix via free radical polymerization. [100] This has a significant advantage that the free reactive groups are highly available also in ‘small’ micrometer-sized 3D architectures such as in channel or pores. Due to this, the biofunctionalization of these structures can be done in 3D. The hydrogel matrices then produced have to be placed into the adhesion protein solution of choice. The structures created in 3D are then dependent on the diffusion of the molecules.

### **1.3 INTRODUCTION TO THE BRAIN AS A POTENTIAL MATRIX ENVIRONMENT**

In their natural environments, cells, are not only within the ECM in proximity with cells of the same type of cells but with a variety of different types for different purposes. An example is the brain as one of the most essential tissues. Here, cells such as neurons, glia cells, cells of the brain ECM, and the endothelial cells for blood vessels are found in the brain. Within the brain and its different areas the proportion of the cell types define the stiffness of a particular brain region. Interestingly, the brain is one of the softest tissues inside the body with elastic moduli ranging from 40 Pa to 20,000 Pa. [101] This range appears due to the high amount of water-absorbing proteins and the low amount of collagen I. They form a structured and very distinct architecture, where designated areas are responsible for distinct functions of the body. Moreover, ventricles filled with cerebrospinal fluid (CSF) can be found. This fluid acts as a damper against strikes, hydrates the brain, and as an additional transport system for hormones and byproducts inside the brain besides the blood vessels.

It is replaced several times a day in a human. [102] This soft tissue is not only protected by the cerebrospinal fluid but covered by several layers (dura mata and pia mata) and embedded into the skull for protection. [101] However, not always can an injury be prevented, and scar tissue is formed. This tissue is called glia scare and will also be formed by the insertion of implants like stiff electrodes, which are not mechanically compatible with the brain cells. The formation of glia scars around implant devices will limit its usability. Interestingly, these scars will be softer than the tissue has been before but will still encapsulate the device and prevent its functionality. Additionally, a reduced stiffness can occur with different diseases, inflammation, or acidosis. [103], [104] As an improvement, implant coatings of softer materials could be applied to the devices to obtain the mechanical compliance.

However, compliance is not solitary the mechanical compliance between a single cell and the matrix material. Another perspective of compliance is for instance the diffusivity of a material or the material relaxation after applied strain. The diffusivity determines whether a material can let nutrition and other molecules pass through. This ability is present in hydrogels. Here, to adapt the diffusivity, the mesh size is important, which also will change the stiffness of the materials, see chapter 1.4. Even though this seems to be an ideal solution, the interaction of the implanted materials e.g. hydrogel and CSF with its proteins and ions should be monitored. [104], [105]



## 1.4 INTRODUCTION TO THE MECHANICAL MATRIX CHARACTERIZATION

### 1.4.1 Stiffness, strains and their slopes

As explained in section 1.1, cells are influenced by the topography and architecture but also strongly from the mechanics of the underlying or surrounding matrix. [19], [106], [107] This part will highlight the various ways of mechanical characterization for matrix materials can be. At first, we have to consider the stiffness of matrix material, as this describes the force applied to the matrix with a reached material displacement. The slope from this curve is the value for this matrix material and material constant. Second, we will consider the elasticity of the materials, which includes Hooke's law as a definition of the spring constant. The spring constant  $k$  in equation (1) is defined as the vertical deflection  $d'$  proportional to the force  $F$  applied for this deflection. The strain  $\varepsilon$ , equation (2), applied to a material is defined as the division of the change of length  $\Delta l$  by the start length  $l_o$ . Further, the stress  $\sigma$  on the matrix is described as the force  $F$  divided by the area  $A$  of the material, equation (3). The stress  $\sigma$  and the strain  $\varepsilon$  together with the Young's modulus  $E$ , describe the elasticity of a material, see equation (4). [108]–[112]

$$k = \frac{F}{d'} \quad (1)$$

$$\varepsilon = \frac{\Delta l}{l_o} \quad (2)$$

$$\sigma = \frac{F}{A} \quad (3)$$

$$\sigma = E \varepsilon \quad (4)$$

For materials with linear force displacement slopes, this law can be taken into account, as the strain and the displacement is directly proportional to the applied force. At third, we have materials with

non-linear force-displacement curves where the stiffness value is increased from a certain displacement on. This stiffness value is stable after reaching a so-called 'plateau region'. This behavior comes from the partly viscous and elastic components inside these materials. It is found in many materials, especially in biological or biomimetic materials such as collagen fibers or hydrogels. In hydrogels, the polymeric network is flexible up to a point where the polymeric chains are strained too far away from the crosslinking point.

#### 1.4.2 Young's modulus and the different models for indentation methods

Classically the Young's modulus is investigated using a tensile test in order to determine the elasticity of a material of interest. However, a tensile test is not always possible, for example, with very soft or small samples. As the materials of choice in this work are mainly hydrogels, the Young's moduli were determined with other methods. The Young's modulus  $E$  is the relation between applied force or stress  $\sigma$  and deformation of a material or strain  $\epsilon$  and describes the resistance of a material against a load. It is a characteristic for the material composition. By adjusting the chemical composition, such as in hydrogels, the crosslinker concentration, the Young's modulus can be easily adjusted. The chemical composition will not only change the Young's modulus of the resulting matrix but can also have an influence on the surface tribology. The tribology properties of the matrix include the adhesive and friction behavior of samples to each other. For the determination of the Young's modulus, several models have been formulated to include different restrictions to the calculations. Importantly, there is to mention the difference between the Young's modulus and the stiffness in general and the terms used in this work. The Young's modulus is a material parameter independently of the sample geometry and shall be the same, whereas the term stiffness can be dependent on the sample form. The most common model is the Hertz model. It assumes a homogenous isotropic and fully elastic material, which is indented continuously with a perfect sphere or a cone. The indentation depth is very small, not more than 10% of the sample thickness and no interaction, no adhesion nor friction, happens between the sphere and the matrix. [109], [111], [113], [114] This model will be used later in this work, see chapter 2 and 4, as the hydrogels examined fit into the descriptions mentioned before.

Nevertheless, other models exist and shall be mentioned here shortly, e.g., the Johnson-Kendall-Robert theory (JKR) and the Derjaguin-Muller-Toporov theory (DMT) included the adhesion between the sphere and the material and assumed contact between solid bodies. While the JKR model assumes the deformation of the two bodies due to surface tension and elastic deformation, the DMT model assumes full adhesion between the bodies involved. With this, the forces for the separation of

the two matrices, mostly van der Waals forces and molecular forces outside the contact zone, can be taken into consideration. [115], [116]

### 1.4.3 Determination of the Young's modulus

The measurement of the Young's modulus can be done in various ways. Two methods are: Indentation and rheometer tests. In indentation tests the matrix material is indented by a known force and indenter type and form. The displacement of the material and the indenter force provides the force-displacement curve. The slope of this curve is calculated with the applicable model for the Young's modulus. Here, the Hertz model will be applied for all indentation measurements. These indentations can be done microscopically using an atomic force microscope (AFM), Figure 5A, or macroscopically with a non-sticking sphere of known size in mm range, Figure 5B. For the AFM a cantilever with known spring constant and bead diameter indent into the matrix and retract. According to the slopes created from the data, a fit from the Hertz model will be laid over the data. Thus, the data from the material can be compared to the Hertz model fit and assessed. Ideally, the Young's modulus of the material will reach a plateau region, as the Young's modulus is material dependent and should stop at a saturation point. As hydrogels depend on their elasticity on their polymeric mesh sizes created from the crosslinker concentration used and the environmental condition during the polymerization, it is highly important to measure the Young's modulus at several positions. [108], [109], [117]

The Young's modulus according to the Hertz model:

$$F = \frac{4E}{3(1-\nu^2)} R^{\frac{1}{2}} d^{\frac{3}{2}} \quad (5)$$

*E* Young's modulus; *F* applied force; *R* Indenterradius; *d* indentation depth; *ν* Poisson's ratio

Another method to gain acquaintance with the mechanical matrix properties is the use of a rheometer, Figure 5C. With a rheometer, a sample is clamped into the sample holder, and oscillatory shear stresses are applied towards the sample. As a result, the complex shear modulus  $G^*$  is created, including  $G'$  and  $G''$  and a complex component  $i$ , see equation (6).  $G'$  is the storage modulus and describes the matrix possibility depending on the storage capacity to store energy and thus describes the elastic part of the material.  $G''$  is the shear loss modulus and describes the viscous properties. Per definition, the proportion of  $G' > G''$  is for an elastic material and  $G' < G''$  for a viscous material. [109], [118]

$$G^* = G' + i * G''$$

(6)

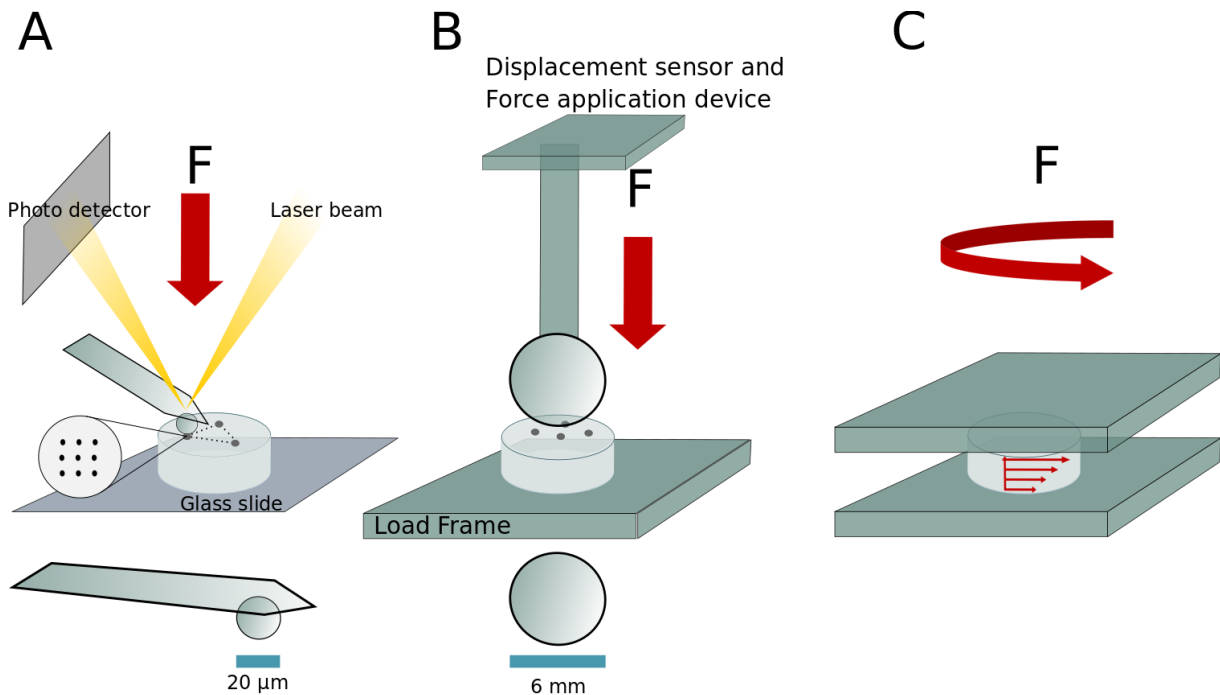


Figure 5 Schematic illustration of Young's modulus evaluation. A) and B) show the general setups for indentation based measurements, which require several points of indentation per sample. The applied force is uniaxial. A) The Schematic set-up of an AFM based measurement. The hydrogel sample is covalently bound to a glass slide to prevent movement of the sample. The cantilever with the attached bead will apply a force to the sample with defined speed until a deflection of the cantilever is measured. The deflection is determined by the laser beam concentrated on the top of the cantilever and reflected towards a photodetector. Each movement of the laser beam is recalculated towards movement and force applied to the sample matrix; the bead diameter is  $21.82\mu\text{m}$ . In B) the macro indentation is depicted. The non-sticking sphere with a diameter of  $6\text{mm}$  will indent a certain depth inside the sample sitting on top of a load frame. C) Depicts the general set-up for rheometer measurements. The force applied to the clamped sample oscillates in  $xy$ -plane.

#### 1.4.4 Determining the polymeric mesh size via mechanical measurements

The polymeric structure defines the mechanical performance of the hydrogel matrix. The matrix characteristics can be described by the average mesh size of the polymeric network  $\xi_a$  (also known as correlation length) which depends highly on the monomers chains or their molecular weight  $M_c$ . The molecular weight is described by the repeating unit and its molecular weight  $M_0$  and the degree of crosslinking  $X$ , see equation (7). The average mesh size also is related to the polymer fraction  $v_p$  in the swollen gel in equilibrium. This polymer volume fraction can be calculated with equation (8),

where  $V_{\text{polymer}}$  the volume ration of the polymer and  $V_{\text{gel}}$  is the volume of the swollen gel. [81], [108], [119]

Additionally, the average mesh size of the polymeric network  $\xi_a$  depends on the crosslinker density  $\rho_x$  and can be calculated by using the equation (11) derived from Pescosolido *et al.*, 2012. [119] Pescosolido *et al.*, 2012 used the correlation between the shear modulus  $G$  and the crosslinker density  $\rho_x$  of the hydrogels, see equation (10). Furthermore,  $\rho_x$  and  $\xi_a$  were related with the assumption of a polymeric network with a regular spherical mesh size. This spherical diameter is the average mesh size of polymeric network  $\xi_a$  is, see equation (11) With the relation between the measured Young's modulus  $E$ , the Poisson's ratio  $\nu$ , and the shear modulus  $G$ , equation (9),  $\rho_x$  and  $\xi_a$  can be calculated.  $R_{\text{gas}}$  is the gas constant,  $T$  the temperature and  $N_A$  is the Avogadro constant. These relations are depicted within the equations (8)-(11) below. [81], [108], [119]

$$M_c = \frac{M_0}{2X} \quad (7)$$

$$\nu_p = \frac{V_{\text{polymer}}}{V_{\text{gel}}} \quad (8)$$

$$G = \frac{E}{2(1 + \nu)} \quad (9)$$

$$\rho_x = \frac{G}{R_{\text{gas}}T} \quad (10)$$

$$\xi_a = \sqrt[3]{\frac{6}{\pi \rho_x N_A}} \quad (11)$$

As the whole matrix system is a system with and in water, the hydraulic properties of the hydrogel are important. An example is the swelling behavior of hydrogels as it is reported that the swelling takes place as long an equilibrium within their chemical potential is not reached. [81], [113] The fraction of water taken up and stored can be described by the volumetric water content  $\theta$  using the weight of the polymeric matrix  $m_{\text{dry}}$ , the weight of the swollen sample  $m_{\text{wet}}$  and the density of the solvent  $\rho_{\text{solvent}}$ , see equation (12). The swelling %S can be described by the ratio of the final  $m_{\text{final}}$  and start  $m_{\text{start}}$  mass, see equation (13).

$$\theta = \frac{m_{wet} - m_{dry}}{\rho_{solvent}} \quad (12)$$

$$\%S = \left( \frac{m_{final}}{m_{start}} \right) 100 \quad (13)$$

The polymeric chain structure and the crosslinking density act here as force, the chemical potential needs to overcome since the polymeric chains will interact with the solvents according to their charges. The same counts for molecules or drugs infiltrated into the hydrogel matrix, which diffuses inside and towards the border of the sample. This diffusion of molecules or release of molecules can apply stress towards the sample via osmotic pressure. It can, in dependence on the type of crosslinking, induce degradation of the material. [81], [89], [113]

## 1.5 INTRODUCTION TO THE INTERACTION BETWEEN MATRIX MATERIAL AND MOLECULES

Notable in this work is the definition of matrix and mesh. The matrix represents the whole hydrogel sample based on its polymeric network in the swollen and unswollen state. The mesh represents the existing polymeric network and its size, depending on the crosslinking density. The mesh is the base of the hydrogel behavior, such as swelling, and dictates in the end, the mechanical properties of the sample. The dimensionality defines whether a sample of any material displays a structure in 1D, like a thread, 2D (plane surface or a nanopattern of Gold-NP or FN); 2.5D or half enclosed structures represent a matrix where every object is exposed to more than a 2D surface but has at least one free side, see Figure 2. 3D is a fully closed structure, such as a channel made from various materials as mentioned earlier in section 1.1.

### 1.5.1 Molecule release from matrix materials

In this part of my work, I want to introduce the topic of interaction between the matrix and molecules, also called substances or drugs. In particular, this section is about passive substance release systems from hydrogel matrices used. Different hydrogel systems from natural as well as from synthetic hydrogels can be found for the substance release to the supernatant to *in vitro* and *in vivo* application. These systems can be based, e.g., on alginates polymerized with ions or covalently crosslinked or IPNs with and from polysaccharides, or nanocarrier systems to overcome the blood brain barrier like biodegradable nanoparticles. [120]–[124]

The considerable advantage of hydrogels as carriers of substances are similar to those of the cell-matrix interactions. It is the ease of substance infiltration due to swelling. The substances can be

nutrition for cells or drugs. With the high water content in hydrogels, aqueous dissolvable drugs can be easily used. The adaption of the mechanical properties is controlled by the mesh size, which also mediates the infiltration and the release of substances. Interestingly, additional features such as electrostatic interactions, the degradability of the matrix, the pH response of the network, and the swelling properties can have a substantial impact on the substance matrix interaction. [125] Each of these factors can either increase the drug release, such as the degradation of the matrix or decrease the release. An example of such behavior would be molecules that are electrostatically attached to the matrix. Additionally, the sample size is also important to consider, as it influences the application. The administration side for *in vivo* studies can be wound dressings for dermal applications or nano-sized applications for pulmonary administration. [125]

### 1.5.2 Sink conditions for *in vitro* experiments

The sink conditions are defined as the maximum substance concentration, which can be released into the supernatant. It usually should not exceed 30%, which means that the solubility limit of a substance introduced into the system is smaller than 30% of the total volume. With this, an artificial saturation of the substance and a decreased release time should be avoided. Several factors need to be considered. Here the three most important sink condition factors are: First, the substance is dissolvable in the respective solvent/solvent-system. Second, the saturation limit of the substance investigated will not be reached during the investigations. Third, the concentration of the substance is within the measurable limit of the technique used. These requirements are called the 'sink' conditions and can be adjusted to each system. [126] From different references, the various volume specifications can be found: The volume of the solvent shall be nine to three times higher than the dissolution limit of the substance inside the respective solvent. [126]–[128] A possible drawback of the sink conditions could appear when the drug release from *in vitro* experiments should predict future *in vivo* applications. *In vivo* situations are much more condensed with a possible smaller volume for the dissolution on the one hand, on the other hand dynamic fluid exchange exists e.g., liquor exchange inside the brain or blood flow is challenging to mimic. [129] Furthermore, increased interaction in the sink condition due to the extended volume can compromise the matrix stability in the case of degradable hydrogels. Switching to non-sink conditions could here bring the results closer to the *in vivo* situation and protect the matrix. However, it can also alter the release kinetics from the matrix to the environment. [130], [131]

### 1.5.3 Release mechanism and kinetics:

Three different types of drug release can be determined. First, the drug release via diffusion from the matrix. Second, the drug release via matrix swelling and, at last, the drug release using chemical changes inside the matrix. [132], [133] Highly significant for all types of release is the infiltration of drugs into the matrices as they influence the release kinetics. For hydrogels, two strategies are mainly used. The first is to include the drug into the hydrogel precursor solution. With this, the matrix is already loaded after polymerization, e.g., hydrogel NP, direct after the polymerization and dried. [134] For the second approach of infiltrating drugs into the prepared hydrogel matrices, these will be further dried and immersed into the drug bearing solution to take up the substance of choice. Later these hydrogel samples are dried again. [134], [135] The diffusion based drug or substance release has to be taken into account for fully swollen matrices. Depending on the substance molecules size and that of the polymeric matrix as well as of the charges of both, the substance molecules will move through the matrix by diffusion and mass transport. An equally dissolved substance inside the swollen sample is assumed without interacting with the matrix and substance charges. The substance release happens then at the interface between matrix and solvent on the chemically potential and concentration gradient. [130] In case of a swollen matrix with mesh sizes smaller than the substance molecules, the matrix needs other release mechanisms such as degradation of the whole, or swelling of the matrix, as friction due to size lowers the diffusion of the drug. In general, the diffusivity of a drug from a hydrogel can be calculated by the equation (14).

$$D = \frac{RT}{6\pi\eta r_{drug}} \quad (14)$$

The diffusivity:  $D$ ; the radius of the drug molecule:  $r_{drug}$ ; the viscosity of the solution  $\eta$

The diffusivity in equation (14) is calculated without steric hindrance and excludes the influence of the mesh size. In the case of meshes and molecules with similar size friction and thus also the delay in the release has to be considered. [125] The substance release based on matrix-swelling acts upon the osmotic pressure, which is comparable to the chemical potential between the matrix and the surrounding. The swelling of the matrix is finished when equilibrium is reached, as in equation (15). [122], [135]

$$\Delta\mu_1 = \Delta\mu_{mix} + \Delta\mu_{ion} + \Delta\mu_{elastic} = 0 \quad (15)$$

Where  $\Delta\mu_{mix}$  describes the chemical potential for mixing term,  $\Delta\mu_{ion}$  the term and  $\Delta\mu_{elastic}$  describes the elastic term of swelling network chains.  $\Delta\mu_1$  describes the chemical potential outside the gel network. [122] In most cases, this type of release relies on dehydrated glassy samples. These



hydrogel samples do not contain any liquid but the dry polymeric mesh. However, their polymeric mesh can still swell and include water. In the dry state, they include the substance for the release either loosely or connected to the matrix mesh. The swelling of the matrix and water uptake into the matrix lead to an increase relaxation of the mesh and a dissolution of the drug into water. The swelling of the matrix, as well as the dissolution of the substance and its release, lead to two boundaries moving in the opposite direction. [135] The substance release based on the matrix alterations is influenced by the chemical changes inside the matrix. These changes can be actively triggered by pH, temperature, or even hydrolysis of crosslinker. The hydrolysis will degrade the matrix and enables enhanced release to the incorporated substance and is an active matrix-substance release system. [132]

For the solvent and substance infiltrated into the hydrogel matrices as well as release from the matrices the behavior can be described in various models. Both, infiltration and release indicate the transport from substances or solvents from one location to another. However, the usage of material matrixes, here hydrogels, requires two thoughts: The idea that the behavior includes the diffusion of solvent and substances within the matrixes to another position or sample surfaces and the diffusion from the matrix to the surrounding supernatant. Several mathematical models for the description of the release kinetics have been established, which can be found elsewhere.

The general release profiles can be determined with the release theory by Ritger and Peppas [136] :

$$\frac{M_t}{M_{00}} = kt^n \quad (16)$$

$M_t$  is the mass of drug released at time  $t$ ;  $M_{00}$  the total mass of released drug;  $k$  a kinetic constant.  $n$  in equation (16) is the diffusional exponent depending on the transport, sample geometry, and polydispersity and is given by the release fraction over one unit of time for the indication of the kinetics of release. With the diffusional exponent  $n$ , the different cases can be described. One case example is the classical behavior of Fickian diffusion with the diffusional exponent  $n=0.5$ . The Fickian diffusion for release is the transport of the substance or solvent in a greater time than the relaxation time of the polymeric structure. For the diffusional exponents  $n<0.5$  or  $n=1$  the release is described as non-Fickian or Case II diffusion. Nevertheless, this is a model and does not include e.g. the individual material properties, possible substance-matrix interaction and sink conditions (mentioned above) or pH of the supernatant. With the release from actual matrices and the substance-matrices interaction can be found to be different. [130], [137], [138]

## 1.5.4 Methods for quantifying released substance concentration

### 1.5.4.1 HPLC measurements and UV-VIS spectroscopy

Various methods can be used for determining the concentration of the substance released into the supernatant. Here, high-performance liquid chromatography (HPLC) and UV-Vis spectroscopy are used to investigate the release of the substances used. For the UV-Vis spectroscopy, a microplate reader determines the absorption of light from substances dissolved in the supernatant. The absorption of light can be determined as the substance molecules change their energetic status when irradiated with a particular wavelength. A valence electron will change its position in the outer orbitals. The energy necessary is described with:

$$\Delta E = h f = \frac{h c}{\lambda} \quad (17)$$

Where  $\Delta E$  is the energy difference necessary to overcome the barrier between the orbitals;  $h$  is the Planck constant,  $f$  the frequency,  $c$  the speed of light and  $\lambda$  the wavelength of the incident light. [139], [140] Another possibility to determine the concentration of the substance can be done by using a calibration curve. The calibration curve is applied measuring various standards with known concentrations. With these results, a calibration curve can be set up and a linear fit is applied. With the slope of this fit and the interception of the axis, the concentration can be determined. It is essential to consider the eventual dilution of the substances before the measurements took place, see equation below:

$$C = \frac{FE \text{ or } A - \text{interception of axis}}{\text{slope}} \quad (18)$$

Where  $C$  is the concentration in  $\mu\text{g/mL}$ ;  $FE$  is the peak area/counts per peak area;  $A$  is the absorbance.

The HPLC was used to measure the concentration of substances released from swollen alginate matrices. Extracts taken from the experimental volume were investigated. The extract is placed together with a solvent into a separating column and is passed through this column by pressure. After passing the column, the liquid passes a detector. This detector determines the diluted substance molecules. Detectors working on the basis of light determine the absorbance of light/the light, which is passed through after the solvent and the extract molecules absorbed parts of the light. Two types are possible to use: first one photodiode and the second an array of photodiodes. The more photodiodes are used the more spectra can be determined at the same time. Other detectors

use the index of refraction for samples without UV-Absorption, fluorescence detectors, electrochemical detectors or evaporative light scattering detectors. Here, the solvent is evaporated, and measurements are taken from aerosols.-After passing the detector, a chromatogram is compiled from the data recorded. The peaks from this chromatogram resulting from the substances within the solvent can vary in height and width according to their concentration. For the determination of a substance concentration from an experiment, the same substance but in various known concentrations called the standard need to be measured. [139], [140]

## 1.6 INTRODUCTION TO QUANTIFYING METHODS FOR THE BIOCOMPATIBILITY OF MATRICES AND THE CELL-MATRICES INTERACTION FOR 2D AND 3D

In this work, different cell types for different experimental setups were used to study different effects of materials properties towards cellular behavior. In this part, the general cell culture is described and used if not stated differently in the experimental part. If not stated otherwise, all cells were cultured in an incubator at 37 °C and 5 % CO<sub>2</sub>-atmosphere with the respective cell culture medium for rat embryonic fibroblasts wild type (Ref 52 wt), fibrosarcoma cells (HT1080 with transfected nucleus NSL- GFP and H2B-GFP) human umbilical vein endothelial cells (HUVEC) or *Acanthamoeba castellanii*. The general cell culture can be found in the appendix, chapter 6.2 “General cell culture methods” on page VI. Adaptions are mentioned within the method sections for the particular chapter.

### 1.6.1 Adhesion assay

The investigation of *in vitro* cell growth on a material and its results provide the information whether a material is adequate for *in vitro* and eventual future *in vivo* applications. The area of adhesive cells covering the matrix surface can be determined by fluorescence microscopy from fluorescently stained cells. For this investigation, the cell cytoplasm is stained with calcein AM, which stains the cytoplasm of the cells. Because of this, the whole area of the cell is visible using fluorescence microscopy and can be determined according to the sample surface in %. For further information, the cells can be stained with Hoechst and Propidium Iodine. The first will stain the nucleus the latter will infiltrate and stain the dead cells. Images taken from the samples with different fluorescent channels can give the information about the cell adhesion, morphology and amount of living and dead cells.

### 1.6.2 Morphology of cells

Each cell type has its unique morphology when adhering to 2D surfaces. For Ref 52 wt and HT1080 on stiff and planar substrates such as the cell culture flask bottom, an elongated, dendritic, and polarized shape is expected. [12], [141], [142] As in other studies found, HUVEC grow preferred in a

densely packed monolayer and appear to achieve a mostly square-like structure when cultivated properly. [143], [144] For the evaluation of cellular attachment and optimal cell growth on produced 2D samples, the cellular morphology assessed as compared to the known morphology on stiff and planar substrates. The difficulty is here that variances in stiffness and topography and especially in architecture (3D) can and will result in different morphological appearances.

### 1.6.3 Cytotoxicity

The influence of different materials on cells and cell cultures are not only measurable with direct contact experiments but with indirect methods. There, not the physical properties but the chemical properties, the excess chemical products, the degraded byproducts of the material are assessed whether they have an influence towards the cells. A useful tool for this is the (3-(4,5-dimethylthiazol-2-yl)-2,5-diphenyltetrazolium chloride (MTT) cytotoxicity test, where the viability of the cells respective to a negative control is determined by the comparison of the metabolic conversion of MTT (3-(4,5-dimethylthiazol-2-yl)-2,5-diphenyltetrazolium chloride into formazan. A negative control is the control, which will be tested for negative cytotoxicity with a sample, which is not cytotoxic. The opposite is the positive control, here, a toxic sample is used to be tested for positive cytotoxicity. The cytotoxicity of the materials in this work is judged in view of the ISO standard 10993-12. The means of the average viability results are compared. In the ISO standard 10993-12 it is stated that a material is not cytotoxic when for the 100% v/v extract as well as for the 70% v/v extract, the percentage of cell viability in respect to the negative control is at 70% or higher [145], [146]. By using the ISO standard 10993-5 and 12 and monitoring the results for different materials, a dissipation from other work and results are possible. A hypothesized difficulty here is that for degradable materials, the extract preparation of 72h might not be extended enough. This is because as the later *in vitro* or even *in vivo* experiments are designed for a more extended period of time, and those degradation products and released excess material will not be examined. One strategy to avoid this is to determine the time frame for the degradation and the point where at least 50% of the sample is degraded. Another critical point is to monitor the sample handling beforehand. The samples used are prepared with different synthesis steps, e.g., hydrogels and can include excess monomers or chemicals despite washing procedures and sterilization steps applied. Here the monitoring of the MTT results, is essential to adjust the preparation, e.g., adjust the washing process with several repetitions as one strategy mentioned. If not stated differently, the assay follows ISO standards 10993-12 and 5 within this thesis.

The cell viability in respect of the negative controls is determined by following equations: [146]

$$OD_{\text{sample}} = OD_{\lambda} - OD_{\text{empty}} \quad (19)$$

$$\text{Viability [\%]} = \frac{\text{OD}_{\text{sample}} \cdot 100}{\text{OD}_{\text{control}}} \quad (20)$$

OD is the optical density determined with UV-Vis. The optical density for the investigated samples  $\text{OD}_{\text{sample}}$  is determined from the density of the blank well,  $\text{OD}_{\text{empty}}$  subtracted from the optical density measured of the sample,  $\text{OD}_{\lambda}$ , at a specific wavelength. The wavelength depends on the sample type, for the MTT assay a wavelength of 570nm will be used. To determine the cell viability in percent in respect to the control, the optical density for the investigated sample is multiplied by hundred divided by the optical density for the negative control,  $\text{OD}_{\text{control}}$ .



## 2 3D CELL-MATRIX INTERACTION

---

### 2.1 INTRODUCTION

In this chapter, I present my work that was carried out to investigate cells *in vitro* in 3D microstructured hydrogel channels. Hydrogels are highly interesting for cell investigations as they provide a close similarity to the ECM. This is due to their hydrated matrix and the straightforward process to tailor them to the appropriate stiffness. With the approach to increase the dimensionality from 2D hydrogel surfaces to 3D enclosed environments with internal interconnected architectural features, new results can be found from the 3D cell-matrix interaction. These results are achieved accordingly to the adjusted amount of the crosslinker concentration of the hydrogel used. Thus, with the hydrogel surrounding the single cell, the mechanical properties will be directly targeted towards the cell and its compartments. In this way, from the cell membrane to the nucleus and further down, all compartments will be influenced by the hydrogel mechanics due to the hierarchically structured connection within the cell as discussed before in section 1.1. [13], [147], [148] As previous studies have shown on 2D samples, the stiffness or elasticity, as well as the thickness of the sample, will influence the cell behavior as a consequence of the cells ability to transform the mechanical signal from the 2D matrix into chemical signals inside the cells (see section 1.1.3). With this mechanotransduction, the structures inside the cells are mediated and react accordingly, e.g., rearranging FAC or the cytoskeleton. [11], [25], [38], [106], [149] Nevertheless, the majority of the *in vitro* studies according to the cell-matrix interaction has been conducted with 2D matrixes. However, for extensive knowledge about the behaviour of the cells the next step is the conversion of the 2D cell-matrix interaction studies into 3D investigations. It is found that with a higher degree of cell-matrix contact, the interaction and influences towards the cells increases with the enlarged surface of the cell. [150]

The impact of this enlarged surface contact of the cell to the matrix can be seen from various cell responses towards 3D environments. Changing the dimensionality for the cellular environment will change the migration behavior from the cells, as documented when 2D and 3D migration is compared. [151] One reason of the changed migration behavior can be the change in the positioning of the nucleus. [3] For two-dimensional migration the nucleus location is known to be at the back of the moving cell. For higher dimensional migration, the nuclei are found to be at the back but also at the leading front within the cell. The nucleus at the front can be used to open small spaces between attached cells in order to migrate through. Another strategy to migrate through tight 3D constrictions with the nucleus are the rupturing of the nuclear envelope or the alteration of the ECM environment. This alteration of the ECM is achieved via proteolytic cleavage. This change of position

will involve the cell compartments around the nucleus, especially those who are involved into the cell migration e.g. such as actomyosin complexes, or the perinuclear actin caps. [3], [11], [13], [152] Other investigations comparing 3D and 2D cell behavior found that the focal adhesion clusters are not firmly located at the adhesion surface like on 2D surface but can be distributed over the cell membrane surface (Figure 1B). Still, they are active and mediate the cell's speed and deformability. [3], [23], [153] Several possibilities can be found to create a 3D enclosed environment. These are, for example, fibrous environments from collagen (Figure 2F) from a natural source without the need for biofunctionalization.

Another option is the use of synthetic materials, ideally transparent materials such as PDMS or hydrogels. The advantage of transparent samples is the option to use light microscopy imaging techniques and the potential for live cell imaging. One option is the creation of macropores inside hydrogels with various techniques. [154]–[157] Mostly, these pores are several times larger than the cells of interests and create pores in sizes of several hundreds of  $\mu\text{m}$ . These pores have a clear advantage for high throughput possibilities. The drawback of these macropores is the imaging of single cell interactions with the matrix. These type of samples lead to excessive amounts of cells. Moreover, few cells are exposed to the material, but the majority will be in contact with cell-cell interactions. [155], [156] However, other options to regulate the cell-matrix interaction in a more controllable way are channels. To date, different types of channels exist for cell-matrix interaction made from different procedures and in various sizes. An example here is a microchannel network in hydrogels such as methacrylated gelatin or poly(ethylene glycol) diacrylate. The 3D environment was produced via 3D printing with a channel diameter from  $100\mu\text{m}$  to  $1000\mu\text{m}$ . [158] However, in order to gain knowledge about processes in single cell confinements or channels with spacing small enough for just one cell are required. To date, several versions of confined (channel) environments for cellular investigations exist. These options are, for instance: Semi-3D channels, where the wall of the existing channel left and right to the cell are made from pAAm gels. From basal, the cells are attached to the glass slide, and from the top, they experience no confinement. [77] In the Lammerding lab, environments from PDMS with defined constrictions are used. [159] Also, other groups work with confined PDMS channels. [42] Straight channels with a defined length and start and endpoint are mostly used. Interestingly, most confined and structures channels used for 3D cell experiments are made from PDMS. Some of these channels are summarized in “Table 2 Selected overview of recent and actual three-dimensional experimental set-ups for cell investigation in channel” on page 58. Remarkably, the cells have contact towards the stiff PDMS and additionally towards a glass coverslip, which closes these constructs to a 3D environment while the knowledge about the impact of matrix stiffness for 2D experiments is proven. Knowing the importance of the



matrix stiffness towards the cells, challenges such as the engineering of soft, and mechanical adapted 3D environments in small sizes for single cell investigations are given.

In view of these challenges, a new 3D microstructured *in vitro* environment needed to be established. This has been done and resulted in a 3D microstructured hydrogel. This hydrogel was created with interconnected channels, as presented earlier. [45] In the following section, I show hydrogels penetrated with free, interconnected channels with different diameter and a small 'vascular like' structure where cells can migrate in and grow. Firstly, I show results from experiments in 3D microstructured hydrogels with pathogenic cells, *Acanthamoebae castellanii* (*A.castellanii*) followed by the results from the investigations of anchor dependent mammalian cells within the 3D structures in dependence of adapted hydrogel mechanics.

## 2.2 RESULTS AND DISCUSSION FOR 3D CELL-MATRIX INTERACTION

In this part of my thesis, I followed a method firstly published by us 2019 [45]. Herein, it was investigated whether pathogenic *A.castellanii* can be captured and investigated for several days, with the effect of decreased cell activity inside the microstructured hydrogels and noticeable decreased cell number in the supernatant. Both results qualify the microstructured hydrogels to be used in the future as a cell capture device. The production details of the 3D microstructured hydrogels are given below in section 2.4.2 and 2.4.3. In short: A sacrificial template from tetrapodal ZnO (t-ZnO) is prepared by pressing t-ZnO powder in a desired size and shape, and sintering the ceramic at 1150°C. Next, a polyacrylamide precursor solution is poured over the ceramic templates. After the polymerization of the hydrogel, the ceramic is removed by hydrolysis in hydrochloric acid. Later, the 3D microstructured hydrogel sample is washed until a neutral pH is reached and prepared for further cell experiments such as described on page 61 in section 2.4.3 "Preparation of 3D microstructured pAAm matrices".

Figure 6 shows the potential of the microstructured hydrogels. A-F show the interconnected structures inside the hydrogels filled with a FITC-Dextran conjugate in solution as described in section 6.5 and imaged with the spinning disc microscopy. Channels from t-ZnO can be varied in size and in packing density. Figure 6G displays the results of the decreased cell number in supernatant due to the microstructures of the hydrogels, which is invaded by the *A. castellanii*.

For further details, the reader is referred to the following publication:

S. Gutekunst, K. Siemsen, S. Huth, A. Möhring, B. Hesseler, M. Timmermann, I. Paulowicz, Y. Mishra, L. Siebert, R. Adelung, C. Selhuber-Unkel (2019): 3D Hydrogels Containing Interconnected

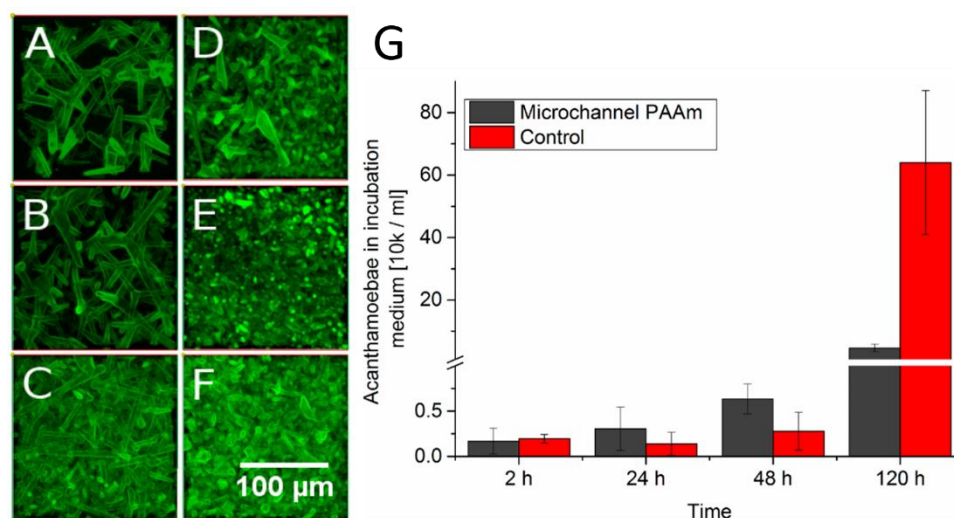


Figure 6) A-F show 3D images of fluorescently filled channels in PAAm from the z-view in a high intensity voxel representation. They present the possibility of various channel densities from the top with  $0.3 \text{ g/cm}^3$  down to  $1 \text{ g/cm}^3$  of t-ZnO as well as the option of varying the production for different sizes and forms of the arms. A-C have been produced with PVB t-ZnO and D-E with EtOH-t-ZnO. G shows the highly important fact and prospective of cell-trap for pathogenic *A. castellanii*. After 120h (5 days) the control was highly flooded with pathogenic cells in the supernatant, while the *A. castellanii* incubated with the 3D structured samples where obviously lower and accumulated inside the structure. A)-G) Reprinted with permission from *ACS Biomaterials Science & Engineering*.<sup>1</sup> [45]

As these experiments showed a high success for the caption of pathogenic cells, the next reasonable step was to implement this sample for human cell types. For this, the ideal experimental and sample requirements for human cells were established and investigated, as described in the following sections.

For further experiments with mammalian cells, several questions need to be answered:

- Does the experimental set-up require adjustments for different cell types?
- Which adjustments need to be taken?
- Can the mechanical properties of the material be adjusted, and to which range?
- Do the mechanical properties of the hydrogel influence the cellular behavior, especially towards the nucleus, and to which extent?

<sup>1</sup> <https://pubs.acs.org/doi/10.1021/acsbiomaterials.8b01009>. Further permissions related to the materials have to be directed to ACS Biomaterials Science & Engineering.

- Do occur more than the expected result of significant influence towards the nuclei diameter within the channels?
- Are the results related to both: the mechanics and the dimensionality?

### 2.2.1 Improving the 3D experimental parameter

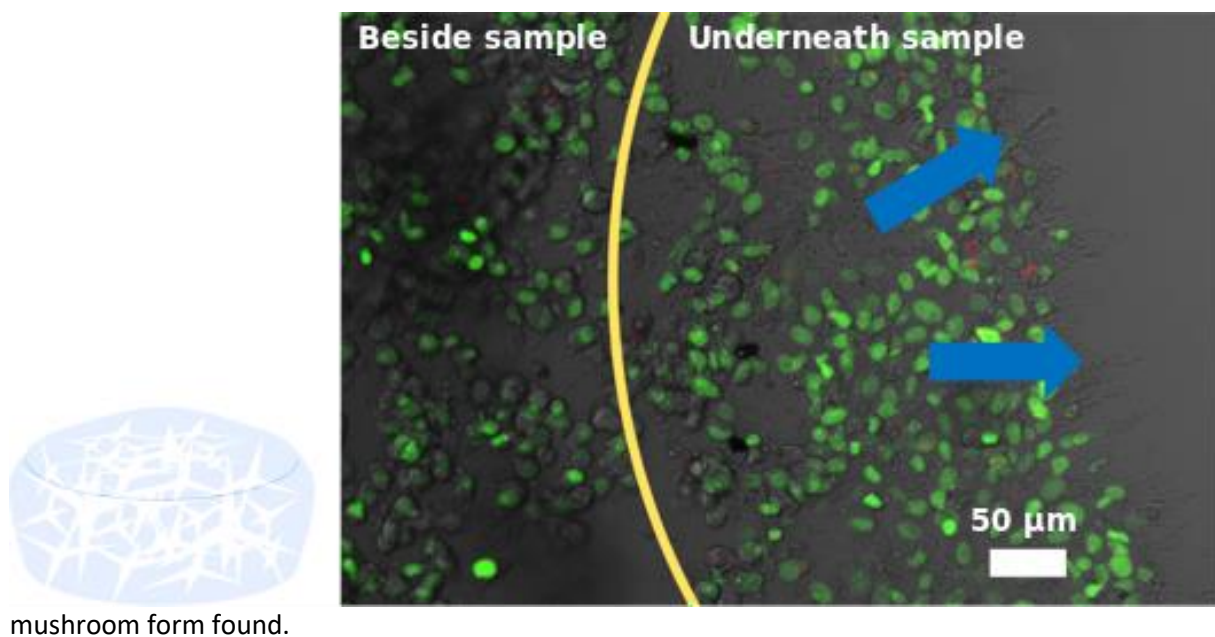
In this part of the thesis, I present the results according to the investigated cellular behavior of HT1080, fibrosarcoma cells, in hydrated 3D environments. Here, empty channels provided the structured environment to investigate whether an overall small constructed setting in combination with different mechanical properties influences this cell type. HT1080 cells, are cancer cells from the connective tissue and serve in this work as model system for soft tissue cells. They were chosen as they are a stable soft tissue cell line, highly motile, and are well established in stiff PDMS 3D environments. [160] The cells in this work were kindly provided from the Lammerding Lab and exhibit a transfected nucleus with NSL- GFP and H2B-RFP. While the first mark the rupture of the nuclear envelope, the protective lipid bilayer membrane around the nucleus with a nuclear localization sequence, the latter mark the histone proteins rich part from the nucleus, which is in the chromatin.

The first question that required to be solved was to obtain the optimal conditions for the sample preparation and fixation. This was followed by the investigation towards the most effective biofunctionalization, as well as to find the best incubation time. Additionally, at the same time, the optimal hydrogel stiffness in range from the 'soft tissues' and the optimal storage timing needed to be determined. The range for 'soft tissue' regimes such as the upper range of the brain (from 40 Pa to 20,000 Pa. [101]) to the upper range of muscles [161] includes values from 1kPa to 50kPa.

A first result was, that the 3D microstructured samples, which can be several millimeters thick for catching the *A. castellanii*, were too high. Aiming for the investigation of the cellular behavior of mammalian cells with focus to the nucleus and the three-dimensional imaging a thin 3D microstructured sample is of advantage. The benefit of thin samples is the opportunity to investigate the samples through all its depth. Due to this, the cells, their nuclei and the mechanical influence is visible in the microscope. Moreover, higher magnification is beneficial for detailed imaging of the 3D structures and the compartments of the cell within the 3D microstructured hydrogels. With this requirement and the consideration, that hydrogels and especially pAAm swells over 2000%, as shown in Gutekunst *et al.* [45], the thickness of the sacrificial template had to be adjusted as well. To enable the imaging through the whole depth of the sample, a hydrogel thickness of 2mm or less should be obtained. For this the sacrificial template thickness of 0.16mm with a diameter of 12mm and t-ZnO density of 0.9g/cm<sup>3</sup> resulted in a manageable template. Both, the height and the diameter of the sacrificial template were necessary to overcome the drawback of the light weight of t-ZnO. In this

work PVB t-ZnO were used, as it displays thin and elongated tetrapodal arms. However, other forms of t-ZnO can be used to achieve an interconnected microstructure with different forms, see above Figure 6D-F from EtOH-t-ZnO. The prepared samples were able to be stored for longer times, up to two years, with prior ozone treatment before usage as the treatment creates free binding sides on the ZnO surface.

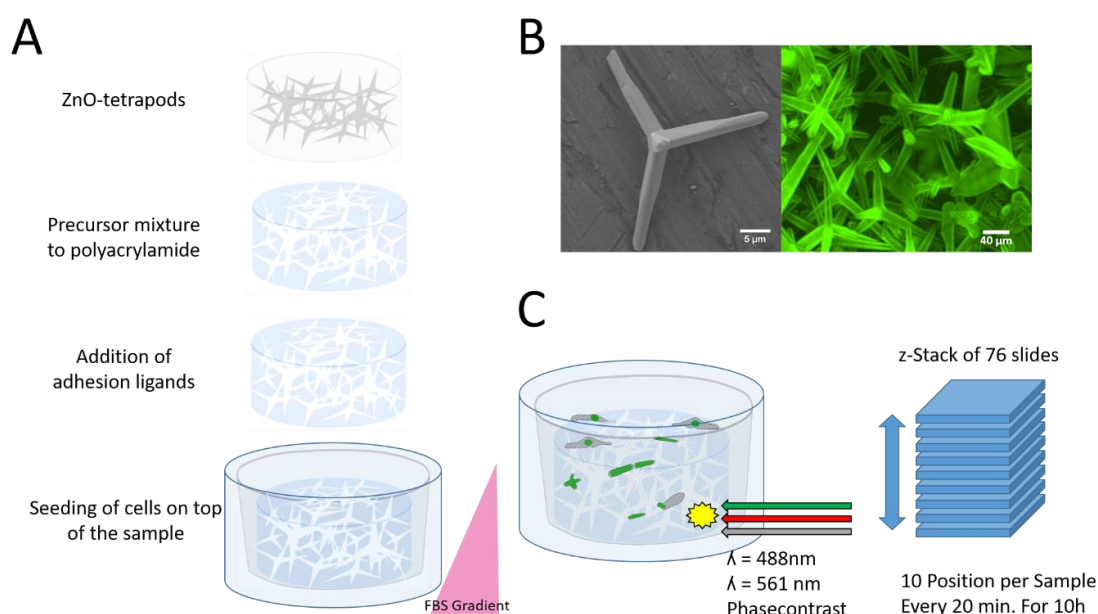
As the motility of the cells and especially the motion of the nucleus were of superior interests in this study, samples without any drift during the investigation are interesting. Imaging without drift from the samples, facilitate the later image analysis. With this consideration first experiments were conducted with microstructures samples fixated on a glass slide. For this purpose, the samples were prepared using the sacrificial templates as described in chapter 2.4.2, page 60, with the addition of a glass slide functionalized with 3-(Trimethoxysilyl)propyl methacrylate in order to form a covalent binding between a glass slide and the polymerizing hydrogel. Hence, the samples could not float around during microcopy. Interestingly, besides the improved sample fixation, a changed behavior and form of the 3D microstructured hydrogel samples was investigated because of the swelling. The fixated samples obtained a 'mushroom' form, with small covalently bound area at the glass surface and a larger convex form of the sample surface similar to Figure 7A. Figure 7A shows a sketch of the



*Figure 7 Left) A sketched microstructured pAAM sample attached to the 3-(Trimethoxysilyl)propyl methacrylate functionalized glass slide is slightly deformed. Right) HT1080 cells invade the space underneath a representative pAAM sample and glass slide despite covalent functionalization. The yellow line indicates the start of the sample. At the left side of the line, the cells are accumulated. The blue arrows indicate protrusions from the cells. Scale 50μm.*

As this present chapter is about anchor dependent cells, the hydrogels pAAm had to be biofunctionalized. It was found that here an already incorporated bio-crosslinker (BCL) is the best choice. The bio-crosslinker molecule act as mediator between the hydrogel matrix and the adhesion proteins of choice, here collagen I. Therefore, acrylic acid N-hydroxysuccimide ester (A-NHS) has been used to incorporate reactive ester groups inside the hydrogel matrix. [100] For the experiments the cells were seeded on top of the 3D microstructured hydrogel samples. However, for the on glass fixated 3D microstructured hydrogel samples cells were hardly found adhering to the convex shaped of the biofunctionalized hydrogel sample. Additionally, cells were not found within the channels. An important aspect is the probable tension within the hydrogel sample, considering the matrix shape. Interestingly, cells preferred to squeeze themselves under the hydrogel sample despite the chemical bond between hydrogel and glass slide, see Figure 7. Beyond the sample the cells form small protrusions to move forward (blue arrows). The cells are at this point on the glass surface directly beyond the hydrogel. These findings are in agreement with work according to curvotaxis, were cells avoid convex surfaces. It is also in agreement with the findings of the invasiveness from cancerous cells, which shows a preferred cancerous cell invasion into confined environments and fits the presented results. [162]–[164] According to these first results, the tension within the matrix was the probable reason for hindered cell invasion into the 3D microstructured hydrogel. With this, all further experiments were conducted with free hydrogel matrices, as sketched in Figure 8. These samples were prepared by a t-ZnO template-mediated synthesis, as mentioned above, using hydrogel matrices with three different Young's moduli. Furthermore, an improvement of the cell invasion inside the 3D microchannels was obtained by placing the hydrogel sample into a transwell with an induced gradient of FBS. Transwells are containers of various sizes with a membrane at the bottom. These transwells can be inserted into petri dishes or well-plates by hanging them on the frame or placing them directly into the well-plate. Their purpose is numerous such as indirect cell-co-cultures in the same well-plate or as migration assays through the pores of the membrane. In the present work, the membrane was from polyethylenterephthalat with 1.0  $\mu\text{m}$  pores for 24well plates. Here, the transwell was used to apply a concentration gradient of growth factors to the hydrogel matrix and the cells. As the cells were seeded on top of the collagen I biofunctionalized microstructured hydrogel sample, the majority had to migrate through the hydrogel to reach the FBS, Figure 8A. Additionally, the growth factors were probable diffused through the pores of the transwell and concentrated inside the hydrogel, and have served as another appeal towards the HT1080 cells to enter the sample. [165] The interconnected and fluorescently filled channel network within the hydrogel matrix is shown in a 3D representation in Figure 8B with one original single t-ZnO. The microstructured and fluorescently filled hydrogel matrixes and were imaged using a spinning disc laser confocal microscope preparing z-stacks. For cell imaging, z-stack and time-lapse imaging were

combined with multiple channels of fluorescence and phase-contrast, Figure 8C. The 3D representation was calculated using the maximum intensity representation and the software Xcellence. To gain knowledge about cellular behavior as close to the *in vivo* conditions, incubation times were improved. According to other work, migration, at least for 2D surfaces, is also influenced by the incubation time. [166] Additionally, the relaxation of the stress inside hydrogel matrices in general influences the cell behavior on 2D hydrogels. It has been investigated that a decreased level of stress within hydrogels results in an increased cell spreading. [167] With this, an enhanced time of incubation will lead to a possible reduction of stress inside the sample due to swelling of the hydrogel



mesh to its equilibrium point, as explained earlier in chapter 1.5.3 (see also Figure 10B).

*Figure 8) Experimental set-up for the preparation of the 3D experiments. A) Preparation of the samples via sacrificial template synthesis, biofunctionalization, and the seeding and cultivation of cells in 3D. B) exemplary images; left: a t-ZnO; right: the hollow channel inside the hydrogel, filled with fluorescent dextran (green) and imaged with the confocal microscope, showing a high-intensity voxel representation. C) Experimental set-up for the imaging process. B) Left image reprinted with permission from ACS Biomaterials Science & Engineering.<sup>2</sup> [45]*

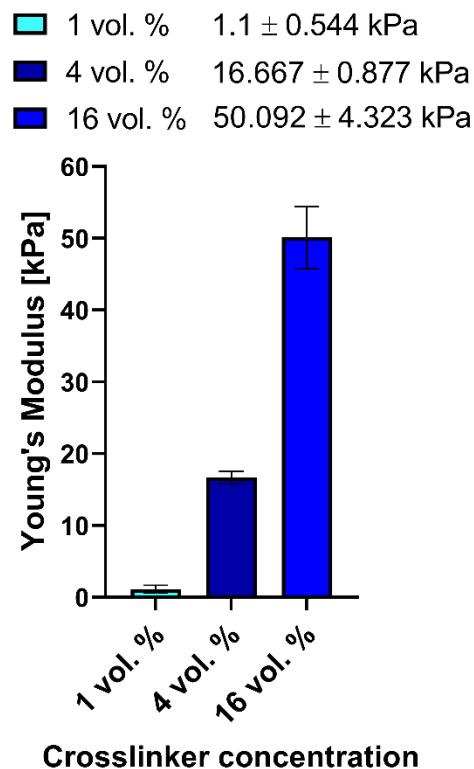
With repeated cell tests with different experimental settings, the cell incubation time was set to five days to reduce possible tension within the samples and provide the required times for the cell invasion. Providing comparable imaging settings to other three-dimensional experiments such as in

<sup>2</sup> <https://pubs.acs.org/doi/10.1021/acsbiomaterials.8b01009>. Further permissions related to the materials have to be directed to ACS Biomaterials Science & Engineering.

the Lammerding Lab, the cell incubation was followed with 10h of microscopy with light exposure every 20 minutes, Figure 8C.

The chosen range of mechanical values of 'soft tissue' from 1kPa to 50kPa within the hydrogel matrices was adjusted with the volumetric crosslinker concentration within the precursor solution.

Three different mechanical values with the respective crosslinker concentration, bisacrylamide, of 1vol.%, 4vol.%<sup>3</sup>, and 16vol.% have been chosen. The mean values of the hydrogels Young's modulus 1.1 kPa  $\pm$ 0.54kPa, 16.67 kPa  $\pm$ 0.88 kPa, and 50.09 kPa  $\pm$ 4.32kPa, further referred to as 1kPa, 17kPa



and 50kPa, were investigated with a homebuilt indenter<sup>4</sup> using the Hertz-model, see Figure 9.

Figure 9 Indentations data from the crosslinker concentration used in vol.% in pAAm samples and their respective Young's moduli.

At last, two different investigations were conducted. Firstly, the influence of the mechanical properties of the hydrogels towards the channel size within the 3D structured hydrogel matrices were investigated. This was because the focus of these investigations is towards the mechanical

<sup>3</sup> Similar volumetric crosslinker concentration as used in the investigation of *A.castellanii* in 3D environments [45]

<sup>4</sup> Described in our the work '3D Hydrogels Containing Interconnected Microchannels of Subcellular Size for Capturing Human Pathogenic *Acanthamoeba Castellanii*' ,[45]

influence of the 3D structures hydrogels on the cells. As the free channels inside the microstructured hydrogels represent the inverse t-ZnO, where the range of the tetrapod sizes is determined [45], the swelling behavior of the hydrogels with different vol.% of the crosslinker and the impact towards the channel sizes were investigated. To reveal the interconnected structures within the hydrogels, the channels were fluorescently filled and imaged. The imaging of the fluorescently filled channels were carry out by spinning disc confocal microscopy, directly after one night of infiltration with fluorescence solution. For the analysis of the channel sizes a 3D representation was calculated and the channels were measured. The channels were measured in their diameter at the tip and the base, which represents the smallest and the widest diameter of the channels. Notably, for cell experiments within confined 3D structures, the channel sizes will influence the ability of cells to enter the channels in view of the nucleus diameter as stiffest cell compartment. As shown in Figure 10A, with increasing crosslinker volume, the diameter for channel tip and channel base decrease slightly, with all mean values below 5 $\mu$ m in diameter, which is below the cell diameter found for *A. castellanii*. [45] The infiltration of the fluorescence solution into the channels is described in the appendix in section 6.5 page XII.

At last, the long-time storage of hydrogels in solution was studied for two different volumetric crosslinker concentration, 4vol.% and 16vol.%. This aims to access the ideal time point of usage for hydrogel matrices and the equilibrium swelling to reduce tension within the hydrogel samples. For this, samples were stored over time in the fridge at 4°C in water. Figure 10 on page 41 shows the influence of the volumetric crosslinker concentration towards the channel sizes and the connected loss of Young's moduli by hydrogel swelling over time within. From initial over 110kPa after one week of storage for 16vol.% and 70kPa for 4vol.% crosslinker, after two weeks of storage, the Young's modulus obtained was in the range from 50kPa and 16kPa with a slow decline towards the stored time of 28 weeks. This relaxation and swelling of the pAAm needed to be considered for all cell experiments with the result that all samples were ready to be used after two weeks in solution, when stored on a fridge at 4°C.

With this information gathered, the questions about the optimal sample preparation were answered:

- Microstructures hydrogel matrixes should not be attached covalently to a glass surface to prevent tension within the hydrogel samples
- The channel size within the microstructured hydrogel matrixes depends slightly on the crosslinker concentration
- The hydrogel matrixes have to be stored for two weeks at 4°C to reach with swelling a stable Young's modulus



- Optimum incubation and experimental time are: five days of incubation followed with 10h of microscopy with light exposure every 20 minutes

The whole experimental setup and preparation are shown in Figure 8, page 38.

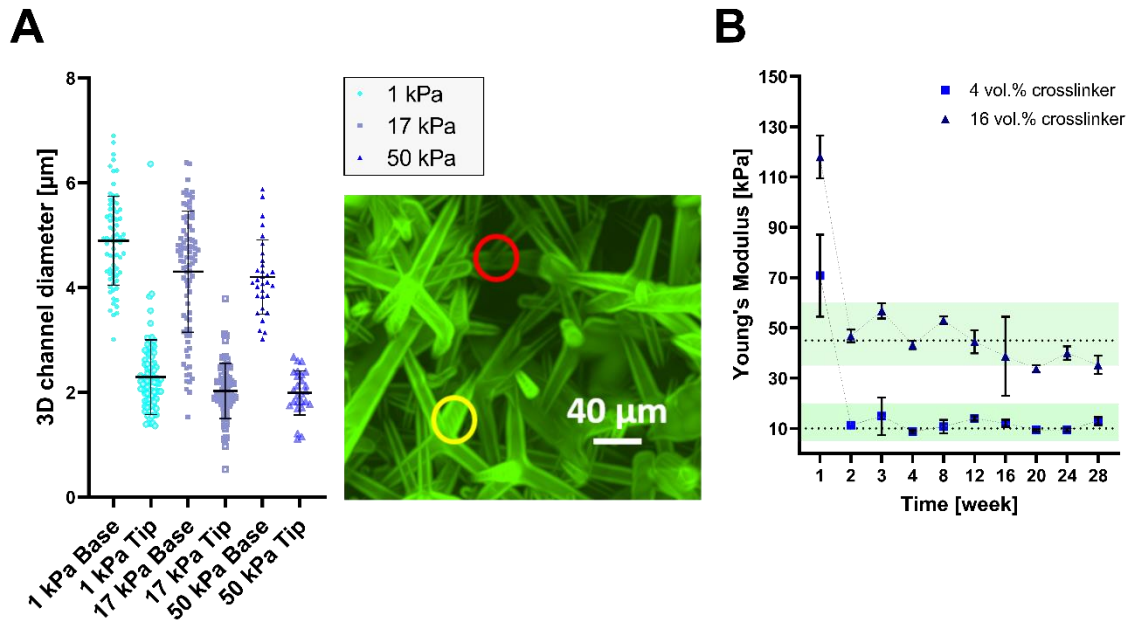


Figure 10 A) Results of the measured diameter of the 3D channel in polyacrylamide. The channels were filled with a fluorescent dextran solution, imaged via confocal microscopy, and a 3D representation image has been calculated from the confocal image. The samples with the channels were dried via an ethanol series and immersed overnight in a fluorescent dextran solution at 4°C. The channel diameters have been measured according to the exemplary three-dimensional voxel image in A. The green channels were measured at the beginning (base, yellow circle) and the end (tip, red circle). The conical form of the channel represents the former structure of the tetrapod. Each dot within the graph represents one channel. B) The graph shows the loss of Young's Moduli over time of polyacrylamide samples with 4 vol.% and 16 vol.% crosslinker concentration stored up to 28 weeks in the water at 4°C. For each measurement, individual samples were prepared and measured three times. The connected dotted lines were included to facilitate the identification of identical crosslinker concentrations.

### 2.2.2 3D cell-matrix interaction with mammalian cells

With the intention to examine cellular behavior in mechanically different 3D microstructured hydrogels, the experiments have been adapted as described above, and the cell culture was done as presented in the method section (see 2.4 on page 59).

The initial questions for the cell experiments were:

- Do different mechanical properties of the hydrogel have an influence towards the cellular behavior, especially towards the nucleus, and to which extent?
- Do more than the expected result occur of significant influence towards the nuclei diameter within the channels?
- Are the results related to both: the mechanics and the dimensionality?

In order to answer these questions, I investigated the acquired data for the following topics:

- The influence of the mechanical properties on the stability of the nuclear envelope
- The cell location inside the 3D sample
- The distribution of the nuclei located within the cell membrane during migration
- The distribution of the nuclei diameter in 2D and 3D
- The speed of the nucleus between image sequences and relation to cell motility

At this point, I want to define the terms motion and migration used in this investigation. Migration refers to the overall movement of the whole cell, including the cell membrane. The term motion used here applies only to the cell nuclei, more specific to the position of the center of the nucleus from one image sequence to the next. Another term I want to clarify is cell diameter: The 3D diameter of the nucleus is the average of the minor axes manually measured, from at least three positions. The nuclei diameter in 2D is measured over the minor Feret diameter. The Feret diameter is the best fit diameter of an object between two parallel planes. Here, the minor axis, the minimum diameter was analyzed automatically using ImageJ. [168]

Earlier, Figure 9 on page 39, the three mechanically differently hydrogels in this part of the work were introduced with the respective volumetric crosslinker concentration 1vol.%, 4vol.%<sup>5</sup> and 16vol.%, further referred to 1kPa, 17kPa and 50kPa. These are the 3D microstructured hydrogel matrices for the subsequent cell investigation using HT1080 cells with a fluorescently transfected nucleus. The nucleus displays two different transfected parts, the nuclear localization sequence

---

<sup>5</sup> Similar volumetric crosslinker concentration as used in the investigation of *A.castellanii* in 3D environments [45]

which will indicate the rupture of the nuclear envelope membrane around the nucleus formed from a lipid bilayer in green (NLS-GFP), and the histone rich part of the chromatin in red (H2B-RFP). The nuclear envelope is of high interest, as it acts as ‘mechanical’ damper to protect the DNA inside the nucleus from destroying mechanical influences. [169] This is crucial, as the nucleus is the stiffest and largest cell compartment inside the cell membrane, storing the DNA. With this, it is by far the limiting parameter for migration in confined environments. This is similar to the *in vivo* environments. [43], [170] Moreover, as the cell-matrix interaction studies are now shifted strongly to experiments in synthetically produced confined 3D environments such as established from the Lammerding group [43], the nucleus is the point to study. [11] However, most of the established constrictions such as labyrinths or channels [42] are made of polydimethylsiloxane (PDMS) in a range much stiffer and not hydrated and with restricted nutrition access. Important in the studies in PDMS environments is the nucleus, its stability, and the stability of the nuclear envelope. The nuclear envelope will take the mechanical impact towards the nucleus and can rupture to decrease the mechanical stress. This is done, e.g., while migrating through small confinements. The rupture of the nuclear envelope is observable with a microscope for fluorescent transfected nuclei. Then the content of the nuclear envelope is released into close proximity of the cell. Similarly, the nuclear envelope can be repaired after passing the constriction, as shown from Denais et al (2016). [160] When the nuclear envelope is repaired, the substance from the nuclear envelope is retrieved and the envelope is resealed. However, the rupture of the nuclear envelope has a damaging impact on the DNA. [159] When such constrictions, in particular channels, are designed within hydrogels, most groups have at least one surface made from glass presented towards the cell. With this, the presented microstructured samples, entirely made from hydrogel, are up to now the most potent choice to investigate the mechanical force from soft tissue towards the nucleus. In particular, it is highly interesting validating the hydrogel channel impact within the range of ‘soft tissue’ towards the nuclear envelope and its stability. Figure 11 on page 44 shows an example of cells migrating through the hydrogel channels over time with the nucleus at the rear, red arrow. It is clearly evident, that the nuclear envelope is striped and ruptured from the nucleus while moving inside the channel, see image D. Figure 11E and F show the position after 0h and 10h of imaging in a high intensity voxel representation. With the nuclear envelope stripped from the nucleus inside the 3D microstructured hydrogels, it shows the importance of the material topography and architecture. This can be the topography for 2D surfaces or architectural conditions in 3D. For this work, samples were analyzed according to the ruptured nuclear envelope for each independent experiment and hydrogel stiffness.

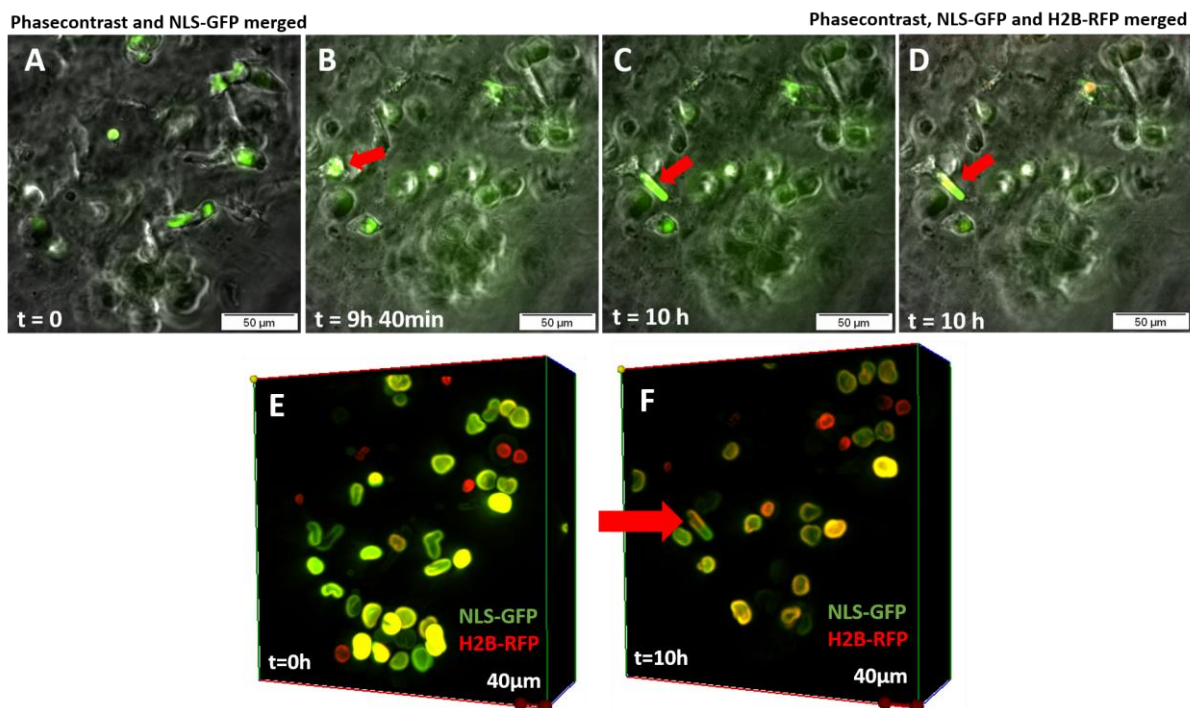


Figure 11 Time-lapse images of a position in a z-stack in a 3D microstructured sample of 1kPa over 10h. Phase contrast in grey, 488nm in green shows the NLS-GFP, and 561 in red shows the H2B-RFP of the cell nuclei. In A), the position is shown at t=0h; In B) and C), the same position and z-slide are shown at 9h:40min and 10h. The red arrow points to a cell that protrudes its cell nuclei at the front in another new channel. In D) all merged channels are shown. It is visible that NLS-GFP and the H2B-RFP do not overlay each other but that the nuclear envelope is sheared from the rest of the nucleus as the nuclear envelope is ruptured. E) Three-dimensional high intensity voxel representation at 0h of imaging F) Three-dimensional high intensity voxel representation at t= 10h of imaging. The red arrow indicates the visible separation of the nuclear localization sequences NLS-GFP from the histones in the chromatin rich part of the nucleus H2B-RFP. Scale bar A-D, 50 $\mu$ m ; E-F, 40 $\mu$ m

The data about the nuclear envelope rupture in dependence of the hydrogel stiffness and the experimental set-up shown in Figure 8, is shown in Figure 12. For the present experimental set-up, it was found that for all mechanical properties, nuclear envelope rupture events take place with a distinct difference from the soft environment (1kPa, 17.75%  $\pm$ 3.91%) towards the stiff environments (17kPa, 59.71%  $\pm$ 11.22% and 50kPa, 41.41%  $\pm$ 18.47%) appears. The influence of the stiffness to the rupture events of the nuclear envelope (Figure 12) is significant ( $p=0.0171$ ) between the 1kPa and the 17kPa hydrogels. The findings of the nuclear envelope rupture are in clear agreement with previous findings in constrictions from a few  $\mu$ m made from PDMS pods [6], [43], [159], [171] but were not often reported in PDMS channels. [42][160]

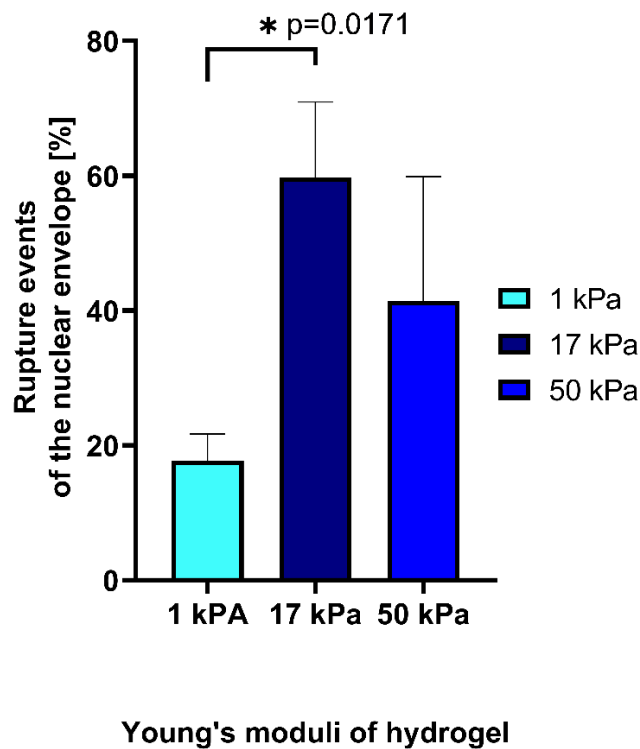
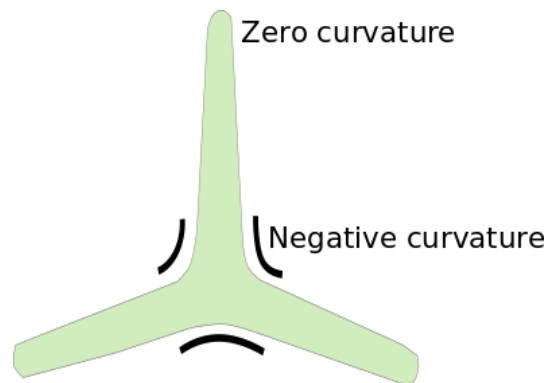


Figure 12 Rupture events of the nuclear envelope in [%] according to the surrounding material stiffness of 1kPa, 17kPa, and 50kPa. The findings are significant for the soft hydrogel towards the stiff



hydrogel.

Figure 13 shows the sketch of a green fluorescently filled channel. The uniaxial channels are connected at the base forming a negative curvature. The curvatures of the single channels are zero due to their uniaxial appearance.

As sketched in Figure 13 and also before in Figure 8B on page 38, the microstructures consist of the inverse structure if the t-ZnO. The channels are uniaxial and interconnected at the base from the channel or at the tip part from the channel. Both, the channels and the cavities inside the hydrogels show curvatures, which is the degree of change within a curve at a surface. The degree of change can be described as Gaussian curvature with zero, negative or positive curvatures, which indicates no

curvature at all, a concave and a convex surface. All three mentioned cases of curvature are present in biological systems, e.g., blood vessels. Figure 13 presents the curvatures existent within the 3D microstructured hydrogels due to the channels. The positions inside the microstructured hydrogel, such as the channels and cavities, have different curvatures, which can have an impact on cellular behavior. Experiments on 2D surfaces from other groups have demonstrated that cells experience, sense, and react to concave and convex forms known as curvotaxis. [172]–[175] The curvotaxis in this work is triggered by the location within the microstructured hydrogels.

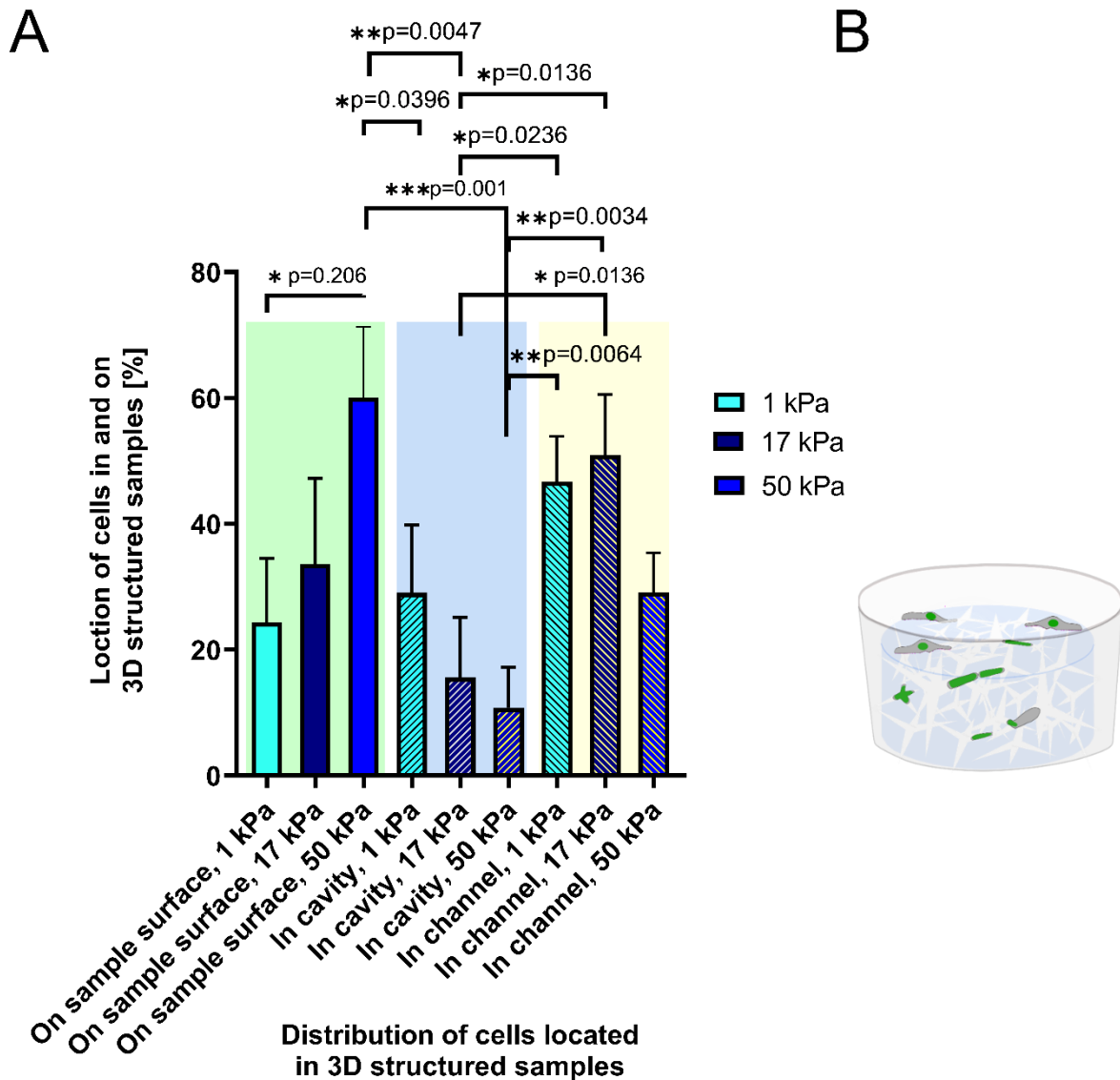


Figure 14 A) The location of the cells in [%] to the sample surface (On sample surface), the sample cavities (In cavity), and the sample channel (In channel) are shown according to the sample stiffness of 1kPa, 17kPa, and 50kPa. The graph shows the mean and standard deviation. B) The sketch depicts the potential locations of cells inside the 3D channels

In addition and to quantify the recorded data, the location of the cells given by the stiffness of the materials has been analyzed. Three locations were compared and defined as: Adherent cells on top of the sample, cells inside the sample cavities with negative curvature, and cells inside the channels with zero, Figure 14. In Figure 14A, the distribution of the cells located in and on the 3D structured hydrogel samples in percentage towards the the Young's moduli are shown. An exemplary sketch of the potential location of the cells is depicted in Figure 14B. For the location on the sample surface, it was found that for stiff samples, the difference in cells located percentage to soft samples is clearly higher ( $p=0.206$ ) for 50kPa hydrogels ( $60.07\% \pm 11.22\%$ ) compared to hydrogels with the lowest stiffness (1kPa,  $24.28\% \pm 10.25\%$ ). When comparing the cavities, a higher percentage of cells were located inside the cavities of soft samples (1kPa,  $29.06\% \pm 10.73\%$ ) then in stiff samples (50kPa,  $10.78\% \pm 6.42\%$ ). For the cellular appearance inside the channels, the percentage of total cells is in a similar range from 1kPa as well as for 17kPa hydrogels (around 50%) but was decreased for stiff hydrogels (50kPa,  $29.14\% \pm 6.23\%$ ). Interestingly, it appears that HT1080 preferably were inside channels with zero curvature, and less inside cavities with negative curvature. This preference of zero curvature is highly visible for the 17kPa channels towards the 17kPa cavities ( $p=0.0136$ ) and the 50kPa cavities ( $p=0.0034$ ). Also, the preference of cell location in channels from 1kPa than in cavities from 50kPa hydrogels is evident high ( $p=0.0064$ ), Figure 14A. The percentage of cells is for both curvatures, zero in channels and negative in cavities, were higher with the 1kPa and 17kPa hydrogels inside channels and cavities than for the stiffest hydrogel with 50kPa. The cell avoidance of 50kPa cavities is evidently shown in Figure 14A (significance  $p=0.001$ ) with a cell percentage in cavities of  $10.78\% \pm 6.42\%$  and cell percentage on the hydrogel surface of  $60.07\% \pm 11.22\%$ . The zero curvature inside channels is more favorable for the cells as the negative curvature of the cavities. The cells inside the 1kPa hydrogels appear not to mind cavities at all, see Figure 14A. Comparing the results to previous work about convexity and concavity structured surfaces on 2D samples, this behavior is in agreement with the general avoidance of concave surroundings with larger diameter and the preference of zero curvature. One explanation for this cellular behavior can be the associated bending of the stress fibers within the cells while residing in positive or negative curvatures. Residing in a location without any curvature reduces the interface area and hence minimized the energy, which is preferable. [174]–[178] Additionally, it appears that the durotactic and architectural cues such as the curvature result in different outcomes for the presented cases mechanical properties of the experiments in this work. With increasing stiffness the importance of the architectures and curvature rose.

For stiff hydrogels, the cells in this work prefer the zero curvature channels over the cavities but mostly adhere to the surface. For softer hydrogels, 1kPa, and 17kPa, the different location and their curvature are less challenging. Interestingly, it has been found elsewhere that the surrounding

curvature influences the lamin levels. In practice: the lamin A level increases with a convex structure and influences the stiffness of the nucleus or the nuclear envelope. [172] [43] This is in agreement with the findings of cancerous cells that are more likely to adhere to surfaces with concave curvature. [179] Hence, these data support the close connection between durotaxis and curvotaxis and my findings from Figure 12. The excitant curvature in connection with the hydrogel stiffness could have influenced the stability of the nuclear envelope by triggering the lamin levels. Additionally, curvotaxis and the stiffness decrease the number of invading cells into the stiff 50kPa hydrogel. In opposite to this, cells invade the channels with both lower Young's moduli and the curvatures act on nuclear stability. With Figure 12A, it shows, that the influence of the curvature is more potent with a higher Young's moduli. Hence, the nuclei rupture events between the 1kPa and the 17kPa were significantly different ( $p=0.0171$ ).

When speaking of positioning, the nucleus inside the cell is always an important part not just for mechanosensing but also as a stiff obstacle that needs to be aligned or squeezed for migration or used as a piston for transendothelial migration. [3] Because of these findings, cell migration was investigated with a view towards the nuclear positioning inside the cell during migration. Importantly it needs to be considered that because of the channel structure, the migration of cells is limited in direction, and options to rearrange the nucleus are rare. [180] Figure 15A shows a sketch of the nuclear position during cell migration, in D are the results depicted.

Interestingly, for all material stiffness, the nucleus was mainly positioned at the center of the cell. For other positions, a preference as a function of stiffness was not found. The findings for the positioned nuclei at the center or the back are clearly different for 1kPa hydrogels, with  $p=0.0201$ .

For 50kPa hydrogels, the findings for the front and the center are clear, see Figure 15A and B.

The question to be answered for these results is now:

-Why is the positioning of the nucleus within a 3D environment of importance?

As described earlier in 1.1, the positioning of the nucleus is essential as it provides the functions of the cell, such as proliferation or migration. It has been reported that different localization positions have been observed in the dependence of the involved cell compartments. Dupin et al. [22] reported an intermediate filament dependent nucleus positioning, which pushes the nucleus towards the back of the cells. There, the level of lamin, despite lamin A, influences the position as the lamin level increase or decrease the stiffness of the nuclear envelope. This is supported by other reports and reviews about cellular migration, where the nucleus is located behind the centromere. [41], [180], [181] However, others reported the nucleus positioned in the front due to topographically, dimensional features, or even *in vivo* due to a changed centromere position behind the nucleus. In these cases, the microtubule actively positioned the centromere behind the nucleus caused by their



connections via dyneins. [3], [41] These findings explain the positioning of the cells for the front and the back. Petrie *et al.* found a positioning of the cell nucleus in the center due to the formation of a piston. This piston is meant to be at the leading front of the cell with a “compartmentalized pressure” (Petrie 2017, page 98) and facilitate the migration. [37] In summary, the mentioned localization options of the nuclei in this work seem to appear in all cases.

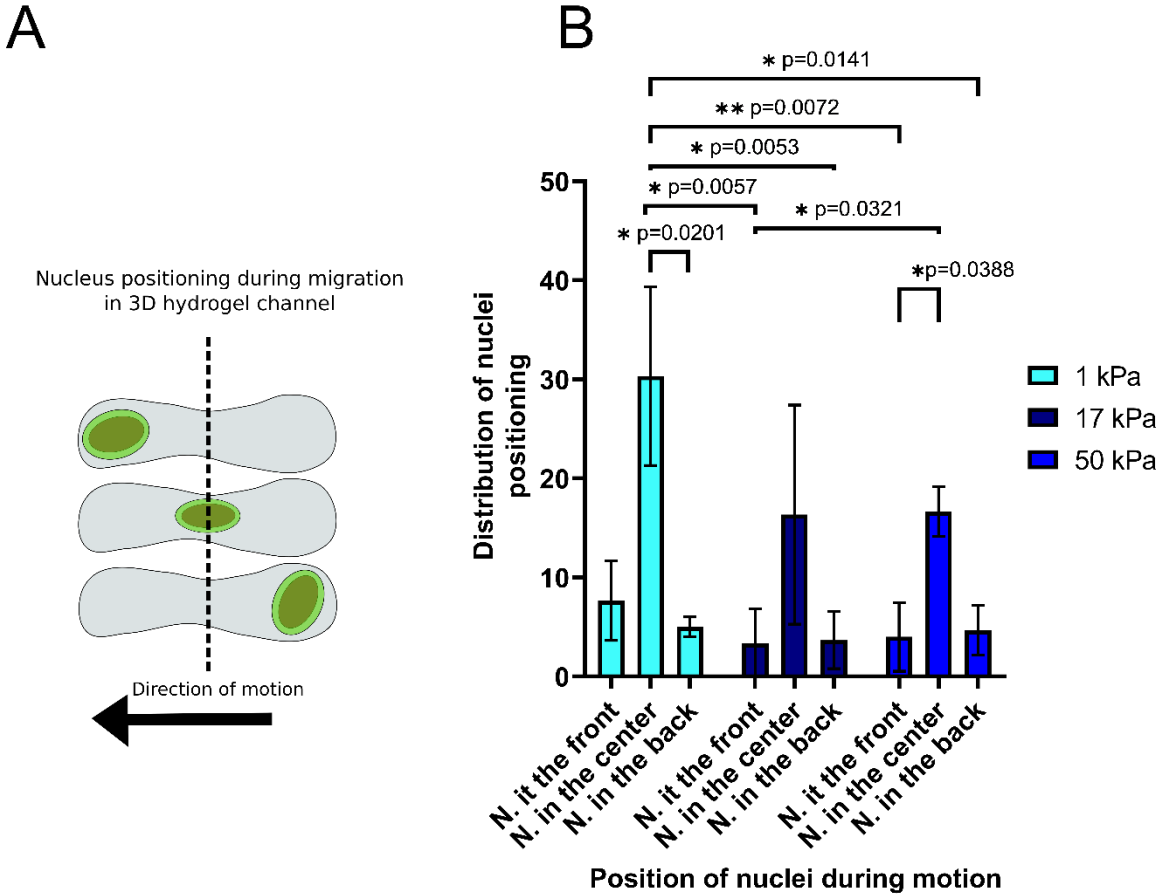


Figure 15 A) Sketch of the nuclei position during migration in comparison to the hydrogel stiffness. A line has been applied to the cell center, and the nucleus was investigated whether it was in the front, in the center, or the back of the cell. D)The graph shows the mean and standard deviation. The significances were determined via the Kruskal Wallis test, means of the averages and standard deviation are shown.

As shown in the data plotted in the figures earlier, the 3D environment, as well as the matrices stiffness, mediates the cellular behavior with respect to nuclear envelope stability and the localization of cell and nucleus during the investigations. Besides these results, the smallest diameter of the nuclei, the minor axis, which can be achieved as a function of the mechanical properties and the diameter of the hydrogel channels is investigated. With the overall confinement around the cells due to the channel structure, the mechanical properties of the matrix can be sensed by the cell and the nucleus. For each nucleus, its diameter, or minor axis, has been determined at three different

time points at 0h, 5h, and 10h of the imaging. The results are shown in Figure 16 on page 51. In Figure 16A, the averaged means for all three experiments of each crosslinker concentration respective of each stiffness are shown for the analyzed images sequences. The distribution of the nuclei diameter after ten hours for all three hydrogel stiffness showed similar and comparable means with a diameter at around  $8\mu\text{m}$  with a deviation from around  $3\mu\text{m}$ . This is contradictory to what was expected due to the result of other studies. There, channel confinements from PDMS as small as  $3.7\mu\text{m} \times 1.7\mu\text{m}$  have been migrated through from cells. [182] To gain a more in-depth insight into the impact of the sole matrix mechanics, the nuclei diameters were analyzed of the control cells. These cells were seeded on top of the unstructured 2D pAAm samples from the same stiffness and treatment. Also, here, a direct impact of the stiffness on the nuclei diameters were not visible, as the distribution and the mean for all experiments are comparable, Figure 16B.

Visualized in Figure 16B (left), the data of the 3D experiments as well of the 2D controls were compared in box-plots as a function of the dimensionality. Here, a significance  $p < 0.0001$  appeared. The data distribution of all minor axis shows the averaged means with  $8.10\mu\text{m} \pm 1.69\mu\text{m}$  for 3D nuclei and  $12.39\mu\text{m} \pm 2.17\mu\text{m}$  in minor axis for 2D nuclei. While the data point distribution for the diameter in their means is comparable, the form of the distribution is slightly different. It is clearly visible that the majority of the minor axis length for 1kPa samples are above the  $8.10\mu\text{m}$  mean value, and for 17kPa and 50kPa, the majority is somewhat below the  $8.10\mu\text{m}$  diameter. These results could be explained by the slight influence of the crosslinker concentration towards the channel diameter, as depicted in Figure 10 on page 41. The crosslinker concentration influences the swelling behavior of the hydrogels, and with this, the channel sized present in the hydrogels. For the diameter of the cell on top of the hydrogel sample, the distribution is similar for 1kPa and 17kPa hydrogels and slightly lower for the 50kPa. However, since no clear trend is visible, a conclusion about these averaged mean values would be more speculative. The data presented in Figure 16B (right) all data points for the single material properties for the 3D experiments as well as for the 2D controls.

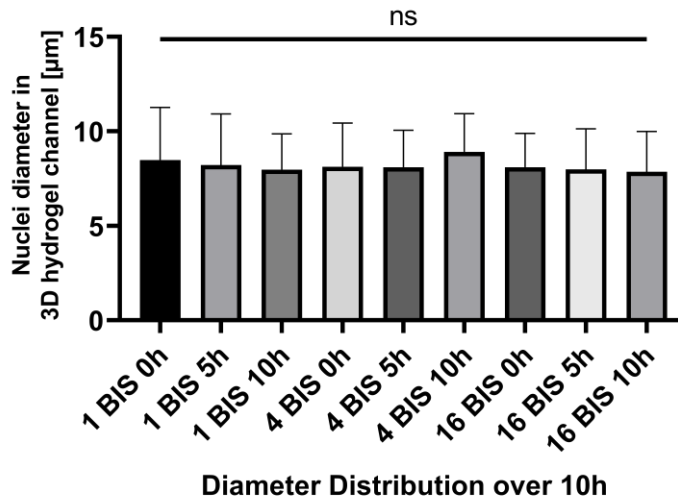
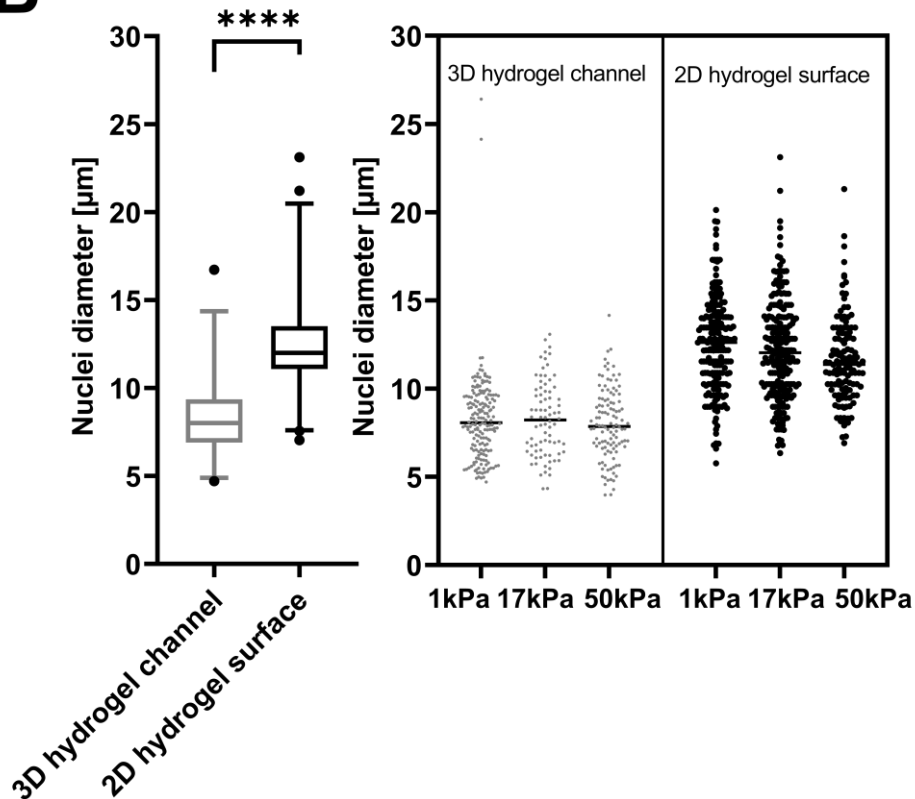
**A****B**

Figure 16 Comparison of the nuclei diameter in 3D channels as well as on 2D hydrogel surfaces. A) No significances can be found for the diameter of the nuclei in 3D channels for three different time points B) Left: The data of all diameter of the cells in 3D at around 8µm and on 2D with around 12µm are compared. The data were analyzed with the Kruskal Wallis test. Right: All data points for the individual matrix stiffness are shown for the 3D hydrogel channel as well as for the 2D hydrogel surfaces.

It is shown in Figure 16 that the data distribution of the nuclei diameter, its minor axis, is not very different. Moreover, the strong impact towards the cell nucleus diameter is from the differences in dimensionality rather than the Young's modulus. On biofunctionalized 2D surfaces, cells can spread much more while adhering to the hydrogel surface. Though the results mentioned above indicated less success in further data analysis, the nuclei were analyzed over time, and the change of the individual nuclei diameter from one-time point to the other, delta t, see on page 52 Figure 17.

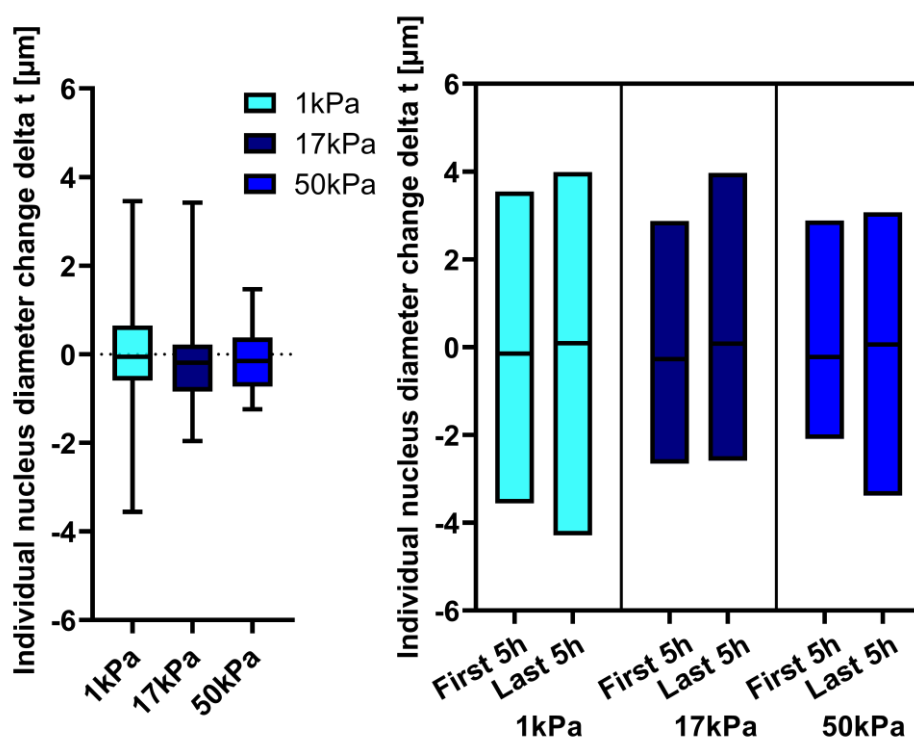


Figure 17 Distribution of the nucleus diameter changes from one time point towards the other, delta t, as a function of the matrix stiffness. The distribution includes the increase and decrease of the diameter as well. Left: Box plots show distribution with mean and the standard deviation. The change within the nuclei is dynamic and decreases with the increase of the crosslinker concentration. Right) Floating boxes show the mean and the standard deviation for the first five hours(left) and the last five hours(right). For all matrices, the change in diameter of the nuclei is larger for the last five hours of the experiment.

On the left side of Figure 17, the averaged means of the changes within the individual diameter between the image sequences are shown as a function of the material stiffness. There, it is visible that the variation within the changes of the diameters minor axis decrease with the increase of the stiffness of the materials. The same figure shows on the right side, the data distribution as a floating box distinguished between the first and the last five hours of the experiment. There, the distribution of the minor axis change in length is larger. The evolving question here is:

-Why is a change within the individual nuclei minor axis occurring?

The change in the minor axis of the cell nuclei can occur for several reasons. Firstly, it is reported that stress is applied to the nucleus, and thus, to the chromatin can lead to chromatin swelling. [41], [183] Moreover, some cells have been reported to increase and decrease the minor axis of the nucleus with tension and compression. [184] This is in agreement with the findings that even in 3D confinements, the actomyosin filaments and other compartments of the cell expose the nucleus to tension and compression during migration in 3D confinements. [185] For the right side of Figure 17, a similar trend is shown for the first five hours and the last five hours. The change of the individual nuclei diameter for the last five hours is slightly larger than for the first five hours. These data for the last hours of imaging support the hypothesis that the chromatin on the nuclei is swelling due to the stress, increasing the nuclei diameter in its minor axis. In Figure 10 on page 41, the distribution of the channel diameter within the hydrogels according to the stiffness and crosslinker concentration is presented and shows larger diameter for the channel in base and tip in 1kPa hydrogels. Due to the lower volumetric amount of the crosslinker, the swelling is larger in 1kPa hydrogels when the equilibrium swelling of the polymeric mesh is achieved. With the swelling and the stiffness of 1kPa, the swelling of the nuclei and its variation can become probably larger as less resistance from the hydrogel matrices is applied. The nuclei investigated are not static in one location but also move within the cell's membrane. This migration, or more precisely, the motion of nuclei in general within the confined cells and the motion speed of the nuclei in between the single image sequences, has been investigated. Firstly, it has been found that within the 3D microstructures the nuclei motion for all hydrogel stiffness occurs over 75%. The highest nuclei motion, the movement of the nuclei within the cell, has been found in 3D microstructured hydrogels with a Young's moduli of 50kPa of 90%, see Figure 18.

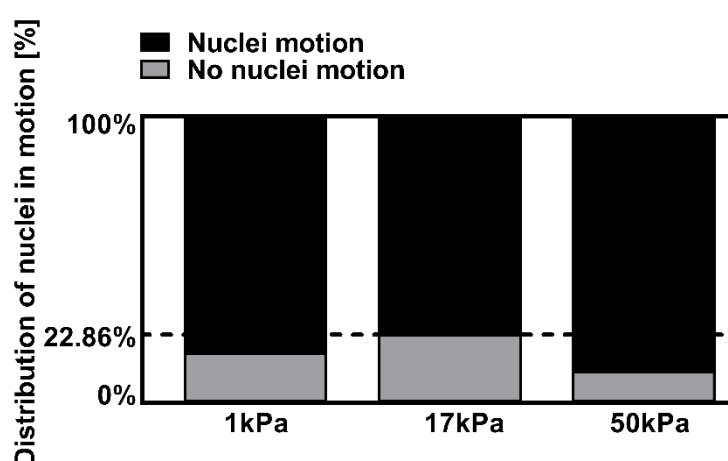


Figure 18 Distribution of nuclei motion inside 3D microstructured hydrogels for all hydrogel matrix stiffness in percent for the different matrix stiffness. The highest fraction of nuclei motion is found for cells in 50kPa hydrogels. The fraction of nuclei motion is found for 17kPa hydrogels.

Connected with the occurrence of nuclei motion is the motion speed of the single nuclei within the cells inside the 3D microstructured hydrogels. For this investigation, the single nuclei were manually tracked, and the shift of the nucleus center was detected. The data in Figure 19 show the average speed of the nuclei in between the image sequences according to the Young's moduli of the hydrogel on the left side. At the right, the nuclei speed distribution for the individual experiments is shown. Clearly, the speed of the nuclei is below 8nm/sec. A significant difference,  $p=0.0043$ , and  $p=0.0037$ , has been found between the overall mean speed between both softer hydrogels with 1kPa, 17kPa towards the 50kPa matrices. The mean of the average speed of the nuclei motion has around 1.2nm/sec and 1.5nm/sec. The speed is prolonged in comparison to experiments within this type of 3D samples conducted with pathogenic *A. castellanii* and without biofunctionalization. The pathogenic cells obtained a speed of 50-340nm/s in samples with 16vol.% crosslinker during the experiments. [45] However, considering the confinement around the single cells and the nuclear envelope rupture events (Figure 12), the speed of the nuclei motion might be reduced in order to limit the stress towards the envelope.

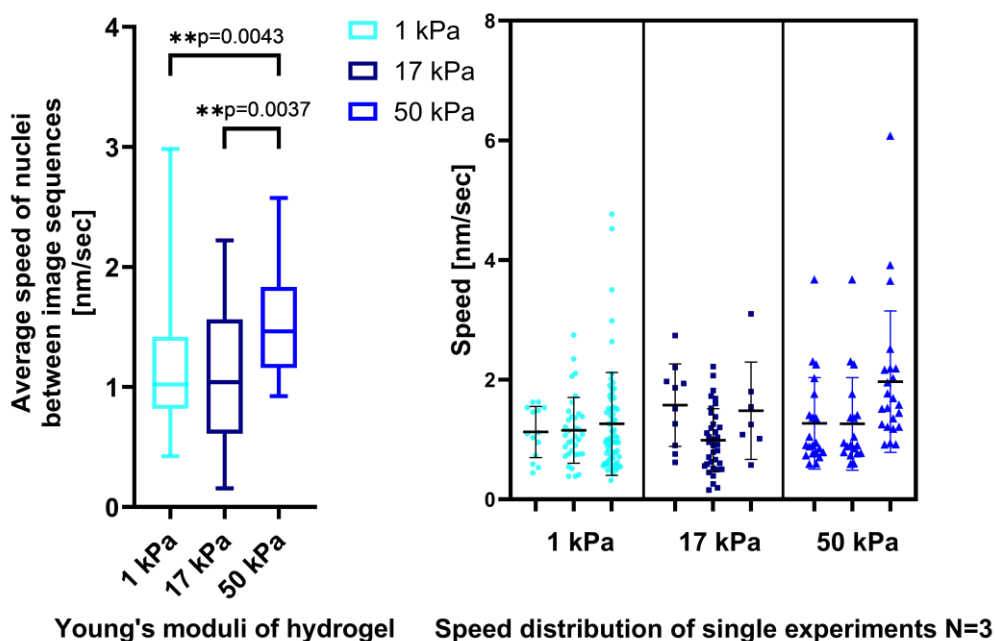


Figure 19 The distribution of the speed of the nuclei motion between the different material stiffness is shown. Left: The average speed of nuclei motion between image sequences in nm/sec per material stiffness is shown. The differences between 1kPa and 17kPa samples are significantly lower than to the 50kPa samples; Kruskal Wallis test. Right: Distribution of nuclei motion speed per individual experiment is shown, mean and standard deviation,  $N=3$  with  $n=10$ .

Nonetheless, in agreement with the literature about cells within 3D constrictions is the speed of cells. In constriction, the speed is increased within smaller constrictions and, as such, with higher stress towards the nuclei. The stiffest matrix shows significantly higher motion speeds from the nucleus

than the other both. With smaller confinements and thus higher stress from the matrix faster cell migration speed has been found in other research mentioned in a review. [186] This is supported by the data in “Table 2 Selected overview of recent and actual three-dimensional experimental set-ups for cell investigation in channel” on page 58.

An explanation could be that with stiffer hydrogels, the adhesion proteins on the cell membrane bind stronger towards the hydrogel. With this, a higher polarization and higher speed are possible. Additionally, the curvature seems to play a role as discussed earlier and is less favorable for the HT1080 cells. Because of this, they migrate faster to get around the 3D confinements. This result is additionally supported with other findings in this work; see Figure 15 on page 49. In Figure 20, control images of the H1080 cells for the control in well-plates, on 2D surfaces, and within the 3D microstructured hydrogels are presented exemplary for each matrix stiffness. The cells inside the channels did not show any distinct morphological appearance as a function of the respective hydrogel stiffness while interacting with the matrix. These morphological changes can be observed on the control images on top of the pAAm surfaces with different stiffness. These surfaces have been treated and were biofunctionalized at the same time as the 3D microstructured samples. A morphology of elongated and spreaded cells was mainly found on the samples with the stiffness of 1kPa. For the other surfaces, the cells were mostly roundish, a sign for less preferred matrix stiffness. Additionally, In the control images, a hydrogel channel overview is depicted and shows the cells with the intact nuclear envelope, but also situations where the nuclear envelope ruptured and is separated localize from the stiff part of the nucleus, see below on page 57. Control images of HT1080 cells as overview are given in Figure 20.

There, the transfected cells in control petri dishes, on control hydrogel surfaces and within the channels are shown. The petri dish controls display no differences in cell morphology. The cells on the hydrogel surfaces show the morphology of the cells on 2D surfaces for the different matrices stiffness. The cells show a more spread and elongated form for 1kPa and 50kPa hydrogels. For the 17kPa hydrogels they are mostly roundish. The different morphologies indicate the preference of the cells towards the soft hydrogel with 1kPa of 2D samples. The morphologies of the cells in 3D are similar in all hydrogels with different Young’s moduli, with mostly cylindrical-shaped forming filopodia into the next segment of the channel or a new channel. The formation of filopodia or protrusions to test the near-by area is also known from other cancer cell types, which form invadopodia. Invadopodia are protrusions that test the properties of the environment. These protrusions can degrade the ECM by protease reactions to adapt to the close environment and create an opening. Moreover, invadopodia can also widen pores mechanically to migrate through or invade tissue. Nevertheless, this behavior depends on the stiffness of the material and, thus, the invasion. [187]

However, in some cases, the cell is captured inside the cavity. In this state, the cell forms a three-arm star form into channels. The cell nucleus is also deformed in this position. A deformed cell nucleus is shown in Figure 20 for the 50kPa hydrogel. There it is visible that the histone rich and stiff part of the nucleus is deformed since this part of the nucleus is transfected with H2B-RFP and is displayed in red. The nuclear envelope is ruptured in this position and the NLS-GFP is distributed in the channel, here in green. These control images show again the importance and differences of 2D and 3D cell culture and the influence towards the cell behavior. The irregularly structured hydrogel samples are not repeatable within its internal channel structures. Thus per sample, ten positions randomly selected were investigated as repetitions. Each sample represented one individual experiment, three individual experiments per mechanical property were carried out with ten repetitive and randomly investigated positions. If not stated differently, the statistical significances were determined by the Kruskal Wallis test for not normal distributed data sets of various sizes, which compares the means to each other.



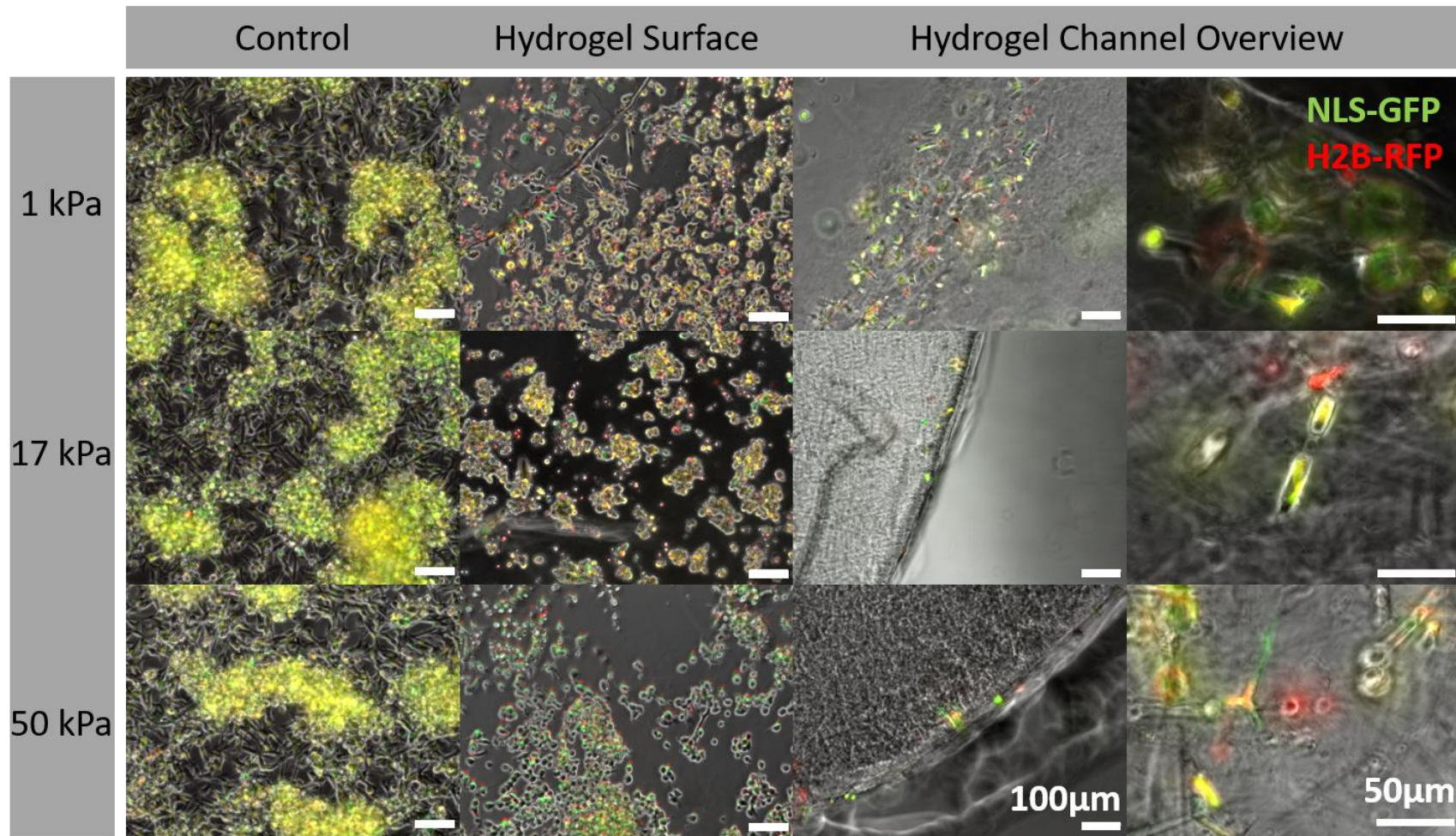


Figure 20 Control images of cells, HT1080, in wells (control), on hydrogel 2D surfaces (Hydrogel Surface), and in hydrogel channel (Hydrogel Channel Overview) for polyacrylamide samples with Young's Moduli of 1kPa, 17kPa, and 50kPa. Images show merged phase-contrast in grey and the transfected nuclei in green (NLS-GFP) and red (H2B-RFP). The overlay of these both transfections depict intact nuclei, while the occurrence of individual colors indicates a ruptured nuclear envelope, where green is the nuclear envelope and red the histone rich part.

Table 2 Selected overview of recent and actual three-dimensional experimental set-ups for cell investigation in channel

Material	Architecture	Stiffness	Spacing	Incubation time	BCL and BF	Cell type	Staining/ Transfection	Speed	Morphology, Migration and Nucleus	Reference
PDMS	Linear channel	1.77MPa	L:20µm H:3.7µm W:11.2-1.7µm	1 week	Fn and Collagen	A125 lung carcinoma cells, MDA-MB-231 breast carcinoma cells, HT-1080 fibrosarcoma cell contractility 100-200nN, and primary breast cancer cells (IFDUC1) of mesenchymal	YES; Hoechst for the nucleus; Cells partly with increased level of lamin A; MDA-MB-231 and HT1080 cells that express enhanced green fluorescence protein (eGFP)-lamin A	Speed increased in smaller confinements; is hindered by the nucleus until it is squeezed in;	Nucleus as major point for resistance	[182]
PDMS	Linear channel		L:150µm H:11µm W:7µm			sphingosylphosphorylcholine (SPC)-treated Panc-1 cells		1-1.2µm/min mean; Depending on cell treatment	Reduced permeation into 7µm channels; Nucleus too large; Elongated nucleus in the center of the cell; Sliding and push and pull mode;	[150]
PDMS	Linear channel		L:- H:10µm W:3-50µm		Collagen	MDA-MB-231	Yes; fixed; Several different have been used for FAC; tubulin; Fluor live cell imaging: transfected fluorescent protein-tagged end-binding protein	Means around 0.8-1.2µm/min for 3µm constriction	Polarized; Decrease of stress fibers and FAC by confinement; Inhibition of myosin, Rho/ROCK, or β1-integrins has no influence on 3µm confinement but in 50µm confinement; confined migration with F-actin is disruption; depends on microtubules	[52]
PDMS	Linear channel	3kPa			Passivated	non-adherent subline of Walker 256 carcinosarcoma		Around 5µm/min in mean of averages	Blebbing Walker cells migrate in confinement without forming specific integrin-mediated focal adhesions; needs a friction	[188]
pAAm	Interconnected channel	1kPa; 17kPa; 50kPa	1.5µm-16µm in variation	5 days	A-NHS: Collagen I	HT1080	Transfected nucleus with NLS-GFP and H2B-RFP	Mean of averages: 1kPa and 17kPa: ~1.2nm/sec 50kPa: 1.5nm/sec	Elongated cell und nucleus; Filopodia; Ruptured nuclear envelope; Position of cells depends on material mechanics;	See chapter 2 in this thesis

## 2.3 CONCLUSION

In this chapter, I answered the questions of whether a soft 3D microstructured hydrogel can be adjusted for the use with mammalian cells, which mechanical range is suitable, 1kPa – 50kPa, and whether these constructs will influence the cellular behavior positively. I was able to adapt the microstructured hydrogel matrices for sample for anchor dependent cells, which invaded and experienced the different Young's moduli from the soft tissue regime. Moreover, I designed the experimental set-up and provided the opportunity of detailed confocal microscopy due to adjusted sizes and relaxed hydrogel matrices. Whereas it has been known from earlier work that cells such as the HT1080 cells will invade into PDMS channels and show a constriction dependent nuclear envelope rupture, the use of soft, hydrated 3D structured samples in order to investigate the nuclei behavior is new.

It was found that nuclear rupture events depend on the mechanical properties of the material. The likelihood of rupturing increased with the stiffness of the material. Additionally, to the mechanical properties, for the rupture events, they are influencing the localization of the cells within the 3D microstructured samples. Furthermore, the localization is also influenced by the curvature of the channels and the cavities. Curvatures in connection with higher Young's moduli are avoided from cells in contrast to those with softer matrices. The Young's moduli influence the motion speed of the nuclei, which are faster with stiffer material. In the end, the materials stiffness, or the volumetric crosslinker concentration, has an influence on cellular behavior as well as the architectural structures inside the samples.

## 2.4 PROCEDURE DETAILS FOR 3D CELL-MATRIX INTERACTION

### 2.4.1 Cells and cell culture:

HT1080; Fibrosarcoma cells. This cell type has transfected cell nuclei, transfected with NLS-GFP, green and H2B-RFP, red. NLS-GFP transfects the nuclear localization sequence, which is located through the nucleus and indicates the rupture of the nuclear envelope. H2B-RFP transfects the histones in the nucleus, which are embedded below the nuclear envelope.

Cells were cultured as followed:

For culturing and splitting, cells were cultivated in cell culture medium DMEM (Biochrom) containing 10% fetal bovine serum (FBS, Biochrom GmbH), 1% Penicillin Streptomycin (penstrep, Sigma-Aldrich).

Cells were splitted 1:10 every 24h to 48h when the confluency inside the cell culture flask reached 80%. For the subculturing and the time for the cultivation of cells with the 3D structured samples in the transwells (Millicell® Cell culture Inserts, Merck) with FBS gradient, the samples were placed into an incubator at 37°C and a 5% CO<sub>2</sub> atmosphere. A day before the experiments, samples, and cells were transferred into a CO<sub>2</sub> independent medium FluoroBrite™ DMEM (in ‚FlouroBrite‘ medium , Gibco) containing 10% FBS, 1% penstrep, 1/50 GlutaMAX™ (Gibco, Germany), and 1/40 2-(4-(2-Hydroxyethyl)-1-piperazinyl)-ethansulfic acid (HEPES, pH 8.5, Sigma) beyond the transwell and 1% penstrep, 1/50 GlutaMax, and 1/40 HEPES (pH 8.5) inside the transwell to gain samples free of phenol red, in order to reduce background fluorescence and increase the signal to noise ratio fluorophores.

Culturing cells in hydrogel scaffolds within trans well plates were prepared as followed: A well of a 24 well plate was filled with 2ml cell culture medium and the transwell was inserted. Inside the transwell, the hydrogel scaffold was placed, and 50 000 cells in cell culture medium were seeded on top of the hydrogel scaffold. Well, plates were incubated for at least 2h to enable cell adhesion to the scaffold, then the cell culture medium medium was exchanged with 600µl of cell culture medium without FBS. This set-up was kept for the whole incubation time until the day before the experiment, then the cell culture medium was exchanged with ‚FlouroBrite‘ medium. The medium beyond and inside the transwell was exchanged daily. For the experiments, the samples were placed into an experiment PDMS chamber with a height of 5mm and a diameter of 8mm filled with ‚FlouroBrite‘ medium. This chamber itself was placed in a petridish with a glass bottom (IBIDI). This petri dish was then later placed into a heating chamber (MI-IBC, Olympus) to provide a suitable surrounding temperature of 37°C for the cells while being imaged.

#### 2.4.2 Sacrificial templates

Ceramic templates were prepared from PVB ZnO-tetrapod powder (provided as curtesy from the AG Adelung tf Kiel and synthesized as shown from Adelung et al. [189]–[191] The loose PVB ZnO-tetrapods were pressed together in a form to yield a round template with a height of 0.16 mm, a diameter of 12 mm and a t-ZnO density of 0.9g/cm<sup>3</sup>. The annealing of the ceramic template was done for 5h at 1150°C, as described previously. [45] The ZnO tetrapods served as sacrificial templates resulting in an inverse structure in the form of microchannels. Most importantly, the templates can be produced at once in high numbers and stored for up to two years as we found that treatment with UV-light and ozone using an ozone oven for 10 minutes increases the hydrophilicity after storage. Without challenges, the hydrogel precursor solution of polyacrylamide can be cast over the template after the ozone treatment.

### 2.4.3 Preparation of 3D microstructured pAAm matrices

The microstructured 3D environment was prepared from polyacrylamide, a synthetic hydrogel material often used in biophysical studies. Additionally, an internal active bio-crosslinker was added during the polymerization to enable the biofunctionalization in the occurring 3D microstructures. The process of the hydrogel preparation is as followed: A solution from Acrylamide (AAm, 40%, Bio-Rad), Acrylic acid N-hydroxysuccimide ester (A NHS, Sigma-Aldrich), N,N'-Methylenebisacrylamide (BIS, 2%, Bio-Rad), bi.dest. water (bi.dest. water, AppliChem, Germany), NaOH (2.5M, Sigma-Aldrich) and 2-(4-(2-Hydroxyethyl)-1-piperazinyl)-ethansulfonic acid (HEPES, Sigma-Aldrich) is mixed as a precursor solution. This solution is degassed to reduce the amount of oxygen. Furthermore, initiators, Ammonium persulfate (APS, 10%, Sigma-Aldrich) and N,N,N',N'-Tetramethylethylenediamine (TEMED, Sigma-Aldrich), were introduced into the solution and carefully mixed. The solution was poured over the template, drop by drop, and a glass coverslip was placed on top to achieve a flat and thin hydrogel sample. After polymerization, the coverslip was removed, and the template with the polymerized precursor solution was immersed into hydrochloric acid (HCl 37%, Sigma-Aldrich) 0.5M, pH 1, until no sign of the ceramic template was left. Then, the now complete hydrogel sample was immersed into bi. dest. water. The water exchange was done until pH 7 was reached. The amount of the components for the hydrogel is shown in Table 3 for a total volume of 500 $\mu$ L.

Table 3: Components of the pAAm hydrogels with the bio-crosslinker A-NHS

		1kPa	17kPa	50kPa
	Crosslinker	1vol.%	4vol.%	16vol.%
<b>Monomer</b>	AAm, 40%	94.69 $\mu$ l	94.69 $\mu$ l	94.69 $\mu$ l
<b>Reactive ester</b>	A-NHS	0.003g	0.003g	0.003g
	H2O bidest.		Fill up to 500 $\mu$ l total	
	HEPES, pH. 8.5	5 $\mu$ l	5 $\mu$ l	5 $\mu$ l
	NaOH, adjust to neutral pH	1 $\mu$ l	1 $\mu$ l	1 $\mu$ l
<b>Crosslinker</b>	BIS, 2%	5 $\mu$ l	20 $\mu$ l	80 $\mu$ l
			Desiccation of solution	
<b>Initiators</b>	APS, 10%, aq.	7.5 $\mu$ l	7.5 $\mu$ l	7.5 $\mu$ l
	TEMED	0.49 $\mu$ l	0.49 $\mu$ l	0.49 $\mu$ l

### 2.4.4 Biofunctionalization:

The sample biofunctionalization has been done with a concentration of 0.5mg/ml collagen (AdvancedBiomatrix). The concentrated collagen solution was diluted with acidic acid (Sigma-Aldrich) solution of 0.02M. All samples were placed for sterilization into EtOH 70vol.% (Walter) for 15minutes and subsequently washed three times with HEPES (pH 8.5), each for 15 min. The samples were then covered with a 0.5ml collagen solution at a concentration of 0.5mg/ml and incubated overnight at 4°C. To cleave all excess collagen from the sample, they were washed three times with phosphate

buffered saline (PBS, Sigma-Aldrich). The covalent binding of the proteins to the samples is possible due to the active ester group of the A-NHS forming an amide bond with the adhesion protein.

#### 2.4.5 Imaging and analysis of 3D experiments with fibrosarcoma cells

Fibrosarcoma cells, HT1080, inside the 3D microstructured hydrogels were investigated conducting spinning disc confocal imaging microscopy. Of high interest was the speed and motion of the transfected nuclei, as well as the rupture of the nuclear envelope as a function of the matrix stiffness. Additionally, the distribution of the cell location, the nuclei positioning, and the distribution of the nuclei diameter were investigated. The imaging was conducted with five dimensions using the 3D dimensions x,y, and z. The fourth dimension is time t, and the fifth dimension is the wavelength of the different channels. For the investigation, all 5D videos were analyzed using Fiji and additional plugins. To exclude the possible sample movement, the drift of the sample was readjusted by the plugin 'Correct 3D drift' to measure the actual movement of the cell. [168], [192] The cell tracking was done by using the plugin 'Manual tracking'. [193] The basis of the cell tracking was always the center of the nucleus. For the diameter of the nuclei in 3D, the hand measurement tool was used at the minor axis of each nucleus at 90° to the channel wall. Each nucleus was measured at least three times at different positions, and the average value of the minor axis was used to be compared with the other nuclei minor axis. From the data obtained, the means and standard deviations from three independent experiments are shown. The results obtained were tested according to their significance by using the Kruskal-Wallis multi comparison test. This test is to be used in cases of non-parametric results and not achieved normal distribution of the results for more than two data sets to compare.

### 3 2D CELL MATRIX INTERACTION

---

This chapter presents the work conducted on 2D cell-matrices interaction. As discussed earlier in chapter 1.1.4, cellular behavior is mediated by the various properties of the matrix (i.e. chemical, mechanical, and topographical). For the chemical properties, the material type and the surface chemistry, particularly the biofunctionalization, have to be considered for *in vitro* cell-matrices investigations. Furthermore, the material type, or better the matrices, need to be biocompatible. Biocompatibility is the ability of a material to be in indirect or direct contact to living cells or tissue without a negative effect on them. [194] The ISO norms 10993-5 and 10993-12 for cytotoxicity tests declare a matrix material as biocompatible when the results of an MTT-assay (see chapter 1.6.3), exceeds 70% cell viability relative to the control for 100 vol.% and 50 vol.% extracts of the respective material. Extracts are prepared by immersing a known amount from the material of interest into cell medium at cell culture conditions. [145], [146] The investigation of these characteristics, the cytotoxicity and the biocompatibility, is highly important for cell experiments. Without them, the interpretation of the cellular behavior on different matrices is not possible. This comparison for different matrixes improves the outcome and the understanding of the cell-matrix interaction. Expanded knowledge about the matrices and the *in vitro* cell-matrix interactions enables the future use of the matrices for *in vivo* application. This is true for hydrogel matrices, which is the focus of this work, but also for other types of matrices such as implants, or even from devices such as biosensors. These biosensors are required to sense *in vivo* bioelectric signals from tissues and can be produced from various matrix materials. Biosensor usage *in vivo* relies on not only the matrix properties of the device but the size as well. This size would then be relative to gain as much information as possible, with minimal invasive implantation. The miniaturization of the devices together with a crimpable material such as the biocompatible NiTi enables the use of biosensors in vessels or for brain applications. [195] A structured biosensor made from NiTi with its different ceramic coatings was investigated towards the 2D cell-matrix interaction and its possible future clinical use as discussed below in chapter 3.1 “Results, discussion, and conclusion for primary cells on biosensors”

Additionally, a second matrix, a hydrogel, was investigated towards the 2D cell-matrix interaction, see chapter 3.2 “Results and discussion for „Engineering of a new bio-crosslinker for enhanced cell adhesion””. In this part of the thesis, a chemically modified hydrogel poly(2-hydroxyethyl methacrylate) (pHEMA) was investigated. The chemical modification resulted from a newly created bio-crosslinker (BCL), which was introduced into the structure of the hydrogel. The BCL was used to

form a covalent bond to specific functional groups of adhesion molecules, which are required to form a bio-active hydrogel for anchor dependent cells. Without chemical modification, the pHEMA hydrogel is inert to protein adsorption and cell adhesion due to its hydrophilicity. This highly hydrophilic behaviour of pHEMA, inhibits the instantaneous absorption of proteins and adhesions ligands from the medium resulting in low numbers of cell adhesion. [196] This also reduces the ability of bacteria to attach to pHEMA besides its high biocompatibility. Its biocompatibility, the property to not have any adverse side effects from its chemical composition towards cells, favors pHEMA as a material of great importance for biological and medical applications. [197]–[199] However, the most common chemical modification and biofunctionalization attempts are based on additional treatments of the hydrogel matrices based on chemical functionalization, e.g., carbodiimide chemistry using EDC, or through UV light irradiation of the sample to activate sulfo-succinimidyl-6-(4'-azido-2'-nitrophenylamino) hexanoate (sulfo-SANPAH) as discussed earlier in section 1.2.5, "Hydrogel biofunctionalization procedures with different chemical components". [86], [200] These are excellent procedures for matrix biofunctionalization at the surface for simple surface structures in 2D. For other sample types with complex structures and higher sample depth, drawbacks could appear. These drawbacks could be limited light absorption for the activation of sulfo-SANPAH or the limitation of diffused chemicals within the depth of the sample. Both challenges would result in a reduced depth of sample biofunctionalization.

The introduction of a bio-crosslinker (BCL) during the synthesis of the hydrogel matrices offers the possibility to obtain a three-dimensional distribution of reactive groups inside the hydrogel for biofunctionalization and later cell adhesion. Therefore, biofunctionalization and cell adhesion could be made possible throughout the whole hydrogel. The newly engineered BCL is made from three parts, the polymerization part, the linker, and the protein-binding part. The protein-binding site consists of a maleimide group, which reacts with thiol-functionalities of cysteine, which are present in fibronectin (FN). [201]–[204] The polymerization part consists of a methacryl group and the linker from diethyleneglycol. Up to this date, few approaches are reported for the use of an active bio-crosslinker during the polymerization. One example of another bio-crosslinker added to the precursor solution is mentioned in this work, section 2.4.4 "Biofunctionalization:" on page 61 in chapter 2 "3D cell-matrix interaction". There, I used acrylic acid N-hydroxysuccinimide ester in a polyacrylamide precursor mixture. Other options for instance biofunctionalization within the 3D volume would be the incorporation of adhesion proteins, e.g., acrylated RGD or monomers decorated with RGD before crosslinking using EDC. [86] All these strategies have slight drawbacks, such as the fast hydrolysis reaction of acrylic-NHS and its property to change the precursor pH strongly. In cooperation with Laura Schumacher, a new bio-crosslinker (BCL) was therefore synthesized to overcome the current limits of instant biofunctionalization.



### 3.1 RESULTS, DISCUSSION, AND CONCLUSION FOR PRIMARY CELLS ON BIOSENSORS

Human umbilical vein endothelial cells (HUVEC cells) were investigated on structured biosensors which base is made from NiTi equipped with Pt electrodes and ceramic insulators. [205] Primary endothelial cells, HUVEC cells, were used in this experimental set-up as they are directly cultivated from living tissue. Moreover, this cell type would be later exposed to the biosensor during *in vivo* applications. Primary cells provide a unique opportunity for representative data close to cells in human tissue. The cytotoxicity was studied using the method discussed in chapter 1.6.3 on page 28 for the different ceramic insulators, YSZ, SiO<sub>x</sub>, and TaO on the NiTi. In short: The material of interest is immersed into cell medium under cell culture conditions for the extraction of excess material and ions. The cell medium, now called the extract, is placed into a cell culture. Cells exposed to the extract will react to the content of the extract by average growth, decreased growth, and even cell death. This growth behavior is checked via a MTT assay. In a MTT assay the MTT, (3-(4,5-dimethylthiazol-2-yl)-2,5-diphenyltetrazolium chloride, is converted into formazan by cell metabolism. Similar is done to a negative control, a cell culture exposed to unedited cell medium. The cytotoxicity of a material or, more precise, the cell viability of the extract treated cells with respect to the control is related to the converted formazan. The amount of formazan can be determined via UV-Vis spectroscopy. All ceramics were found to be biocompatible with cell viability over 90% relative to the control independently from the extract concentration. [205] Interestingly, for the direct adhesion assay, the cells showed a distinct reaction, as depicted in Figure 21. The HUVEC cells were stained with calcein AM (green) and Hoechst 33342 (blue) to obtain information about the cytoplasm and nucleus. In Figure 21A, HUVEC is visible on the control, and the NiTi samples covered with Pt electrodes, light grey, and coated with a ceramic insulator. It is visible that HUVEC preferred the control surface and the TaO coating over the YSZ coating with the result, that the biosensor coating of TaO may be more suitable for cells. The least preferred coating was that with SiO<sub>x</sub>. All these observations are in agreement with previous work. This agreement shows, that cellular behavior towards the ceramic insulators is a general one and unaffected from other components of the biosensor. [206]–[211]

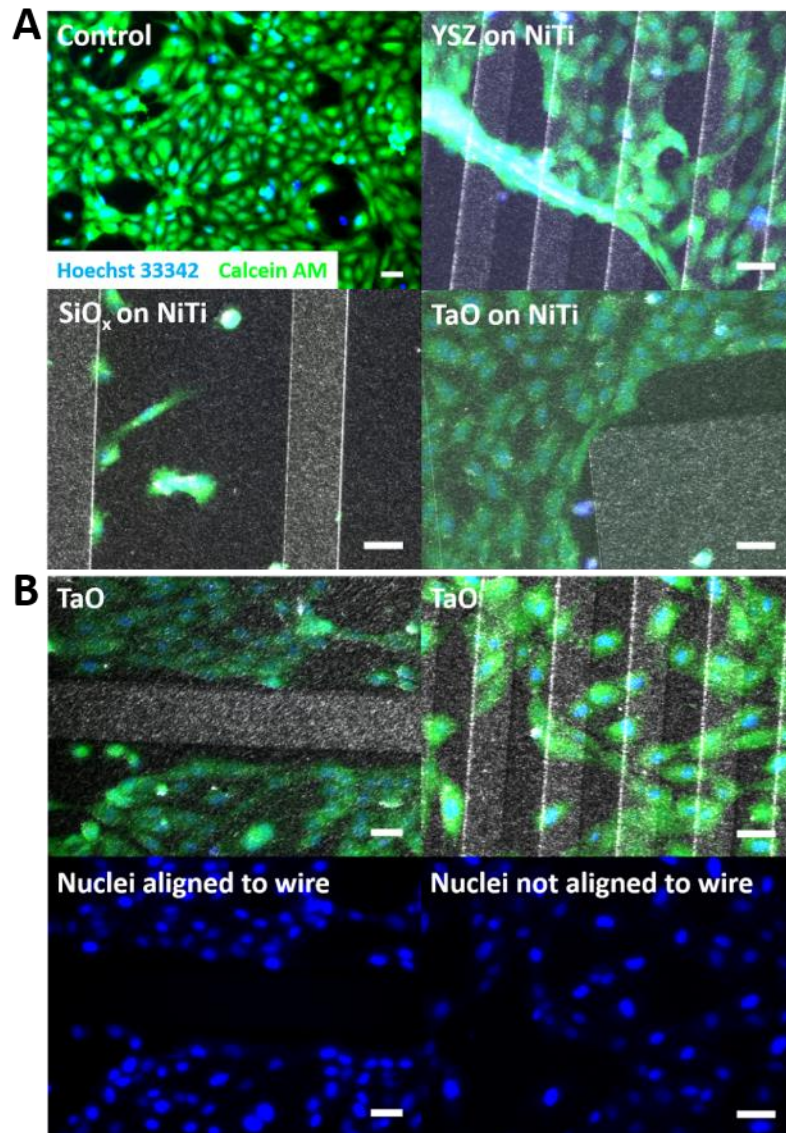


Figure 21 HUVEC growth on structured biosensor surfaces stained with calcein AM (green and for live cells) and Hoechst 33342 (Blue and for the nucleus). The Pt wires with a width around  $50\mu\text{m}$  are coated with the ceramic insulator. The Pt areas with a width larger than  $50\mu\text{m}$  are not coated. These are the electrodes A) Shows the cell growth on the structured biosensor surface with the different ceramic insulator coatings YSZ,  $\text{SiO}_x$ , and TaO and the control. B) Shows the HUVEC growth influenced in their orientation by the Pt wires of different width. Scale  $50\mu\text{m}$ .

In Figure 21B, an example of the cell growth on the structured biosensor is shown. The cell growth is influenced by the width of the Pt wires and their coating. The top row in Figure 21B depicts the layered images with calcein AM for the cytoplasm in green, Hoechst for the nuclei in blue, and reflective light microscopy in grey for the biosensor compartments, while the lower row shows nuclei stained in blue. The light grey represents the Pt wires, the dark grey the ceramic insulator. The width of the Pt wire mediates the direction of cell growth. For the wires larger than  $50\mu\text{m}$  (left) and without coating the cells are aligned along the wires. For the coated wires with smaller width ( $50\mu\text{m}$ ), the cells grow over the structures. The growth there is nearly perpendicular to the structure. This

becomes visible when the cell nuclei are compared along their major axis. The major axis is the widest length of the epileptically formed nucleus. This observation indicates that HUVEC aligns with the structures, which are larger than 50µm. Considering the production of the biosensor, this is reasonable as a marginal topography appears, which guides the cellular behavior, as discussed in chapter 1.1.4.1, “Topographical influences on adhesion and migration of cells” on page 5. The Pt wires are on top of the NiTi and coated with the ceramics using reactive sputtering techniques. [205] This might form a discrete curvature for the cells possible to sense and to grow over comparable to the cells on the small structured YSZ coating. This is in agreement with work about surface structures with curvature. [174]–[177], [212] The alignment of the cells shows that not only the basic material properties and negative cytotoxicity is important for the design of an implant, but also the topography as described in section ‘Cell interaction with 2D matrix surfaces’ on page 3. In conclusion, the miniaturized biosensor is highly biocompatible and in compliance with sensible human primary cells. Additionally, the potential of the intended structuring of future micro biosensors was shown for guided cell growth. [170], [213]

For further details onto the biosensors, the reader is referred to the following publication:

C. Chluba, K. Siemsen, C. Bechtold, C. Zamponi, C. Selhuber-Unkel, E. Quandt, R. Lima de Miranda (2020): Microfabricated bioelectrodes on self-expandable NiTi thin film devices for implants and diagnostic instruments. *Biosensors and Bioelectronics*, 153, 112034.

### 3.2 RESULTS AND DISCUSSION FOR ‘ENGINEERING OF A NEW BIO-CROSSLINKER FOR ENHANCED CELL ADHESION’

Engineering chemical functional molecules require the knowledge of the final application and the required properties. This part of this thesis will highlight the synthesis of an initially protein inert hydrogel, poly(2-hydroxyethyl methacrylate (pHEMA), into an immediate reactive hydrogel for biofunctionalization and cell adhesion. Furthermore, the effectiveness of the BCL was determined with cell adhesion assays and investigated cytotoxicity of the hydrogel matrix with incorporated bio-crosslinker (BCL). The bio-activity of the former protein inert hydrogel pHEMA was based on the thiol-maleimide reaction which is possible because of the reactive new BCL, 3-maleimidopropionic acid diethyleneglycole methacrylate. For this instant bio-activity and increased reactivity of the pHEMA hydrogel towards adhesion proteins, the new BCL needed to be distributed throughout the whole three-dimensional polymeric pHEMA structure. The incorporation of the BCL into the hydrogel

was ensured by choosing a methacrylate group, which can react with its vinyl group in a free-radical polymerization. The vinyl group of the methacrylate group reacted with the monomer hydroxyethylenemethacrylate (HEMA) and crosslinker (CL) ethyleneglycoldimethacrylate (EGDMA) and formed the hydrogel pHEMA. Diethyleneglycol (PEG2) was chosen as non-toxic linker between the polymerization part and the protein-binding. The protein-binding part, a maleimide group was synthesized from  $\beta$ -alanine and maleic anhydride. [204] The maleimide group is highly susceptible to thiol groups, which are present in amino acid functionalities like cysteine groups in fibronectin. This construction, the new bio-crosslinker incorporated into the pHEMA structure and connected to fibronectin (FN), resulted in a biofunctionalized pHEMA for enhanced cell adhesion. The details for synthesis and incorporation of the BCL are discussed in section 3.4.1 and 3.4.2, starting on page 75.

In order to facilitate the reading of this work and the figures, a short code with definition is introduced. The crosslinker concentration, CL, which link the monomer chains together, is given in wt.%. The bio-crosslinker, BCL, links the adhesion protein to the polymeric structure with the concentration given in mol.%. The concentration of fibronectin (FN) is given in  $\mu\text{g}/\text{mL}$ . The abbreviation pHEMA\_1CL\_5BCL\_1.5FN represents a pHEMA hydrogel with 1wt.% crosslinker EGDMA, 5mol.% bio-crosslinker biofunctionalized with fibronectin of a concentration of 1.5 $\mu\text{g}/\text{mL}$ .

To observe the biocompatibility of the newly created bio-crosslinker (BCL), 3-maleimidopropionic acid diethyleneglycole methacrylate, the BCL was incorporated into a pHEMA hydrogel. From the synthesized hydrogel matrices MTT assays were conducted following the ISO 10993-5 and ISO 10993-12 to evaluate the cytotoxicity of the material using extracts from the hydrogels. The extracts were prepared by the immersion of the respective material of interest into cell medium under cell culture conditions as described earlier.

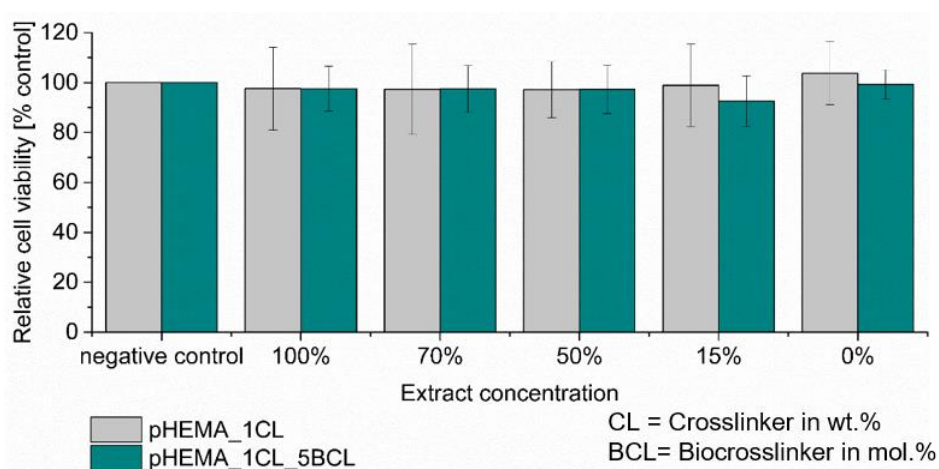


Figure 22 Results of the *in vitro* MTT cytotoxicity tests presented with means value and standard deviation for different extract concentrations. All materials are biocompatible, and cell viability relative to the control is over 90% for all tested samples. CL refers to the crosslinker EGDMA in wt.%; BCL refers to the bio-crosslinker in mol.%.

Figure 22 shows the result of the MTT cytotoxicity tests. Here, no extract concentration had been found to be under 70% cell viability relative to the control. Moreover, the extract concentration for 100vol.% and 50vol.% have been similarly over 90% cell viability, as seen Figure 22. Both, pHEMA with and without the BCL, can be rated biocompatible according to the ISO 10993-12, as discussed above. [146]

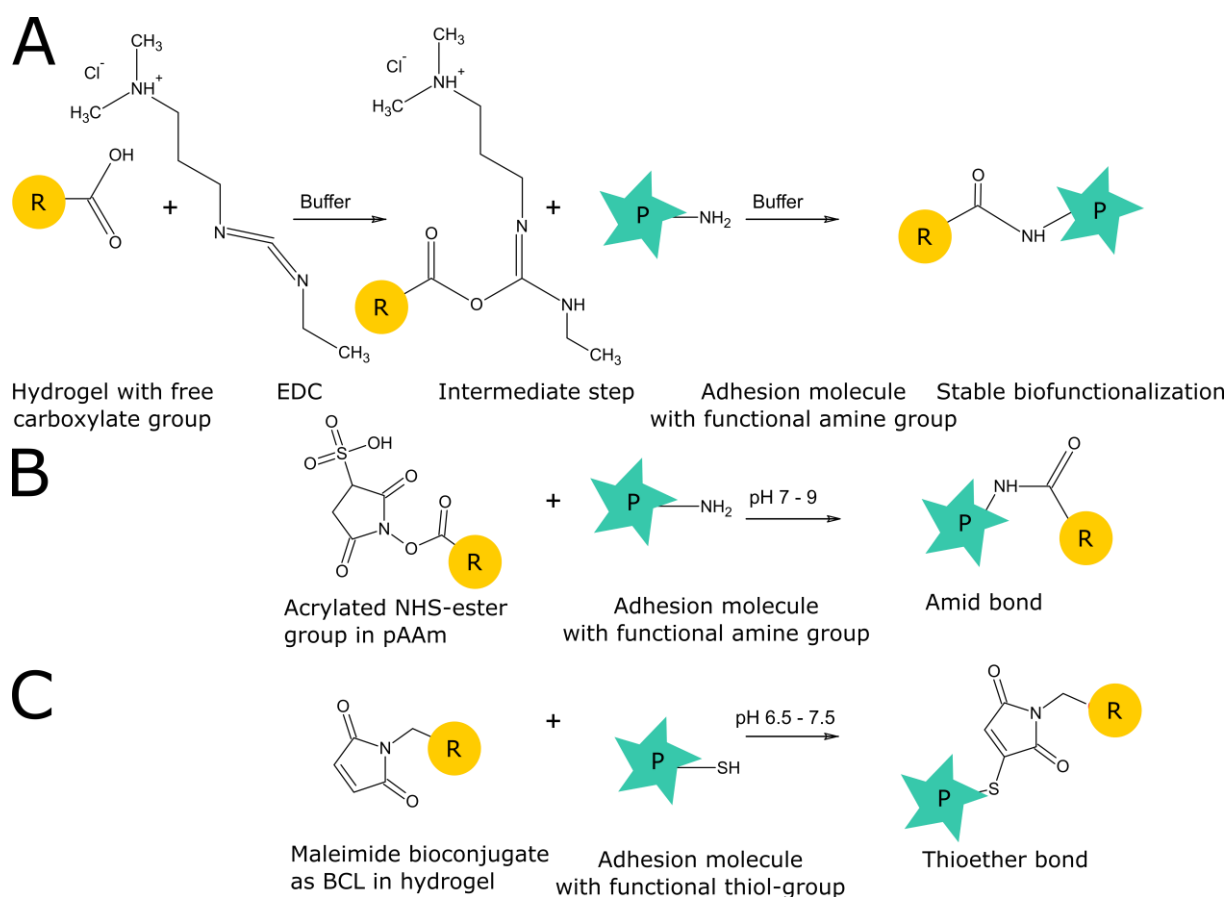


Figure 23 Schemes of biofunctionalization with three variation. P depicts the rest of the adhesion protein; R depicts the rest of the molecule A) Functionalization of carboxylate groups using EDC in a buffered solution. In the end, a stable bond is formed. However, during the synthesis, the intermediate step is prone to hydrolysis. B) A-NHS is adapted as BCL towards the hydrogel of interest, forming stable amid bonds when adhesion molecules come across the fixed A-NHS groups. C) depicts the reaction of the new BCL between the maleimide group of the incorporated BCL with a thiol-group of an adhesion molecule.

In Figure 23, adhesion protein coupling using EDC and A-NHS [94] are shown as a comparison to the coupling with the new BCL. While both are working, EDC coupling in our experimental work has shown to require more time due to several synthetic steps, while A-NHS molecules are slightly unstable during hydrogel synthesis as their hydrophilicity is increased as a result of the sulfonate group. The biofunctionalized hydrogels were studied for their cell adhesion properties. For this, various concentrations of FN were used. The sample weight was chosen to be approximately 100mg

in order to have comparable amounts of BCL, with the assumption of an even distribution. The high affinity of fibronectin towards the BCL was anticipated, resulting from the high affinity of the maleimide group towards thiol- or amine groups, dependent on the present pH. [214] Since fibronectin is rich in cysteine (containing a thiol side group), reaction with the maleimide results in an organosulfide, specifically a thioether. Figure 23C depicts the scheme for the biofunctionalization using the synthesized BCL. For the evaluation of hydrogels with BCL implementation, cell adhesion tests were carried out for two matrix types. Matrices without BCL and matrices with similar crosslinker (CL) ratio and with BCL were used. Interestingly, for both matrix types, cell adhesion was shown. The cell adhesion for pHEMA matrices with BCL was expected to be successful to be enhanced over cell adhesion on pHEMA without BCL. It was also expected that the cell adhesion and the cell covered surface area, variate with the FN concentration. At a closer look, Figure 24, a porous structuring of the samples has been found at the sample surface. The porous structure is visible due to the composite image of the merged bright field and fluorescence images. The cells in green were stained for their cytoplasm with calcein AM, and also for their nucleus and dead cells. These fluorescent dyes, Hoechst and propidium iodide, were adsorbed into the hydrogel sample, visible with the purple surface in Figure 24. Cell adhesion on these structures is in agreement with the literature, where different types of hydrogel matrixes, with specific topographies on 2D surfaces, enables cell adhesion without BCL or FN on protein inert hydrogels. [73], [177], [215]–[217]



*Figure 24 Shows a composite image of a porous pHEMA sample surface from a pHEMA\_1CL\_10FN sample with adhering cells. The composite image shows the merged bright field and fluorescence images from the fluorescently stained cells. Cells were stained with calcein AM, green, for their living cytoplasm, with Hoechst for their nuclei in blue and additionally with propidium iodide for dead cells, red. The cells are visible in green, the fluorescent dyes Hoechst and propidium iodide were adsorbed from the hydrogel matrix, depict the sample in purple. The sample is composed of 1wt.% EGDMA crosslinker and no bio-crosslinker. The sample was exposed to 10 $\mu$ g/mL FN. Scale bar: 50 $\mu$ m.*

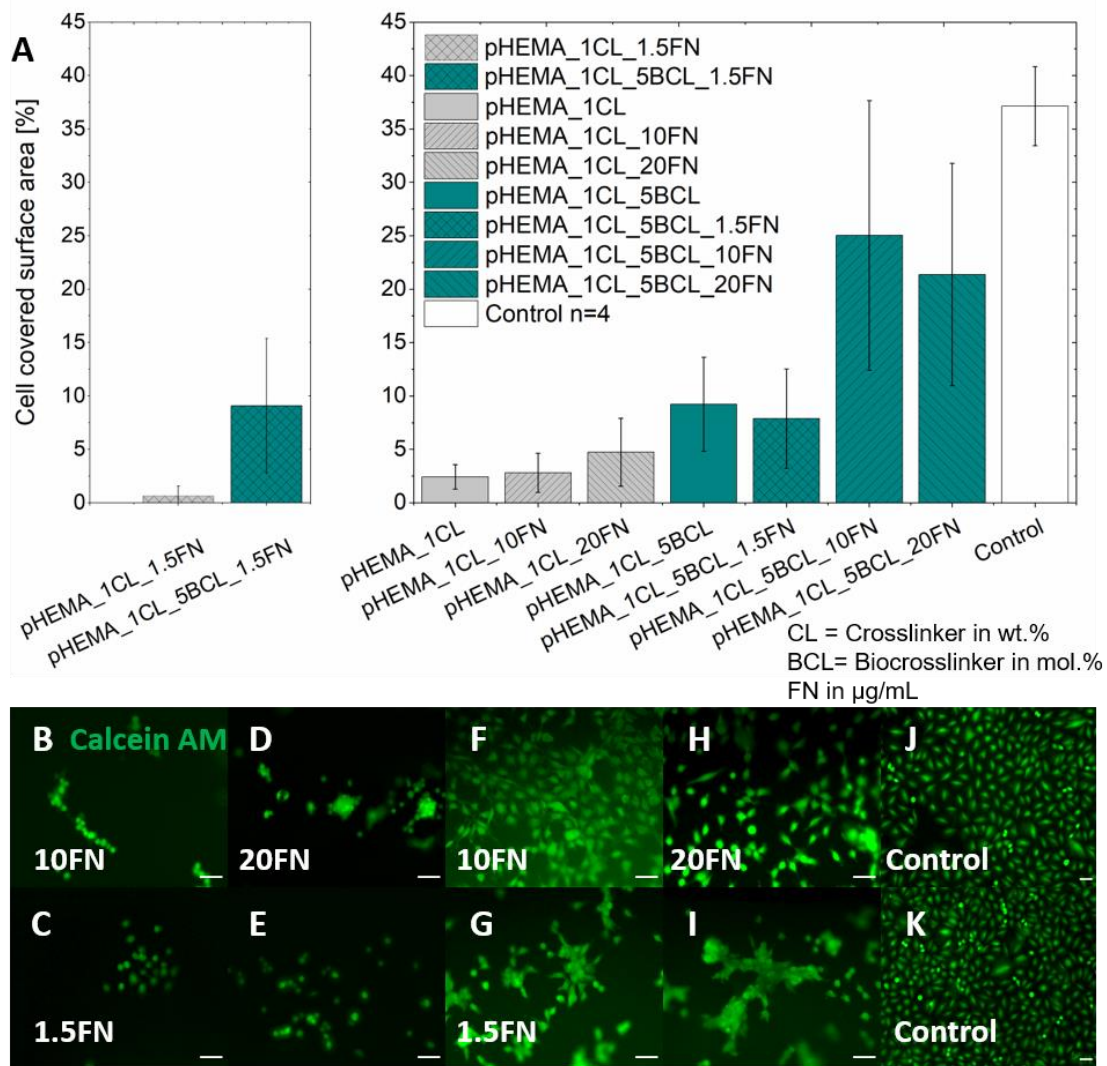


Figure 25 ) Shows the result of the cell adhesion assays and exemplary images. The concentration of the crosslinker (CL) is given in wt.%, the concentration of the bio-crosslinker (BCL) is given in mol.%. A) Shows the results of cell covered sample surfaces with the mean value and standard deviation in dependence of the fibronectin concentration after 24h of incubation. Cells were fluorescently stained with calcein to determine the adhesion area. Left four repetitions are shown, at the right side one repetition with another batch of BCL shown. Samples with 5BCL are covered with more cells compared to samples with no BCL. B)-I) show the cell morphology of Ref 52 wt cells on sample surfaces. Ref 52 wt cells were stained with Calcein AM, green. B) – E) are pHEMA sample surfaces with 1CL and no BCL. B) pHEMA without BCL and 10FN C) pHEMA without BCL and 1.5FN D) pHEMA without BCL and 20FN and E) pHEMA without BCL without FN. All cells show a similar round morphology without lamellipodia. F)-I) are pHEMA sample surfaces with 1CL and 5BCL F) pHEMA with BCL and 10FN H) pHEMA with 5BCL and 20FN G) pHEMA with 5BCL and 1.5FN I) pHEMA with 5BCL and without FN. All cells show lamellipodia and a stretched morphology compared to the pHEMA surfaces without any BCL. The best distribution of cells at the surface can be found in for a biofunctionalization with 10FN and 5BCL(G). K) And L) show the distribution of Ref 52 wt cells in control wells. The distribution is evenly, and the cells are spread over the surface. Scale bar:  $50\mu\text{m}$

In Figure 25 the cell adhesion on matrices without BCL was found to increase, with an increase of FN concentration. This agrees with the finding in other work on pHEMA, where the surface topography was altered, due to pHEMA brushes, resulting in an increase of protein absorption. [218] However, a

mean of over 5% cell covered surface area were not reached. The morphology of the attached cells was roundish, with less or no visible lamellipodia, a sign for unspecific and poor adhesion, see images above Figure 25B-E on page 71. For the pHEMA matrices with BCL, the mean of the cell covered surface area has been experimentally shown to be above 7%. These results were also found for matrices with BCL but without added FN. The usage of cell culture medium where proteins are available, in combination with the surface topography and available BCL molecules for protein absorption, lead to cell adhesion. Moreover, the morphology of the adhering cells shows spreaded and elongated cells with visible lamellipodia. Additionally, the cells were not just clustered together but were found with a larger distribution over the surface, see Figure 25F-H, similar to the control cells J-K.

The data and experiments within the sections 3.2 and 3.4 will be part of a manuscript 'A polymerizable bio-crosslinker for implementation in pHEMA hydrogels to covalently link fibronectin for enhanced cell adhesion' by myself, Laura Schumacher, Clement Appiah, Christine Selhuber-Unkel, and Anne Staubitz. My contribution to this manuscript was the idea and conceptual design of the study, the supervision of Laura Schumacher during her master thesis, parts of the cell experiments and their evaluation, and the lead part of the scientific writing. I worked in the lab of Prof. Dr. Christine Selhuber-Unkel as well as Laura Schumacher as part of her master thesis. Mainly, she worked in the lab from Prof. Dr. Anne Staubitz from Bremen University as well as Clement Appiah.



### 3.3 CONCLUSION AND PERSPECTIVES FOR 2D CELL MATRIX INTERACTION

In the current chapter, the work conducted on 2D cell-matrix interactions on biosensors and pHEMA matrices was presented. Both matrices of profoundly different materials showed high biocompatibility, which enables them to be used in the future, in both *in vitro* and *in vivo* applications. The first part of this chapter, 3.1, showed the investigation of primary cells on miniaturized biosensors and their impact on cellular behavior. The biosensors, with its different coatings, proved to be highly biocompatible with all ceramic insulator coatings in relation to the control. The cell adhesion assays showed to be in favor of the TaO coating. Additionally, the insulating surface coating and the Pt wire mediate the cell growth. This indicates that indeed active guidance in cell growth in biosensors is possible. This active guidance could be used for directed cell growth and alignment on future biosensors or implants. Guided cell growth on the implants could facilitate the interaction between the implanted devices and cells from the tissue environment.

In the second part of this chapter, 3.2, a novel synthesized biocrosslinker 3-maleimidopropionic acid diethyleneglycole methacrylate for the use inside of hydrogels was described, especially for the use with protein inert hydrogel matrices. The introduction of the new BCL during the hydrogel synthesis is a possible strategy to overcome the current difficulties in 3D biofunctionalization of protein inert hydrogel samples. It will open the way of high-throughput cell-matrix interaction tests for different types of adhesion proteins investigated from one sample. Moreover, in comparison to the actual method for the 3D biofunctionalization used in chapter '3D cell-matrix interaction' the here presented method is less invasive to changes in pH inside the precursor mixture and with this more stable to use. Interestingly, the single original educts for the bio-crosslinker 3-maleimidopropionic acid diethyleneglycole methacrylate are known but they have not been synthesized together up to this point to obtain a new bio-crosslinker.

## 3.4 BIO-CROSSLINKER SYNTHESIS AND SAMPLE PREPARATION

### 3.4.1 Creating and incorporating the bio-crosslinker

The synthesis of the newly created bio-crosslinker (BCL) 3-maleimidopropionic acid diethyleneglycol methacrylate was done with its functional groups chosen according to the necessary requirements and aims. These aims are the enhanced cell adhesion to protein inert hydrogel matrices, the synthesis of a biocompatible hydrogel, and reactive groups susceptible to adhesion proteins. The BCL requires for its application a possibility for free-radical polymerization for the polymer binding part and the susceptibility of the protein binding part to specific functionalities of adhesion molecules. For this objective, the ECM adhesion protein fibronectin (FN, BioMatrix) was chosen as adhesion molecule. The adhesion protein FN includes a sequence to which cells adhere, the RGD-sequence (Arg-Gly-Asp). Additionally, FN contains large quantities of cysteine whose thiol functional groups can be addressed by several chemical reactions. [201]–[204] In this work, a maleimide group was chosen as the protein binding part because of the reactivity towards thiol groups and the stable formation of a thioether bond. The maleimide group was synthesized from  $\beta$ -alanine (Alfa Aesar, Germany) and maleic anhydride (Roth), as depicted in Figure 26 on page 75.  $\beta$ -alanine and maleic anhydride were synthesized in the presents of dimethylformamide (DMF), N-hydroxysuccinimide (Apollo Scientific) and dicyclohexylcarbodiimide (DCC, Merck) with a yield of 54% under nitrogen atmosphere forming 3-maleimidopropionic acid-N-hydroxysuccinimide ester, Figure 26A. The polymer binding group and linker were synthesized from diethylene glycol (PEG2, Jkchemicals) and methacrylic acid. First, diethylene glycol was stirred in the presents of para-toluenesulfonic acid monohydrate (*p*TSA, Sigma Aldrich), toluene (Walter) and methoxyphenol (Sigma Aldrich). Next, methacrylic acid was added to the stirred solution. A yield of 71% was obtained from the product 2-(2-hydroxyethoxy)ethyl methacrylate, Figure 26B. After both products were obtained, Figure 26A and B, they were cleaned and purified before they served as educts for the synthesis of the bio-crosslinker, as depicted in Figure 26C. The bio-crosslinker 3-maleimidopropionic acid diethyleneglycole methacrylate was synthesized from 2-(2-hydroxyethoxy)ethyl methacrylate and 3-maleimidopropionic acid-N-hydroxysuccinimide ester, Figure 26C. Triethylamine (Fluorochem) was added to 2-(2-hydroxyethoxy)ethyl methacrylate in ethyl acetate (Fischer Chemicals), followed by 3-maleimidopropionic acid-N-hydroxysuccinimide ester. The suspension was heated under reflux and observed via thin layer chromatography. The product was reduced with evaporation and purified with column chromatography. As the BCL is able to co-polymerize with HEMA and EGDMA because of its methacryl functionality, the BCL will be distributed throughout the whole hydrogel volume crosslinked to the three-dimensional polymeric structure.

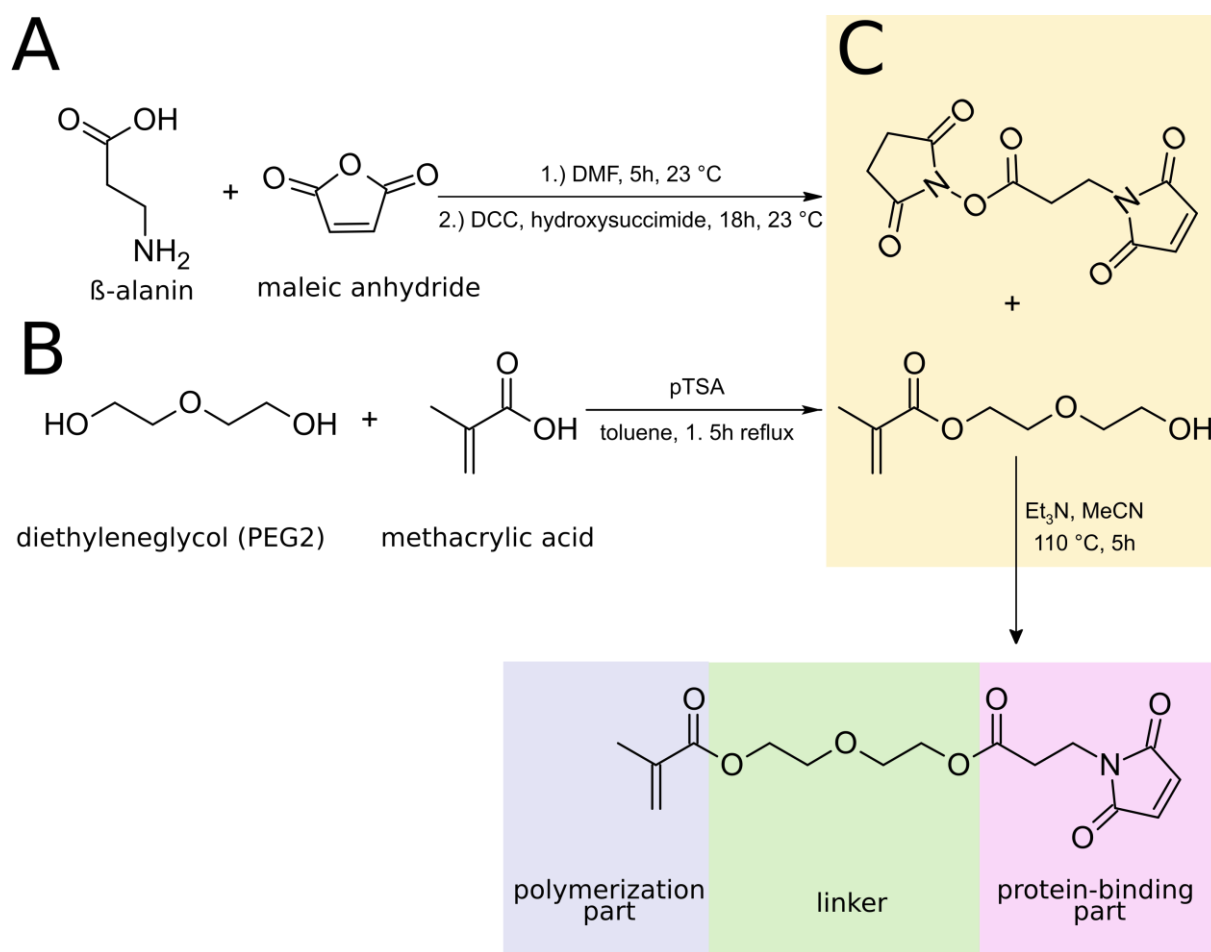


Figure 26 Scheme of BCL synthesis established with and by M.A. Laura Schumacher. A) Synthesis of the building block for the protein-binding part from  $\beta$ -alanine and maleic anhydride. B) Synthesis for the polymerization and linker part from diethyleneglycol and methacrylic acid. C) Synthesis of the BCL from the products of A and B.

### 3.4.2 Synthesizing pHEMA with the new bio-crosslinker

The binding of the new bio-crosslinker into the pHEMA structure is enabled due to its methacryl functionality. The methacryl functionality has a vinyl group that will participate in free-radical polymerization used for various polymers and hydrogels. One of these hydrogels prepared via free-radical polymerization is pHEMA. Free radicals initiate the polymerization from the reaction initiators such as ammonium persulfate (APS, Sigma-Aldrich). The reaction is accelerated with the use of N,N,N',N'-Tetramethylethylenediamine (TEMED, Sigma-Aldrich). The radical polymerization is propagated from one monomer to the other until no monomer can be accessed and transfer the radical, which indicates the end of the polymerization process. Several factors have to be considered during the polymerization process i.e., temperature, UV-light, or pH. In the precursor solution, a pH value too high or too low affects the initiator's effectiveness. High temperature or UV-light can form in most polymer solution radicals itself and increasing the consumption of monomers with the result of shorter monomer chains. Low temperatures and low numbers of radicals can lead to the opposite

effect. The propagation for single chains works at its best, with a low chain conversion, which results in continuous long chains. Both cases will change the material properties of the hydrogel, such as the molar mass of the single chains and the hydrogel stiffness accordingly. [219] In the present work, the BCL, the monomer HEMA (100 mg, 0.77 mmol), water (0.10 mL), the crosslinker EGDMA (0.1 – 15 wt. %), and the initiator APS (0.1 wt.%, Sigma-Aldrich) were added into a pre-dried vial with a septum, purged with N<sub>2</sub>-gas for minutes and stirred with a magnet. Additionally, the solution was mixed in an ultrasonic bath (Bandelin electronics) for 5 minutes. Both procedures were done to obtain a hydrogel with equally distributed BCL. In order to reduce the oxygen amount in the precursor mixture, the solution was degassed. Furthermore, the precursor solution was heated to 80°C for 5 minutes before the second initiator TEMED (0.15 wt.%, Sigma-Aldrich) was added with a syringe (Braun). This mixture was again mixed in the ultrasonic bath for one minute. For the polymerization, the final solution was placed in a water bath of 80°C and polymerized in the absence of oxygen. After the polymerization, the hydrogels were detached from the vial and washed for three days in distilled water (AppliChem).

### 3.4.3 Biocompatibility, biofunctionalization and cell adhesion on BCL containing pHEMA

In order to examine the biocompatibility of the newly created bio-crosslinker 3-maleimidopropionic acid diethyleneglycole methacrylate and the efficiency of cell adhesion, cytotoxicity via MTT-assays and adhesion assays were conducted. For all assays, Ref 52 wt cells were used. The MTT-assay was conducted as described in section 'cytotoxicity' on page 28 using the ISO standard 10993-5 and 12. [145], [146] For the adhesion assay 50 000 cells per well in FlouroBrite medium (Gibco, USA) with 10 % Fetal Bovine Serum (FBS; Biochrom, Germany) and 1 % penstrep were cultured for 24 h on the sample surface. For the biofunctionalization, which proves the availability of free reactive groups of maleimide, the adhesion protein fibronectin was used. Samples were sterilized in 70vol.% ethanol (Walter) and rinsed with a 50mM solution of 2-(4-(2-Hydroxyethyl)-1-piperazinyl)-ethansulfonic acid (HEPES, Sigma-Aldrich). Next, the samples were incubated overnight in a fibronectin solution of preferred concentration (1.5µg/mL up to 20µg/mL). After this, the samples were washed with phosphate buffered saline (PBS), and cells were seeded on top of the sample. The samples were then incubated for 24 h, after which staining solutions were added to observe the cell adhesion by fluorescent microscopy. For the examination of the direct influence of the samples towards the cell adhesion and morphology, the cells were fluorescently stained in their cytoplasm as well as in their nucleus using several dyes Calcein AM (BD Science) for the living cells, propidium iodide for the dead cells, and Hoechst for the nucleus. For the imaging, the BX43 (Olympus), as well as the IX81

(Olympus), were used. For the controls, the same number of cells were seeded into a 12well plate and treated similarly.

For the determination of the sample area covered by cells in percentage, the area of the fluorescently stained cells was assessed using Fiji and its function of particle analysis. [168] All data presented show the means and standard deviation, averaged from the different positions and samples investigated.



## 4 SWOLLEN HYDROGEL MATRICES AS DRUG-RELEASE RESERVOIRS

---

### 4.1 INTRODUCTION

Hydrogels have been in use for substance and drug release in several applications. To name some, oral administered anticancer agents or ant-acids are available. [220]–[222] The ability of hydrogels to take up solutions, to swell, and to release the substances or drugs provide ideal conditions for the use in future *in vivo* or *in vitro* applications, where soft matrices are required. Even a release over hydrogel of nanoparticles to the respiratory system or the skin is reported. [223] Necessary for the treatments using drug release is the successful delivery to the aimed location. In case of the desired location of the brain any orally or dermally taken substance needs to go through the blood brain barrier. This barrier is around the brain and separates the brain from the rest of the immune system. [220] To overcome this barrier, the applied dosage must be tremendously high for reaching a low concentration at the local site within the brain. By positioning therefore a drug loaded and hydrated hydrogel directly inside the patient, e.g., inside the brain, high substance dosages towards the body could be avoided. [224] Advantageous for *in vivo* application would be degradable hydrogels to spare the patient additional invasive treatments. [225]–[227]

However, studies of the *in vitro* applications of drug release towards single cells or organotypic tissue slices are important to increase the knowledge about the effectiveness. Nevertheless, as first step the release and influence of the substances or drugs of choice from and to the matrices need to be investigated. One drug of interest for such investigation is ethosuximide (ETX), which is a water-soluble drug to treat childhood absence epilepsy. [228], [229] Childhood absence epilepsy affects the patient in a way, that activities, e.g., drawing or chewing, are abruptly paused for some considerably time of several seconds. During this timeframe, seizures within the brain can be made visible with electroencephalography. The electroencephalography shows spike waves for the seizures, which starts without pattern, but that can be reduced with anti-seizure drugs such as ETX. It is suggested, that ETX can block the respective T-type calcium channels, responsible for the synchronized activity of the neurons in charge. [91], [230] Another drug of choice for the investigation of the release from hydrogels in suspension would be curcumin. Curcumin is a hydrophobic favoured substance to be used in different approaches. It is a bioactive compound and known for its anti-inflammatory effects on the skin. [231] However, it is hardly water soluble and self-assembles within water. [231]–[233] In this chapter, I present the investigations regarding substance release from hydrated matrices in suspension to achieve an understanding of whether drug release from mechanical adapted and swollen hydrogels can appear over an extended period of time. For this, two different types of hydrogels were used, first a natural and degradable hydrogel based on alginate, and secondly, a

synthetic hydrogel, polyacrylamide. The substances used were ethosuximide (ETX) and curcumin (Cur).

## 4.2 RESULTS AND DISCUSSION FOR ALGINATE-BASED HYDROGEL DRUG RELEASE

In the drug release study based on degradable alginate-based hydrogels and ethosuximide (ETX), the alginate samples were prepared by covalently crosslinking using adipic acid dihydrazide (AAD) and 1-ethyl-3-(3-dimethylaminopropyl) carbodiimide hydrochloride (EDC) for the formation of a hydrazine bond. The hydrazine bond was required to avoid the traditionally method of physical crosslinks with  $\text{Ca}^{2+}$  ions as described in section 1.2.3.1 on page 11. The  $\text{Ca}^{2+}$  ions will form a chelate complex with the guluronic building blocks of different alginate molecules. Thus the alginate solution polymerizes and forms a hydrogel. However, as the alginate was intended to be used for studies in combination with anti-seizure drugs *in vitro* and later *in vivo* inside the brain, any use of  $\text{Ca}^{2+}$  ions inside the hydrogel would challenge the effect of ETX on the T-type calcium channels of the neurons. The detailed procedure for the alginate samples is described in section 4.4.1. on page 95. Shortly, a 2wt.% alginate solution was prepared in a buffer solution of 3-(*N*-morpholino)propanesulfonic acid (MOPS). The crosslinker AAD was added to the alginate solution. In total, three different concentrations, 0.094M, 0.15M, and 0.2M, were prepared, later referred to as AAD<sub>low</sub>, AAD<sub>medium</sub>, and AAD<sub>high</sub>. Next, the EDC solution was prepared in MOPS buffer. After cooling and degassing, the respective alginate-AAD solution and the EDC solution were mixed in the ratio 1:1 and poured into a mold. After the polymerization the hydrogel samples were washed to remove the excess crosslinker educts. After these steps, the hydrogels were infiltrated with the substance of interest, here ethosuximide (ETX), as described in section 4.4.2, see also below (Figure 32). In short: Hydrogels were dehydrated in an ethanol (EtOH) series, where the volumetric concentration of the ethanol was increased from 70vol.% up to 99vol.%. After taking with a tissue any additional EtOH from the hydrogel matrices, they were immersed in an aqueous solution with the respective drug of favored concentration. After the infiltration, the hydrogel matrices were immersed into glass flasks with lid filled the storage solution, an artificial liquor (aliquor), which represents the cerebrospinal fluid within the brain. The glass flasks with lid were placed in cell culture condition, 37°C and 5% CO<sub>2</sub>-gas, on a shaker to avoid static release conditions.

Initially, the degradability of the lowest crosslinker concentration (AAD<sub>low</sub>) was studied to gain knowledge about the time frame when a material loss of at least 50% was achieved. The material loss indicates the matrix degradation and the accumulation of degradation products in the static storage solution. The storage solution was not exchanged during this process. In a later stage, and depending on the application, the storage solution can be diverse such as cell culture medium or another physiological solution like artificial liquor (aliquor), which represents the cerebrospinal fluid in the



brain. This is important since the accumulation of excess material and degradation products in static *in vitro* conditions could lead to cytotoxic effects in later investigations, as discussed in section 1.6.3 “Cytotoxicity” on page 28. With the accumulated excess material and degradation products, the cytotoxicity was determined for the respective material. The alginate matrixes, without any dehydration processes treated, showed after seven days of incubation at room temperature in bi. dest. water, a weight loss of  $50.06\% \pm 13.21\%$ , and after 15 days a weight loss of around  $60.44\% \pm 10.14\%$  (Figure 27A). This is due to the hydrolysis of the hydrazine bonds in water and agrees with other work. [78], [227] Interestingly, the weight loss curve of the untreated hydrogel samples here presented has not a steep slope but seems to stabilize after 15 days. Within these 15 days, a degradation rate of  $4.03\% \pm 0.68\%$  per day is found.

Additionally, samples with three different AAD concentrations were evaluated according to their swelling behavior in bi. dest. water, as these results assign the optimal time point of equilibrium swelling and the ideal point for cell seeding on samples. In the following section, it is referred to as the lowest crosslinker concentration with  $AAD_{low}$ . To the medium, crosslinker concentration is referred with  $AAD_{medium}$ . The highest crosslinker concentration is indicated with  $AAD_{high}$ . Again, untreated samples were taken, dried at room temperature on air for some time, and next placed into bi. dest. water (3ml). Remarkably, from the air-dried samples, the significant swelling of the samples could be observed after the initial 2h. Samples with the lowest AAD concentration ( $AAD_{low}$ ) swelled with a mean of 2612%, for  $AAD_{medium}$  a mean of 706%, and for  $AAD_{high}$ , a mean of 574% was observed. After the first 2h, further swelling was, in its extent, neglectable, see below (Figure 27B). Nevertheless, it is shown with its low mean values but large standard deviation, which is ranging into the negative, that samples lose weight as if they degraded instantly when placed into bi. dest. water. Since the biocompatibility of samples used for *in vitro* and *in vivo* tests is highly required, the cytotoxicity was indirectly measured via MTT-assays. Due to the findings mentioned above, according to the degradability, the cytotoxicity of the samples and their degradation products were tested after the incubation and degradation for 8 days in 5ml cell culture medium. For the different concentrations of crosslinker used, all concentrations were biocompatible, see below (Figure 27C). The means of the cell viability relative to the control were at 70% or higher for all extracts prepared, as discussed in section 1.6.3 “Cytotoxicity” on page 28 . This agrees with the findings and prior experiments about the biocompatibility of covalently crosslinked alginate. [78]

For the direct test of cell-sample compliance, Ref 52 wt were seeded on top of biofunctionalized samples to assess whether they would grow with a healthy morphology, as discussed in section 1.6.2.

The cell morphology is different for the different cell types. A prediction of whether a cell morphology on a new sample material of any type indicates healthy cells is possible when the favored morphology of uncorrupted and healthy cells is known. Ref 52 wt cells are known to grow on cell culture well plates favorable in an elongated, polarized form with visible lamellipodia or focal adhesion cluster (FAC) formation. Cell adhesion was tested by seeding cells (Ref 52 wt) on top of covalently crosslinked alginate biofunctionalized with fibronectin or collagen I, as depicted in Figure 27D and B on page 83. While the cells on the fibronectin biofunctionalized samples were imaged after 24h, the collagen I functionalized samples were imaged after 8 days of incubation. On both samples, elongated cells were found, indicating a not cytotoxic sample in direct contact. For the sample with collagen I biofunctionalization and long term incubation, a network of connected Ref 52 wt cells is visible despite or especially due to the fact that the covalently crosslinked samples degrade over time. A hydrogel sample can be under stress, which would act on the adhering cells. The stress within the sample would act on the cells as if they would adhere to a stiffer matrix. The degradation of the hydrogel matrix could be responsible for relaxing the stress within the hydrogel. [167] Consequently, the stress relaxation within the cells would release the stress sensed from the adhering cells.

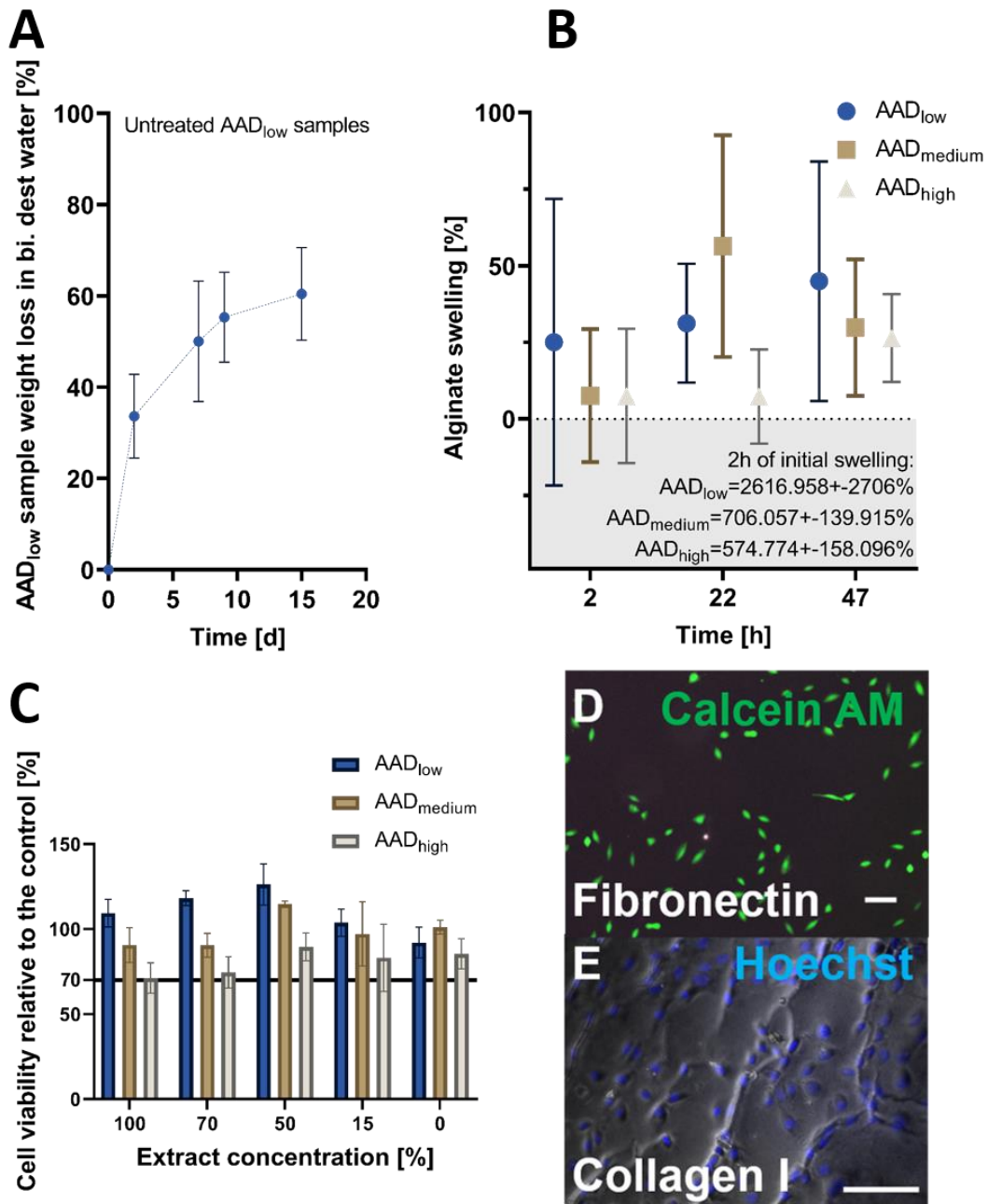


Figure 27 Weight loss and swelling behavior of covalently crosslinked alginate as well as the cytotoxicity evaluated via MTT-assays and representation of successful direct cell-sample interactions on 2D surfaces. A) Degradation of covalently crosslinked alginate, untreated, with the lowest amount of crosslinker used (AAD<sub>low</sub>) over 15 days, mean and standard deviation, n=12. B) Swelling data of untreated samples of all crosslinker concentrations after an initial swelling of 2h, mean and standard deviation, n=3. C) Cell viability relative to the control [%] assessed via MTT-assays, mean, and standard deviation, n=3. D) and F) exemplary cell adhesion images of cells on covalently crosslinked alginates biofunctionalized with fibronectin and collagen I. F) shows the cells on alginate, where MES buffer was used for the synthesis and fibronectin for the biofunctionalization. The cells were stained with calcein AM (green). E) Also, Ref 52 wt cells; alginate sample prepared with MOPS buffer and biofunctionalized with collagen I. Cell nuclei were stained with Hoechst (blue). bar:100µm

The mechanical properties are important for matrix-cell interaction *in vitro* (as discussed in section 1.1.4.2 on page 7) and especially for future *in vivo* applications as they mediate external cellular behavior and cell internal processes. Consequently, the intention for the alginate-based hydrogels was the creation of a soft hydrogel with a Young's modulus below 20kPa but also to assess the optimal mesh size for the release of substances within the brain. The optimal mesh size for drug release from hydrogel matrices depends on the molecular size of the investigated drug and the preferred release mechanism. If the hydrogel mesh is much smaller than the drug molecule, the release can take place due to swelling or degradation of the hydrogel matrix. Similar sized hydrogel mesh and drug molecule would interact with each other depending on the electrostatic charges of both. In a polymeric mesh much larger than the drug molecule the interaction between both would be limited and the release would be due to diffusion. However, the potential location for the drug release needs to be considered with the possible impact of the drug releasing matrix. The usage of hydrogel matrices with smallest polymeric mesh sizes would prolong possibly the drug release, but the small mesh size would increase the hydrogel stiffness. This increased stiffness could impact the tissue of the future application location adversely, leading to foreign body reaction. Nevertheless, the hydrogel matrices also needed to be in a state, where they were stiff enough to be easily handled for possible implantation procedures. This reasoning led to the chosen crosslinker concentrations, AAD<sub>low</sub>, AAD<sub>medium</sub> and AAD<sub>high</sub>. For the examination of the materials, the alginate with the lowest and with the highest concentration of crosslinker was analyzed using AFM. Thin alginate layers of 100µm-300µm were prepared on glass slides, washed, dehydrated, and immersed into bi.dest. water before investigation. For the evaluation of the data, only the saturated curves were taken into account for the evaluation of the Young's modulus using the Hertz model. [234] For the samples using a low concentration of crosslinker (AAD<sub>low</sub>) a distribution of different Young's moduli has been found. Figure 28A shows these values in box plots, where two samples displayed a relative mean value of 19.18kPa and 21.84kPa, while a third sample displayed a mean of 10.74kPa. The samples with a higher amount of AAD (AAD<sub>high</sub>) showed mean values of Young's modulus at around 6kPa. The data in Figure 28B show for the single positions measured at the samples a more random distribution within the Young's moduli. This indicates a diffused concentration of actual crosslinks within the hydrogel at different positions. The reason for this could be due to diffusion inhomogeneity or particularly due to the natural component alginate. The molecules of the sodium alginate display a range of sizes and could influence the crosslinking. The average mesh sizes of polymeric network  $\xi_a$  were calculated from the Young's moduli values, as explained in chapter 1.4. with following equations using the shear modulus  $G$  and the theoretical crosslinker density  $\rho_x$ . [108], [119] The shear modulus  $G$  and the Young's modulus  $E$  are related over the Poisson's ratio  $\nu$ , equation (9). Followed with the relation

of the shear modulus and the crosslinker density  $\rho_x$  of the hydrogel in equation (10). The average mesh size of polymeric network  $\xi_a$  is then related to the crosslinker density  $\rho_x$  with unit volume assuming the meshes as a network of spheres, (11). The diameter of the spheres is then the average mesh size of polymeric network  $\xi_a$ .  $R_{gas}$  is the gas constant,  $T$  the temperature and  $N_A$  is the Avogadro constant.

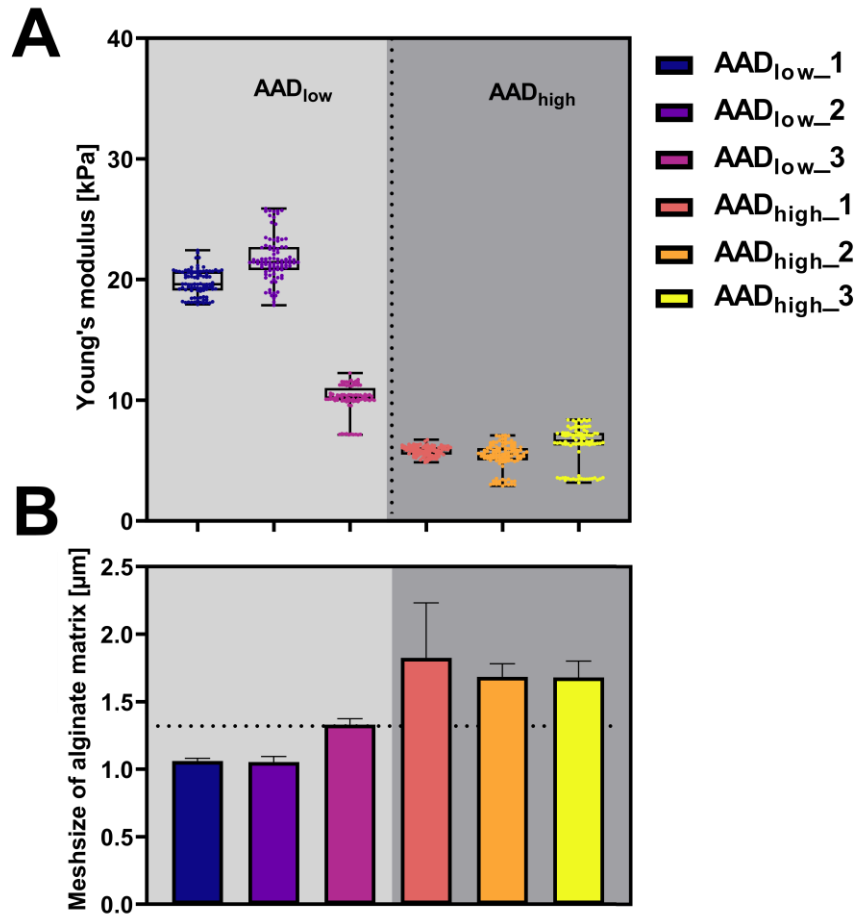


Figure 28 Distribution of Young's moduli and calculated average mesh size of the covalent crosslinked alginate matrices. A) Young's moduli from alginates with two different crosslinker concentration, and B) the relation of the Young's moduli to the mesh size. In A) all data points from single samples are presented together in boxplots. These data points are specified for single positions per sample in together with the mean and the standard deviation of the calculated mesh sizes as bars in B).

$$G = \frac{E}{2(1 + \nu)} \quad (9)$$

$$\rho_x = \frac{G}{R_{gas}T} \quad (10)$$

$$\xi_a = \sqrt[3]{\frac{6}{\pi \rho_x N_A}} \quad (11)$$

The Young's moduli values for the AAD<sub>high</sub> alginates were unexpectedly comparing the swelling results from the investigations of the swelling behavior found (Figure 29A). The swelling of the alginates with the high amount of the crosslinker adipic acid dihydrazite, AAD<sub>high</sub>, was less prone to take up water, which is usually explained by the higher amount of crosslinker, which results in smaller mesh size. The reason could be an oversaturation of the AAD and their hydrazine groups, which form brittle intramolecular crosslinks, which are in agreement with other work. [78] It has been shown earlier that the Young's modulus is strongly related to the mesh size of the polymeric part and its ability of swelling. [80], [81] Hydrogels can be produced with a huge range in their stiffness from 0.5kPa up to 5MPa [235], which depends highly on their average polymeric mesh size. For drug release investigations most studies report mesh sizes in a range of 5nm-100nm. [125] With equations (9)-(11) the polymeric mesh size of the covalently crosslinked alginate was calculated to range between 0.5µm-3µm, see Figure 28B. For the investigations of the swelling behavior as result of the drug infiltration the hydrogel samples were treated as described in section 4.4.2 on page 96. In consequence the alginate matrices were dehydrated in an ethanol series, weighted and immersed in a solution with known concentration of the favoured drug. In this part of the work, ETX was used with three varying concentration. The ETX concentration ranged from 2M, 1.5M, and 0.5M, and water. It is to report that the 2M solution was an oversaturated solution which formed 'oil' droplets after resting and was a non-transparent solution after agitation, a sign of a supersaturated solution. [222], [236] The infiltration of the ETX solutions showed an influence on the covalently crosslinked alginate matrices and their swelling behavior with respect to the concentration of ETX as depicted in Figure 29.

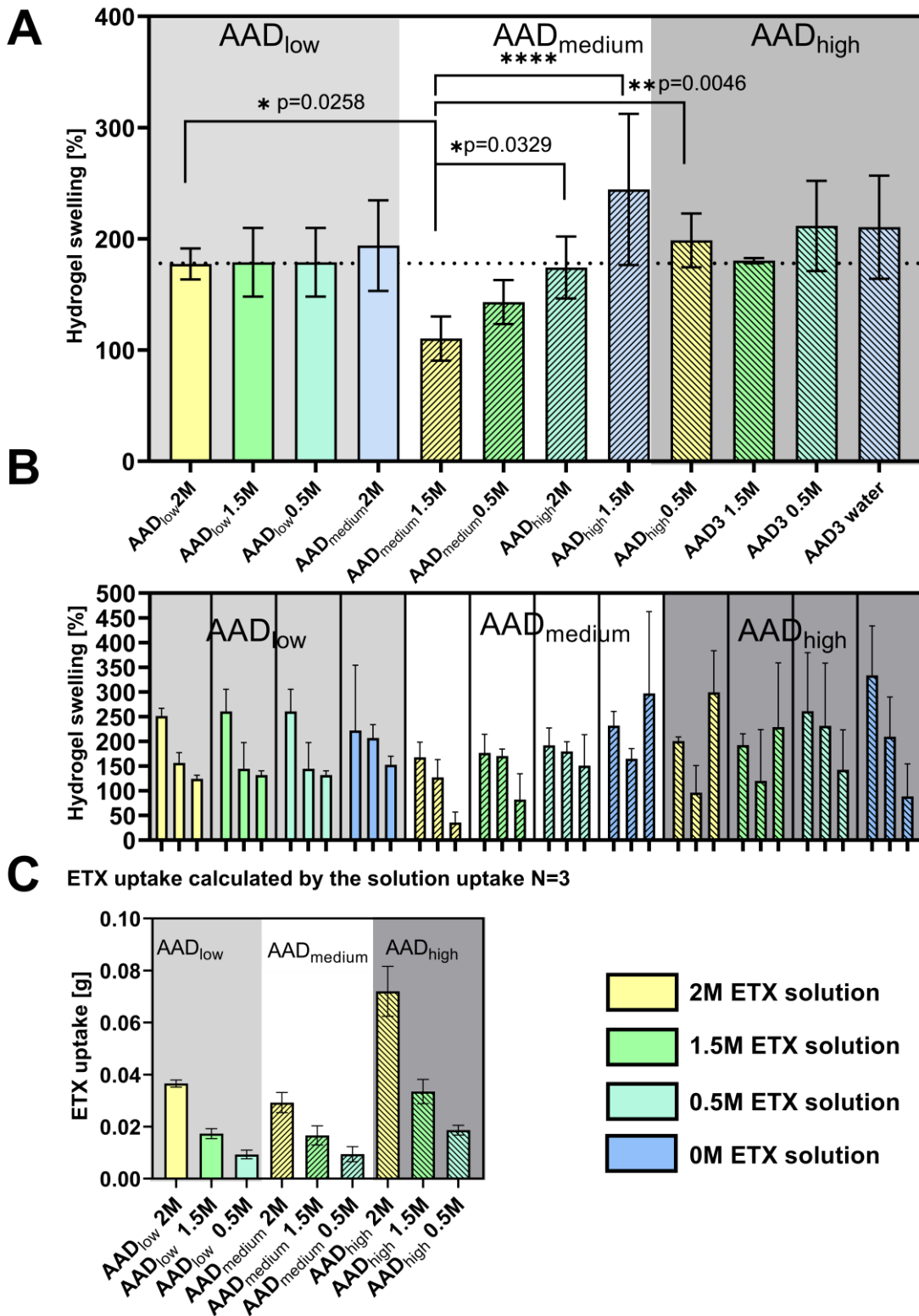


Figure 29 Swelling behavior of alginate matrices with respect to their crosslinker and ETX as well as the theoretically calculated amount of ETX. A) shows the mean and standard deviation of all three independent experiments for the swelling behavior. In B) the means and standard deviations for the single independent experiments are depicted. The theoretically calculated amount of ETX inside the matrices are depicted in C) with means and standard deviation of all experiments.

While the lowest and highest AAD concentration had slightly similar swelling results shown as means with standard deviation from three independent experiments, see Figure 29A. The swelling for the medium crosslinker concentration shows in the same graph an increase of swelling with a decrease of the ETX concentration. The swelling of the samples was tested for statistical significance between the samples of the same crosslinker concentration and among the same solution concentrations of ETX. For this, results were tested positive for normal distribution of data, and an ANOVA test (uncorrected Fischer's LSD test) was performed. As shown (Figure 29A), the differences of the swelling in 2M ETX solution between the medium crosslinker concentration and the other both are significant. Moreover, for the medium crosslinker concentration, AAD<sub>medium</sub>, the swelling behaviors for the different ETX concentrations were also clearly different to each when comparing the results from the 2M towards the 0.5M and 0M solutions. This performance indicates a strong molecule-matrix interaction of the AAD<sub>medium</sub> samples and less dominant for the samples of other crosslinker concentration. These samples seem to have too large mesh sizes to interact as strongly with the ETX inside the solutions, 0.5 $\mu$ m-3 $\mu$ m, as calculated earlier. Figure 29B shows the swelling of the samples in three independent experiments. Clearly, the range of hydrogel swelling differs for each experiment. This is in agreement with the fact that the sodium alginic acid salt used is a natural product with a varying range of molecular sizes. Due to this, variations within different batches can be considered as expected. From the uptake of the solution into the matrix, a theoretical infiltrated ETX amount was determined, see Figure 29C, assuming a homogeneous distribution of ETX inside the solution. The theoretically calculated ETX amounts were below 40mg, with one outlier of AAD<sub>high</sub> with the 2M ETX solution. Interestingly, the concentration of ETX released from the samples and measured via HPLC was higher than calculated, see Figure 30. Considering the supersaturation of the 2M ETX solution, this is a reasonable consideration. Two phases formed from water and highly concentrated 'oil' droplets could have been not distributed evenly in the ETX solution. This could have lead to a not evenly infiltration of the ETX inside the samples and inside the matrix for different experiments. The release of ETX from fully swollen alginate matrices was evaluated for 20 days. During this time, the hydrogel matrices infiltrated with ETX were incubated under cell conditions, in artificial liquor (aliquor), and agitated at 80rpm. Additionally, every 24h, the whole release medium was exchanged with fresh aliquor to mimic the dynamic exchange of fluids inside the body. Via HPLC and double proof, an ETX concentration was detected even after 72h. Figure 30 presents data of two independent experiments, each with three samples. The data show the means and the standard deviations of the investigated ETX release, where A shows the ETX concentration in mg/ml, and B shows the total amount of ETX measured. For the alginate with the lowest crosslinker concentration, AAD<sub>low</sub>, infiltrated in 2M, 1.5M, and 0.5M ETX, different concentrations of released ETX were found. These



measured ETX amounts were respective 104.63mg  $\pm$ 51.22mg, 61.69mg  $\pm$ 0.019mg and 26.64mg  $\pm$ 15.11mg obtained after 3h of incubation. These values were strongly decreased after 72h to 0.13  $\pm$  0.07mg, 0.02  $\pm$ 0.02mg and 0mg ETX. An increase of ETX concentration was found for the medium crosslinker concentration, AAD<sub>medium</sub>. Similar to the findings for AAD<sub>low</sub>, the ETX concentrations decreased with time, Figure 29 and Figure 30.

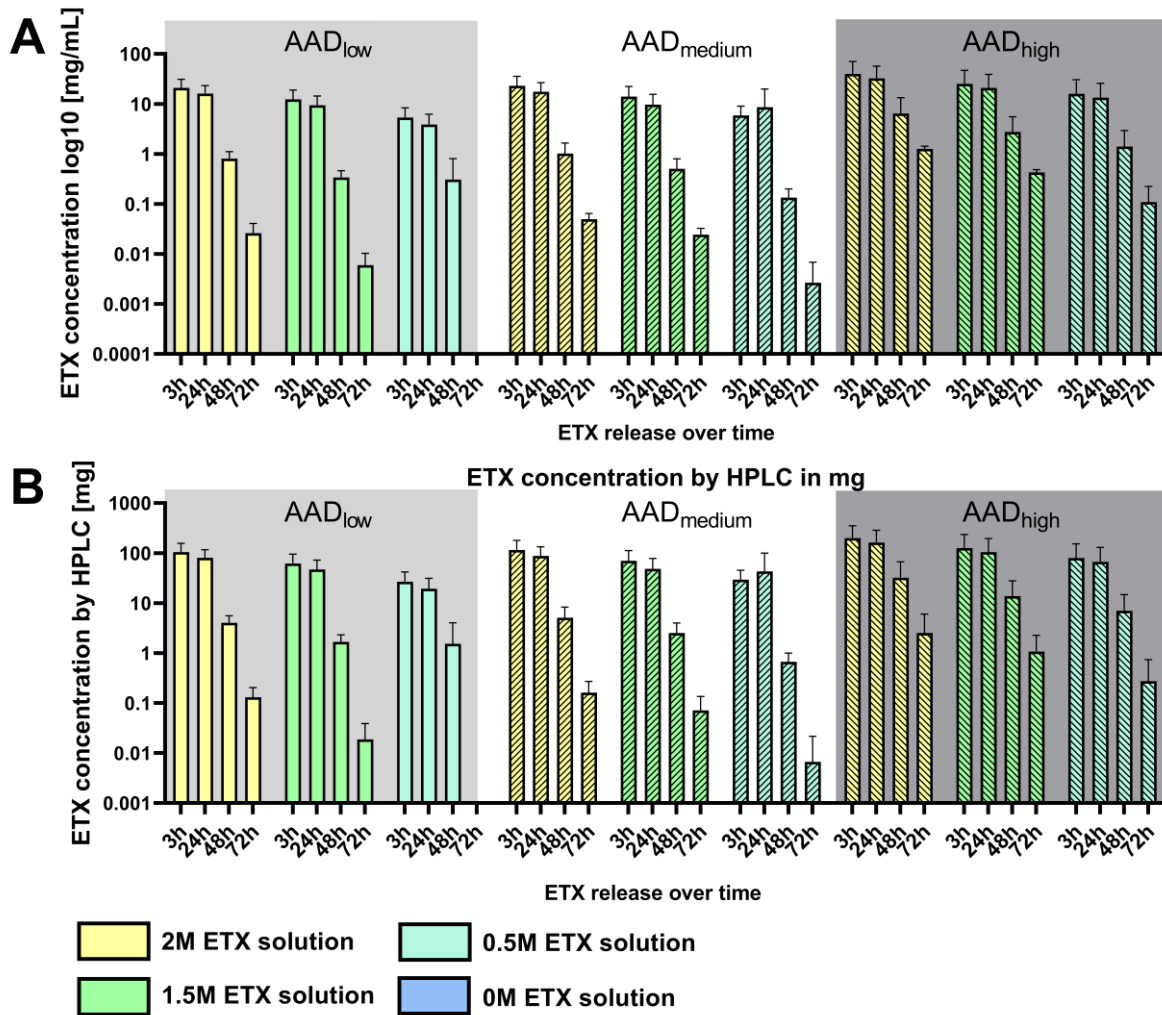


Figure 30 Results of the ETX concentration measured via HPLC using a logarithmic axis. In A) the ETX concentration is represented in the concentration mg/mL while in B) the whole concentration found in 5mL supernatant in mg is shown.

The highest amounts of released ETX were found for samples with the greatest crosslinker concentration, AAD<sub>high</sub>. Here, following amounts were found after 3h of incubation: 199.25mg  $\pm$ 153.03mg, 126.31mg  $\pm$ 108.27 mg, 73.46mg  $\pm$ 74.069mg. These were decreased after 72h of incubation to: 2.54mg  $\pm$ 3.49 mg, 1.07mg  $\pm$ 1.19mg, 0.27mg  $\pm$ 0.47mg. The data show that the ETX concentrations found in the aliquor decreased as expected with time and infiltrated concentration. The range of the concentration found inside the AAD concentration increased with the increase of crosslinker (Figure 30). This indicates an interaction with the matrix, specifically with the crosslinker

involved as the ETX amount found increased with the crosslinker despite the large mesh sizes calculated from the Young's moduli obtained with AFM measurements. As the matrices were already fully swollen, the polymeric matrices did not need time to swell or to dissolve the ETX. Thus, the samples released the ETX instantaneously via diffusion and mass transport from the sample into the supernatant around the hydrogel matrices. The matrix degradation inside the drug release condition was partly faster than described in other work, where alginate based hydrogels crosslinked with adipic acid dihydrazide without infiltrated substances were investigated. [78], [227], [237], [238]

Substantial for the matrix degradation could have been here the prior treatment of the hydrogel matrices, which includes the washing process, the dehydration of the matrices, and the infiltration of substances onto the matrices. Moreover, also the drug release with the incubation conditions was also responsible for the degradation of the hydrogel matrices. These treatments introduced the interaction between the crosslinker and the drug ETX into the matrices as well as a probable osmotic pressure due to a concentration gradient within the hydrogel matrices filled with ETX and the supernatant. All treatments and interactions introduced probable stress towards the polymeric mesh and the covalent crosslinks. The impact of the stress on the hydrazine bonds could have made them more susceptible to hydrolysis and thus reduced the degradation time. A table of the time point of visual sample degradation can be found in the appendix in section 6.7 "Degradation of covalently crosslinked alginate" on page XIII.

#### 4.2.1 Conclusion

In this chapter, I presented the approach for swollen and degradable alginate matrices infiltrated with ETX, a drug for the treatment of absence epilepsy. The matrices were adapted to the lowest stiffness possible to achieve for usage. Whereas it is known that alginate can be used as degradable drug release matrices in various forms, from beads, NP or simple tables for the oral and systemic use [120], [123], [221], [239]–[242] few adjustments have been made for possible direct local application inside the brain. The here presented results could be useful for the possible application directly into the brain to gain a time window without adding drugs towards the patient. The fully swollen matrix enabled the direct release after insertion into the liquor reservoir. With its soft degradable matrix, no mechanical harm will probably be done towards the future surrounding tissue. With its proven biocompatibility and degradability, it is ready to be tested in *in vivo* application. A first initial *in vivo* test in cooperation with Anna Buschhoff and Eva Peschke was conducted with much smaller hydrogel matrices (volume of 20µl) as investigated *in vitro*. The tests showed that the hydrated alginate matrices can be incorporated into the brain of a rat. The animal showed no adverse reaction either to the implantation nor to the material. The next steps would be to increase the ETX concentration within the hydrogel matrices in order to decrease the seizures measured via EEG, and to investigate the degradation of the hydrogel matrices with magnetic resonance imaging (MRI). Future adaptations of the matrices could be done to enlarge the time window of the drug release. This adaptation could be a second layer of a degradable and biocompatible hydrogel with a smaller polymeric mesh size. This could slow down the drug release from the hydrogel matrix.

### 4.3 RESULTS AND DISCUSSION FOR FREE CURCUMIN RELEASE FROM PAAm MATRICES

Above I presented the findings for substance release from degradable alginate-based hydrogels. In this part, I present the investigated data of substance release from a synthetic PAAm based hydrogel. The substance used here was free curcumin. The aim is to investigate the release behavior from free curcumin (Cur) to gain a soft, hydrated, and curcumin releasing substratum for organotypic brain slice cultivation. Samples with 16vol.% BIS (Young's modulus around 50kPa after equilibrium swelling) were prepared and treated as described below. Shortly: samples were dehydrated in an ethanol series, infiltrated with Cur, and immersed into a storage solution in a well plate for the investigation of the Cur release. The well plate was agitated and heated from below. For the infiltration Cur solutions with different molarities, 10 $\mu$ M, 20 $\mu$ M and 50 $\mu$ M were used. Samples and curcumin solution were incubated for three days in a fridge at 4°C to generate an uptake of curcumin by swelling. The release set-up and the measurements are described below, see 4.5.1 on page 97. Also here, the supernatant was exchanged every 24h to mimic the aliquor exchange inside the brain. The cumulative release was determined via UV-Vis with double determinations of micro-volumes from each well. The data in Figure 31 were determined using a calibration curve. The calibration curve was prepared for each measurement with data from a blank (just glass absorption was measured) micro-volume plate and Cur solutions with known concentrations. An adjustment of the calibration curves was necessary since some blanks showed deviations in the absorbance while the absorbance for the known Cur concentrations was stable. With this, the data for the blanks were set to known and right data points, which resulted in an adjusted calibration curve.

For the first 24h inserted into a new solution, the curcumin release from the pAAm samples was a burst release (Figure 31). A burst release is an initial release of the substances or drugs showing a steep slope at first, which decreases rapidly after the first release. In the present case, all curcumin molecules from the pAAm surface and close to it seem to be released into the supernatant with the burst release. After the burst release, the following three days were stably from release day one to three. An enhanced release is seen after the exchange of supernatant within the first eight hours, as shown in Figure 31 on page 93. The cumulative release data points after 24h were slightly decreased. This directs to two possibilities: First, considering the fact that the release of the curcumin is enhanced in the first hours after the exchange of the supernatant due to large concentration differences of curcumin between sample and supernatant, the release is diffusion based. A later re-adsorption into the matrix could have taken place using the different chemical potentials important for the drug release.

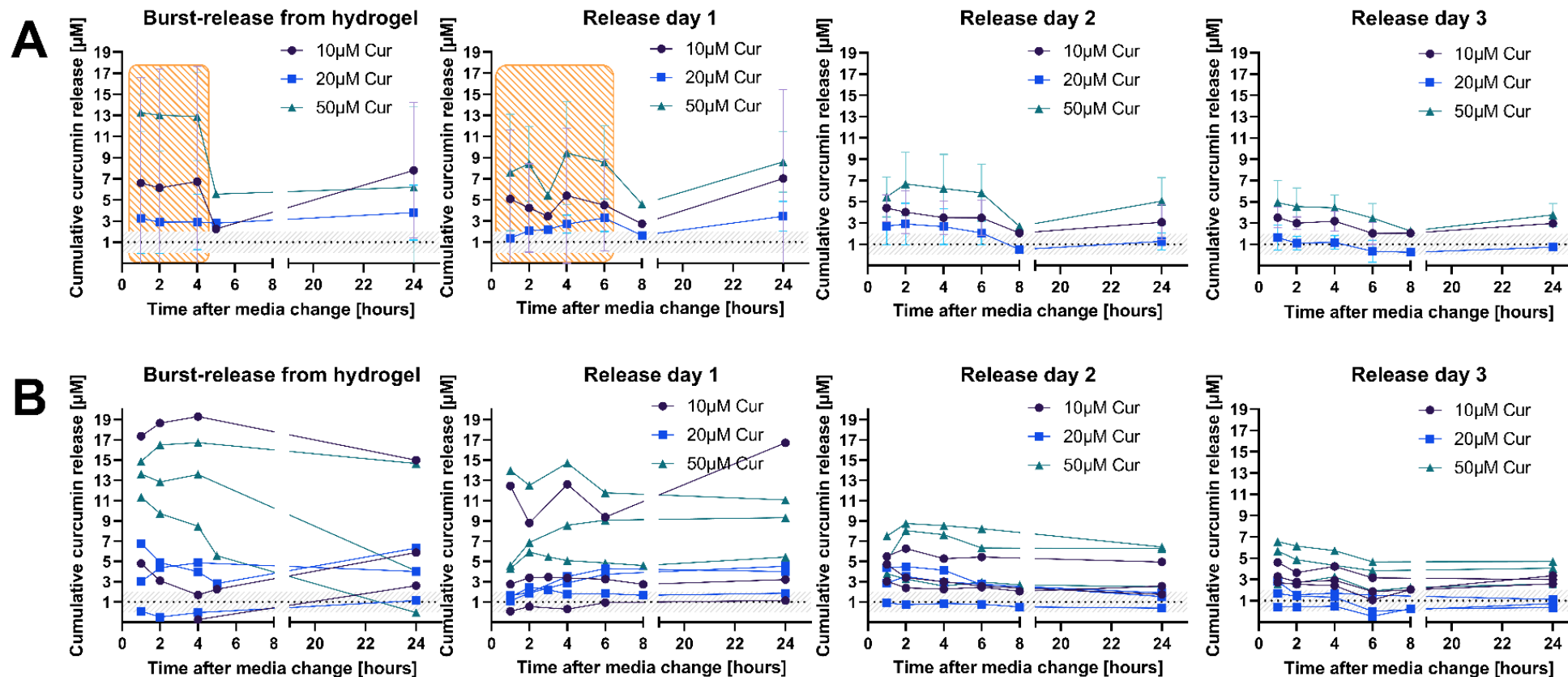


Figure 31 Data of the cumulative free curcumin release from polyacrylamide samples with 16 vol.% crosslinker. The release shows initial burst release followed from another three days of stable release for different infiltration concentrations (10µM, 20µM and 50µM curcumin) A) Data of cumulative release as mean and standard deviation from three samples. B) Curcumin release of single samples.(Calibration curve was adjusted and set stable for the determination of the blank (glass))

The curcumin could be released from the high concentration inside the hydrogel mesh towards the supernatant (water) until an equilibrium is reached and back. Second, the hydrogel sample is still swelling and takes up a solution. With this effect ongoing over time and a slow swelling assumed, the curcumin is released but also taken up from the sample again. Both hypotheses seem probable, but the latter has to be taken into account more strongly. The reasons to consider the re-infiltration of Cur into the pAAm matrices are the storage, swelling, and initial infiltration conditions. As discussed earlier in this work in chapter 2, "3D cell-matrix interaction" from page 31 on and in section 2.2.1 "Improving the 3D experimental parameter" on page 35, the equilibrium swelling required two weeks within a fridge, see Figure 10C on page 41. The storage and swelling of hydrogels inside a fridge have been investigated over several weeks as found that pAAm tends to swell for some time. Here, it was found that an equilibrium and a mean stiffness was reached after two weeks of storage. With the dehydration of the hydrogel matrices and the infiltration Cur for three days within the fridge, the full swelling capacity of the pAAm matrices could have been still available. This would lead to swelling samples within the release solution. Interestingly, the data found for 20 $\mu$ M curcumin were different and not comparable towards the 10 $\mu$ M and 50 $\mu$ M results. Here, the release was superior for the 10 $\mu$ M and 50 $\mu$ M and barely visible for 20 $\mu$ M. Since the samples for the experiments came from the same batches, it cannot result from a material property or strong aberration during the infiltration. This molecule-matrix interaction seems to depend on the curcumin concentration and its eventual clustering of molecules in a certain size.

#### 4.3.1 Conclusion

In this part of the chapter, I presented a polyacrylamide substratum infiltrated with curcumin. The release of curcumin was determined with UV-Vis. The hydrogel matrices showed a release of curcumin for several days with a large initial burst release followed with a more stable decreased release. The presented results show for each solution exchange an increased release with a decreased cumulative release after 24h. With this, the samples released the curcumin via diffusion due to concentration differences and re-absorbed the curcumin from the supernatant because of a not reached equilibrium swelling during the infiltration. The experiments showed the advantageous future applications of hydrogel substratum for *in vitro* organotypic brain slices or other organotypic cultured tissue slices. These substrates are hydrated, molecules, or substances below a certain size can enter or diffuse through to bring nutrition towards the slices. More importantly, hydrogels can generally be mechanically adapted for mechanically investigations of organotypic tissue slices similar to for the use of single cells.

## 4.4 METHODS FOR DEGRADABLE ALGINATES FOR DRUG RELEASE

With the focus to produce a biodegradable and highly biocompatible hydrogel for future localized drug release towards the brain, a well-known component, alginate, was chosen. [84][237]

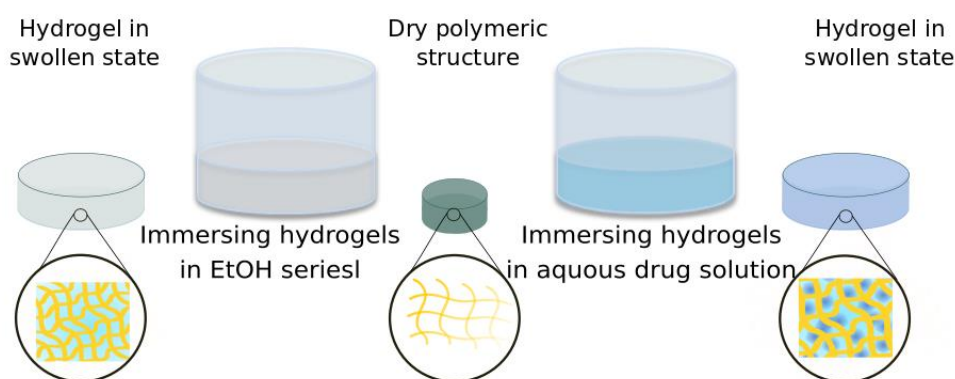
### 4.4.1 Sample preparation and characterization of degradable alginate matrices

The covalent crosslinked alginate-based hydrogel was prepared by a 2%.wt alginate solution in a 0.1M Buffer solution. The Buffer was adjusted from the traditional used 2-(*N*-morpholino)ethanesulfonic acid (MES, Sigma-Aldrich) to 3-(*N*-morpholino)propanesulfonic acid (MOPS, Sigma-Aldrich). In consequence, the comparable structure/size from MES and ethosuximide (ETX, Sigma-Aldrich), which has been overlaid with each other during the first HPLC measurements, did not give false-positive results. The crosslinker used was adipic acid dihydrazide, which formed with the free carboxylate groups of the alginate mediated by 1-ethyl-3-(3-dimethylaminopropyl) carbodiimide hydrochloride (EDC, Alfa Aeser). This bond is degradable by the hydrolysis of the resulting hydrazine bonds between the carboxylate groups and the adipic acid dihydrazide (AAD, Sigma-Aldrich). [78], [227], [237] Three different AAD concentrations, 0.094M, 0.15M, and 0.2M, dissolved in 2wt.% alginate (Sigma-Aldrich) have been assessed for mechanical and substance release as well as biocompatibility and cell adhesion properties. The EDC concentration has been kept constant with 0.104M in MOPS buffer. For the biocompatibility, the samples of 800 $\mu$ L starting volume were washed twice and placed into an EtOH series, 70%.vol - 99%.vol, to dry the structure. Immediately after, the samples were washed and placed into sterilized bi.dest. water overnight for swelling. Following, the samples were placed in 5ml cell medium (DMEM, 1% penstrep, 10% FBS) into an incubator for seven days before the cytotoxicity tests have been performed. For the cell adhesion tests, the samples were washed, sterilized in 70%.vol EtOH for 15minutes and washed with 2-(4-(2-Hydroxyethyl)-1-piperazinyl)-ethansulfonic acid (HEPES, Sigma-Aldrich) with pH 8.5. Cell adhesion was checked with fibronectin as well as with collagen I biofunctionalization to test the consequences about the carboxylate groups already used for the crosslinking and the direct impact on the cell adhesion morphology. In order to characterize the mechanical properties of the covalently crosslinked alginates and to determine the matrix mesh size, AFM measurements were applied and analyzed with the Hertz-model. The samples with the lowest and the highest concentration of crosslinker were investigated. For this, samples of an initial height were produced, washed twice, and placed into bi. dest. water for 24h in order to create similar mechanical and mesh size conditions for the characterized samples as well as those used for drug release investigations. The alginate samples were attached to functionalized glass slides and later glued into petri dishes so that they could not move around while measuring the stiffness. The glass slides were functionalized as described in 6.4 "Hydrogel fixation on glass slides" on page X in the appendix, which serves as an interface for

covalent bonding with the alginate hydrogel. For the covalent bonding, the alginate was poured into a PTFE mold, and the functionalized glass slide was placed over the solution. [243]–[246] Calibration of the spring constant  $k$ , bead attachment, and measurement of the sensitivity from the cantilever were done before the AFM measurements. For each sample, three different macro positions were chosen, at least 1mm apart from each other. Each macro position was determined with nine micro positions 25 $\mu$ m apart from each other, measuring ten times each micro position. This was followed by measuring one micro position 100 times to assess eventual viscous behavior from the sample. The resulting force spectra curves were evaluated using the Hertz-model with the matlab code written from Huth et. al..

#### 4.4.2 Drug infiltration into hydrogel samples

For the substance infiltration, the whole procedure is depicted below (Figure 32A). The samples were dried with an EtOH series. Afterwards the excess EtOH was taken from the samples with a tissue and weighted. Subsequently, the samples were placed into the ETX solution for 24h to transform from the glassy polymeric state towards the swollen and drug-loaded state. Later, 24h after immersion into the drug bearing solution, the samples were measured again. From the up-take of the solution, the theoretical drug loading was determined as the concentrations of the ETX were known. Three different ETX concentrations were examined: 0.5M, 1M, and 2M ETX. For the dissolution of ETX bi.dest. water was used, and the vortex was used. For the 2M solution, it was visible that a supersaturation took place. Once the solution was agitated, a fine whitish suspension appeared into the solution following with a clearing of the suspension and the materializing of ‘oily’ droplets into a clear solution as described in the literature.[236], [247]



*Figure 32 Sketch of infiltration routine for the substances such as ETX and curcumin into the hydrogels. Polymerized hydrogels in the swollen state are immersed into an EtOH series to remove the water from the hydrogel matrices. This is followed by wiping the EtOH from the matrices. Next, matrixes are immersed in an aqueous solution inhibiting the favored substance.*



Each sample was placed into 1ml ETX solution, which was agitated directly before adding the sample into a 24 well plate. For one independent release experiment, each ETX concentration was infiltrated into three samples of each alginate sample type characterized after the three AAD concentration. For the control measurements, the different alginate samples were immersed into bi. dest. water. In order to determine the drug release from the swollen samples as close to *in vivo* conditions as possible, the release was conducted inside an incubator to mimic the temperature conditions and agitated at 80rpm with a plate (KS 130 basic, IKA) in order to mimic the *in vivo* dynamics. Moreover, the liquid system in which the swollen samples were immersed was an artificial buffer system of 5mL (recipe see appendix 6.9 “Artificial brain liquor for release experiments” on page XV in the appendix) and was exchanged every 24h for 20 days from glass vials with lid (22mm diameter x 50mm height, avantor). This exchange was applied to mimic a dynamic solution exchange like the brain liquor inside the brain. Extracts were taken at various time points 3h, 24h, 48h, 72h and 7d, and placed in tubes directly into a freezer at -20°C for storage. From the collected extracts, the accumulated ETX concentration was determined via HPLC measurements. The HPLC measurements of ETX concentrations have been kindly conducted from Hanna Götsche in the group ‘Pharmazeutische Technologie and Biopharmazie’ of Prof. Dr. Regina Scherließ at the Institute of Pharmazie at Christian-Albrechts-Universität zu Kiel. Consequently, the exchange of artificial liquor was performed for 20 days. Each day, the samples were visually examined whether the alginate matrix has been completely degraded.

## 4.5 PAAM AS HYDROGEL MATRIX FOR MOLECULE RELEASE

### 4.5.1 Sample preparation and characterization

For the initial study of the release of free curcumin from a hydrogel matrix, a synthetic non-degradable hydrogel, polyacrylamide (pAAm), has been prepared. This project has been conducted in cooperation with Christina Schmidt from the group of Priv.-Doz. Dr. rer. nat. Kirsten Hattermann-Koch of the Institute of Anatomy. The polyacrylamide has been prepared with 16vol.% crosslinker to the whole solution. For the whole precursor solution 1000µL AAm, 800µL BIS; 3075µL bi. dest water, 50µL HEPES and 75µL APS has been mixed, and degassed for at least 5 minutes. Next, the last initiator, TEMED, has been placed into the beaker glass and the solution was thoroughly merged by resuspension.

Following, 800µL precursor solution was poured into a PTFE mold with a diameter of 1.5mm and a height of 5mm. Samples were washed in bi. dest. water and immersed for swelling for two weeks. Next, the pAAm samples were immersed in EtOH and a series of concentrations from 70 vol.% to 99 vol.% to remove the water from the matrix, as shown above (Figure 32). The samples, now in a glassy

state, were measured and immersed into 2mL curcumin (Sigma-Aldrich) solution of different concentrations. Consequently, the samples took up the solution, and the curcumin were infiltrated into the matrix. The concentration used were 10 $\mu$ M, 20 $\mu$ M, and 50 $\mu$ M and as control bi. dest. water. After three days immersed at 4°C in the dark, samples were measured to determine the swelling and the curcumin concentration available.

For each weight measurement, the excess solutions were swabbed away with a paper, and the supernatant was collected for quantification. For the examination of the release, the samples were placed into 2mL water in a 12-well plate (Sarstedt) on a shaker (IKA) at 300rpm. Heating was administered from beyond with 37°C. The cumulative release was determined for every 24h for 1h, 2h, 4h, 6h, 8h for in total four days. The supernatant was exchanged accordingly, every 24h to mimic a dynamic system. The extract was taken in a volume of 2 $\mu$ L, and the concentration was determined with UV-Vis at 202nm wavelength in a micro-volume plate (Biotech).

## 5 CONCLUSION AND PROSPECTS OF THE PRESENTED WORK

---

In this work, the trinity of bio-matrix interaction from the surface to volume with additional drug release has been investigated. The determination has been done towards an enhanced understanding of cell-matrix and substance-matrix interaction. These are the keys and major objections necessary for augmented implant designs within soft tissue aiming for local substance release. For this superior aim, this work was divided into the sections 3D matrix-cell interaction, 2D cell-matrix interaction, and drug release.

In the first part, mammalian cellular behavior within 3D microstructured as function towards the mechanical properties have been investigated in pAAm hydrogels. The range of the mechanical properties was chosen according to the range of soft tissue within the human body. The lower set-point was the brain as the softest tissue possible. Here I reached a Young's moduli of  $1.1\text{kPa} \pm 0.54\text{kPa}$  with a 1vol.% crosslinker concentration. The highest set-point was chosen to be in the range of muscle tissue and reached a Young's moduli of  $50.09\text{kPa} \pm 4.32\text{kPa}$  with a 16vol.% crosslinker concentration. For the necessary biofunctionalization with collagen I, a bio-crosslinker was incorporated within the precursor with a successfully proved concentration of  $35.47\mu\text{M}$ . With these approaches, I was able to show a relation between the cellular behavior in soft 3D environments connected with the architectural sample features. The cells did not just react towards the mechanical clues, e.g., with rupture events of the nuclear envelope, but had a strong preference of location within the structured matrix. Here it is conclusively shown that an implant not just needs to be compliant in a mechanical point of view but must display architectural features that support the preferred cellular reaction. Prospects for this approach of 3D microstructured *in vitro* samples are live cell staining for migration related cell compartments to gain more in-depth knowledge about the use of myosin or actin based migration path within soft structures.

As the lamin concentration mediates the nuclear envelope stiffness, additional tests with varying lamin concentrations in cells and stained or transfected adhesion proteins like zyxin would broaden the information gained during the experiments within the microstructured hydrogels. With this sample type the use for traction force microscopy (TFM) could be used extensively in order to investigate the 3D cell-matrix interaction inside pre-structures environments. This would be beneficial as some influencing factors can be excluded, such as the need for cells to find a new path through the embedding environment.

The investigations of 2D cell-matrix interaction followed this work. Here, the main emphasis was on the cell interaction towards a protein inert hydrogel pHEMA with an incorporated newly designed bio-crosslinker. This bio-crosslinker can be incorporated into any hydrogel, which is synthesized using radical polymerization. The free protein binding unit is highly susceptible to cysteine, which is present in large amounts in fibronectin. For the protein inert hydrogel pHEMA it was possible with the new bio-crosslinker to increase the cell attachment. After 24h the pHEMA surface was covered with cells over 25%. For this the surface was biofunctionalized with 10 $\mu$ g/ml fibronectin. The favorable biocompatibility of pHEMA was maintained with the bio-crosslinker incorporated. For this work, prospects and next steps are the applications if the BCL not only in pHEMA but also in other hydrogels such as in pAAm and applicate the BCL for 3D microstructures hydrogels. Moreover, establishing this new bio-crosslinker to a standard BCL for biomaterials would reduce the time necessary for biofunctionalizations and enable high throughput investigations.

Since local substance release was an essential feature in the last part of my work, I demonstrated the drug release from two different systems. In the first approach, it was shown that a time prolonged release in dependence of the internal hydrogel structure is possible. The drug ETX was released even after 72h, and the degradability of the covalently crosslinked alginate matrix was existent in the present of the infiltrated substance. This shows the availability of this system for future *in vivo* application. For the second approach, a release from non-degradable matrices of pAAm was established with curcumin, an anti-inflammatory substance. It was shown here for both approaches that the drug concentration is an essential factor for the successful release. In the future this acquired knowledge can be used for future *in vivo* and *in vitro* applications. The degradability, biocompatibility, and compliance of covalently crosslinked alginate with ETX made it to a perfect hydrated implant for local drug release *in vivo*. More, applying a degradable layer on top could prolong the release much further. For the second approach, it has been shown that substance such as curcumin can be steadily released from hydrated matrices. This can be used in order to create a softer substratum for organotypic tissue slices, e.g., brain slices, in order to investigate various stiffness influences.

Overall, the common objective of these studies was the augmentation about the knowledge of matrix interaction in regard to cells with different dimensionalities and the matrix substance interaction. All three topics are related through three mayor points necessary to consider while working with biomaterials: matrix structural size, matrix topography or architecture, and dimensionality. Each point will feature reactions and emphasize the importance when designing biomaterials for actual clinical use.



## 6 APPENDIX

---

### 6.1 LISTS OF CHEMICALS AND DEVICES

Tab. A. 1 Companies of chemicals and cells part 1

Chemicals and Cells	Company
1-ethyl-3-(3-dimethylaminopropyl) carbodiimide hydrochloride	Alfa Aesar
2-(4-(2-Hydroxyethyl)-1-piperazinyl)-ethansulfonsäure	Sigma-Aldrich
2-(N-morpholino)ethanesulfonic acid	Sigma-Aldrich
(3-(N-morpholino)propanesulfonic acid)	Sigma-Aldrich
6-well plates	Sarstedt
12-well plates	Sarstedt
24-well plates	Sarstedt
3-(Trimethoxysilyl)propyl methacrylate	Sigma-Aldrich
Acrylamide solution 40%	Bio-Rad
adipic acid dihydrazide	Sigma-Aldrich
<i>Acanthamoeba castellanii</i>	
Acetic acid	Sigma-Aldrich
Accutase	Biochrom
Ammonium persulfate	Sigma-Aldrich
Acrylic acid N-hydroxysuccimide ester	Sigma-Aldrich
Alginate sodium salt	Sigma-Aldrich
Ammonium iron(II) sulfate hexahydrate	AppliChem
$\beta$ -alanine	Alfa aesar
Bead for cantilever	glass, microparticles GmbH
Bi distilled water	AppliChem
Calcein AM	BD science
Calciumchloride	AppliChem
Collagen I	BioMatrix
Curcumin	Sigma-Aldrich
diethyleneglycol	Jkchemicals
DetachKit (C-41210; PromoCell, Heidelberg)	PromoCell
Dulbecco's modified eagle medium	Biochrom
Dimethylsulfoxid,	Sigma-Aldrich
Dimethylformamide	Acros Organics
Disodium hydrogen phosphate heptahydrate	Roth
Ethylenglycol dimethacrylate	Sigma-Aldrich
Ethanol	Walter
Ethosuximide	Sigma-Aldrich
Fetal bovine serum	Biochrom
Fluorescein isothiocyanate – Dextran 500.000 – Conjugate	Sigma-Aldrich

FluoroBrite™ DMEM	Gibco
Fibronectin	BioMatrix

Tab. A. 2 Companies of chemicals and cells part 2

Chemicals and cells	Company
D-glucose	Sigma-Aldrich
Glue, biocompatible two component glue , Reprorubber	Islandia, USA
Glue; UHU Plus Schnellfest	UHU GmbH & Co. KG
GlutaMAX™	Gibco, Germany
N-hydroxysuccinimide	Apollo Scientific
Hydroxyethyl methacrylate	TCI
Hydrochloric acid 37%	Sigma-Aldrich
HUVEC medium	PromoCell
Hoechst	ThermoFischer
Ethyl acetate	Fischer Chemicals
Fibrosarcoma cells	courtesy of the Lammerding lab
Fibronectin	BioMatrix
Glass vials (Schnappdeckelgläser 22mm x 50mm)	avantor
Isopropanol	Walter, Germany
Maleic anhydride	Roth
Magnesiumchloride	Sigma-Aldrich
methacrylanhydride	TCI
MEM Earle's	Merck
Methacrylic acid	TCI
Magnesium sulfate monohydrate	AppliChem
N,N'- Methylenebisacrylamide	Bio-Rad
Sodiumhydrogencarbonate	VWR chemicals
Sodiumhydroxide	Sigma-Aldrich
p-Tolousulfonic acid	Sigma-Aldrich
Phosphate buffered saline	Sigma-Aldrich
Penicillin Streptomycin	Sigma-Aldrich
Primary Human Umbilical Vein Endothelial Cells	PromoCell
proteose peptone	BD, Sparks
Propidium Iodide	ThermoFischer
petri dish with glass bottom	IBIDI
t-ZnO synthized in presents of PVB	courtesy of the Adelung lab
polydimethylsiloxane	Sylgard 184
Potassiumchloride	Roth
Potassiumdihydrogenchloride	Roth
Poly ethyleneglycol	Jkchemicals
polydimethylsiloxane	Sylgard 184
Proteose peptone	BD science

<i>peptone yeast glucose (PYG) 712 medium</i>	
Rat embryonic fibroblasts 52 wild type	
Sodium alginate	Sigma
Sodium citrate· 2H <sub>2</sub> O	Merck
N,N,N',N'-Tetramethylenediamine	Sigma-Aldrich
Transwell (Millicell® Cell culture Inserts)	Merck
Trypsin/EDTA solution	Merck
Tetrapodal zinc oxide	courtesy of the Adelung lab
Yeast extract	BD science

Tab. A. 3 Companies of devices and software

<b>Devices and software</b>	<b>Company</b>
Andromeda	Till Photonics
Atomic force microscope, Nanowizard3	JPK Instruments
BX-43	Olympus
C-9100-13	Hamamatsu
C-9300-221	Hamamatsu
Cantilever; MikroMasch HQ:NSC36	Innovative Solutions Bulgaria Ltd.
CO <sub>2</sub> -Incubator C150	Binder
DFK 31BF03	Imaging Source
CellSence	Olympus
Excell	Microsoft
Fiji (Is Just ImageJ) 2.0.0-rc-71/1.52p	
GraphPad	Prism
IC Capture	theImagingSource
iChrome MLE	Toptica Photonics AG
Java 1.8.0_66	Oracle
IX-81	Olympus
MATLAB 2013a	MathWorks
MI-IBCD-F1-AF	Tokai HIT
Microplate reader and micro-volume plate Take 3	BioTech
Motorized Stage SCAN IM 120x80	Merz
MT20E	Olympus
Nanowizard Control Software version 4.3.5	JPK Instruments
KS 130 basic	IKA
Origin	OriginLab
Progress MF cool camera	Jenoptik
ThermoMixer C	Eppendorf
U-FSHA	Olympus
Ultra-sonic bath	Bandelin electronics
Vortex Genius 3	IKA
Xcellence RT	Olympus
IX2-UCB	Olympus
sola light engine	sola light engine



Syringe	Braun
DFK 31BF03FC	theImagingSource
U-RFL-T	Olympus
10x UPlanFLN	Olympus
4x UPlanC N	Olympus
20xUPlanFL	Olympus
<b>40xUPlanFL</b>	Olympus

## 6.2 GENERAL CELL CULTURE METHODS

### 6.2.1 Rat embryonic fibroblasts and fibrosarcoma cells

The stable cell lines rat embryonic fibroblasts wild type (Ref-52-wt), and the fibrosarcoma cells (HT1080 with transfected nucleus NSL- GFP and H2B-RFP, as a courtesy from the Lammerding lab, Cornell University) were cultured similarly. All cells were cultured in an incubator at 37 °C and 5 % CO<sub>2</sub>-atmosphere (ThermoScientific, Heraeus VIOS160i). The medium for the cell culture was prepared from Dulbecco's modified eagle medium (DMEM, Biochrom, Germany), 10% Fetal bovine serum (FBS, Biochrom, Germany), and 1% penicillin streptomycin (penstrep, Sigma Aldrich, Germany). Cells were subcultivated when they reached at a confluency of 80% within the cell culture flask to keep inside the exponential growth phase. Firstly, the old cell culture medium was removed, and the cells washed with sterile phosphate buffer saline (PBS, Sigma-Aldrich). Accutase (Merck Millipore, Germany) was then added 1ml/25cm<sup>2</sup> surface, and the culture flask was 5min incubated. The cells were then detached from the flask, rinsed with cell culture medium, and centrifuged (Heraeus Megafuge8, 800 g, 4 min). Consequently, the cells were seeded into another cell culture flask for cultivation or seeded on to the experiments and cultured there.

### 6.2.2 Human umbilical vein endothelial cells (HUVEC)

Primary human umbilical vein endothelial cells (HUVEC, primary cells, PromoCell, Germany) were examined in an experimental set-up to investigate *in vitro* the biostability of a future neuroimplant. For the subcultivation, the recommended medium (C-22011, PromoCell, Germany) has been used in combination with the recommended DetachKit (C-41210; PromoCell, Heidelberg). The subcultivation has been conducted as recommended from PromoCell. Cells were not used for experiments above the 10<sup>th</sup> passage to ensure the morphological and cellular stability

### 6.2.3 *Acanthamoeba castellanii* (AC)

*Acanthamoeba castellanii* were cultured at room temperature outside from an incubator in peptone yeast glucose (PYG) 712 medium. The medium exchange and the cell subcultivation was conducted at least once a week. For the subcultivation, the cells were detached from the cell culture flask by agitating and pounding the flask bottom. Detached cells were taken to a falcon tube and centrifuged at 800 g for 4 minutes. The resultant cell pellet was resuspended, and cells were counted with a Neubauer counting chamber to determine the cell concentration per mL. Depending on the task, cells were seeded with a preferred concentration either to a culture flask for subcultivation or to an experimental set-up. The PYG medium contained following ingredients: 20 g proteose peptone (BD, Sparks, USA), 1 g of yeast extract (BD, Sparks, USA), 34 mL of 0.1 M sodium citrate· 2H<sub>2</sub>O (Merck, Germany), 10 mL of 0.005 M Fe(NH<sub>4</sub>)<sub>2</sub>(SO<sub>4</sub>)<sub>2</sub>·6H<sub>2</sub>O (AppliChem, Germany), 10 mL of 0.25 M

Na<sub>2</sub>HPO<sub>4</sub>·7H<sub>2</sub>O (Roth, Germany), 8 mL of 0.05 M CaCl<sub>2</sub> (AppliChem, Germany), 10 mL of 0.25 M KH<sub>2</sub>PO<sub>4</sub> (Roth, Germany), 950 mL of distilled water, 10 mL of 0.4 M MgSO<sub>4</sub>· 7H<sub>2</sub>O (AppliChem, Germany), and 50 mL of 2 M glucose (Sigma–Aldrich, Germany).

#### 6.2.4 Cell adhesion assay

The standard procedure after seeding and cultivating the cells to the sample surface is the staining of the cells. Therefore, a staining solution on the according to cell medium of 1/1000 calcein AM, propidium iodide (PI), and Hoechst was prepared and given to culture wells. These culture wells with samples and cultivated cells were then incubated for 20 minutes in cell culture environment and for 10 minutes at room temperature in the dark. The samples were washed three times with PBS to remove all excess dyes from the background. If not stated differently, the respective cell medium was pipetted to the cells to prevent the cells from drying and imaged immediately. Samples, which were not investigated immediately after the staining were placed back into the incubator.

The analysis of the calcein stained areas was done manually with ImageJ as well as automated (Fiji is ImageJ). [168] The threshold has been adapted manually because due to different foci planes existent in one sample. This has been done when not stated otherwise.

The averages and standard deviations of the different positions and samples were calculated. Control experiments showed the cellular behavior in cell culture wells and served as an essential check whether the cell growth, behavior, or morphology was corrupted. All controls for the adhesion assays were positive for expected cellular behavior and morphology according to the particular cell type.

#### 6.2.5 Cytotoxicity assay

First, the cell type, according to the investigated cause, was selected, if not stated differently for most experiments, Ref 52wt were chosen. Second, the samples to determine were sterilized with 70 vol.% EtOH and placed in the respective cell culture medium for 72h. The third step was to seed 10 000 cells per well in a 96 well plate with 100µL medium for 24h. After this 24h the extracts of different concentration (100 %, 70 %, 50 %, 15 %, 0 % v/v) with the respective cell culture medium was added to the cells for another 24h. Next, the 50µL MTT solution, 1mg/mL MEM Earle's (Gibco, USA), was added to the cell culture for 2h to be metabolized. The sixth step included the exchange of MTT with 100µL isopropanol in order to destroy the cell membrane and dissolve the formatted formazan in an amount respective to the viability of the cells. The quantification of the cell viability as the last step of this method is done by UV/Vis. A microplate reader (EPOCH<sup>2</sup>, BioTek Instrument Inc. Switzerland) was used at the wavelength of 570nm. [145], [146]

### 6.3 IMAGING THE CELL-MATRIX INTERACTION

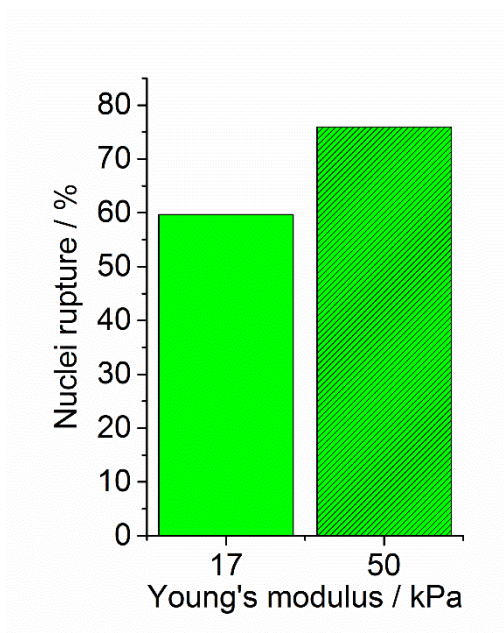
For the presented studies on 2D samples, two different microscopes were used to obtain phase contrast, fluorescence, and reflective light images. The first microscope, an inverted IX81 (Olympus, with the software CellSense) was used for phase contrast and fluorescence imaging as it can be used for transparent samples only. It is equipped with a digital camera (Orca 1, HAMAMATSU), a system controller (IX2-UCB), and a laser (sola light engine).

Another microscope (BX 43, Olympus with the software IC capture) was also used for phase contrast and fluorescence imaging as well as for bright field imaging for non-transparent samples. This microscope is equipped with a DFK 31BF03FC camera from Imaging Source, a burner (U-RFL-T, Olympus). For both microscopes, the objectives 10x (Olympus, UPlanFLN) and 4x (Olympus UPlanC N) were used.

In the study about cellular behavior in 3D microstructured hydrogels, the cellular movement, in particular, the motility and deformation of the nucleus in 3D, was investigated for a duration of 10h. In general, different compartments of the cell, such as the fluorescently transfected nuclear envelope and histone rich part and the cell membrane restricted through the hydrogel channel in the phase-contrast mode, were highly interesting. For this, fast capture times and adapted light intensity for extended imaging processes were required. With these requirements spinning disc confocal fluorescence microscopy was conducted for the possibility of three-dimensional images live cell imaging obtained over time with different channels, phase contrast, and fluorescence. The set-up used is based on an inverted microscope (IX81, Olympus) with the following devices equipped and used: A C-9100-13 digital camera, a spinning disc confocal unit (Andromeda), a laser combiner (iChrome MLE) with a motorized bright field shutter (U-FSHA). Additionally, the motorized stage was used (SCAN IM 120x80) as well as a heating station (MI-IBC, Olympus) for prolonged live cell imaging. The objective 20x (Olympus, UPlanFLN) was used. For the controls the inverted microscope IX81 mentioned above was used with 10x (Olympus, UPlanFLN) and 40x (Olympus, UPlanFLN) objectives.

### 6.3.1 Experiments conducted at Cornell University in the Lammerding Lab:

The results from chapter 2, 3D cell-matrix interaction, with mammalian cells, would not have been possible without the initial experiments at Cornell University at my research stay abroad with the support from the Lammerding lab. Here I present how the initial experiments with the initial indication of a correlation of mechanical properties and nuclei rupture have been conducted (Figure 33):



*Figure 33 First indicating results of a correlation between sample stiffness of 3D microstructured samples and the rupture events of nuclei.*

Samples were placed in a custom-built PDMS (Sylgard 184) experiment chamber and imaged with a confocal laser microscope from Zeiss, LSM 700, AxioObserver. The PDMS experiment chambers were placed into a custom-built heating stage (Phillip Isermann) and heated from above to keep the cells at 37°C. The software used was ZEN black. Acquisition settings were set with chosen channels: GFP(green)  $\lambda=488\text{nm}$ , and RFP(red),  $\lambda= 555\text{nm}$ , which excites transfected nuclei of the cells. Additionally, the white light path, T-PMT, was chosen. Within the confocal mode, optimal pinhole size was set with 1AU. Depending on sample height and incubation time, the imaging of z-stacks and time series varied. In each case, a position check was made to show viable (green fluorescent nuclei) cells within the samples. In the case of the experimental timeslot of z-stacks were done to show the distribution of the cell nuclei within the hydrogel scaffold. Time-lapse imaging was done over at least 3h, best 13h. In the optimal case, time-lapse and z-stack imaging was done combined in one overnight experiment. Time intervals and frame numbers in z-stacks were varied to find the best

solution for cells in the hydrogel scaffold. Depending on the complexity of image acquisition and scanning time frame sizes vary between 1024x1024 and 512x512 Px. For videos, a 10x objective has been used for control images, a 20x objective. With this 5D imaging was conducted, since 3D images in x,y and z direction in time-lapse t and with the wavelength  $\lambda$  of the different channels were taken.

#### 6.4 HYDROGEL FIXATION ON GLASS SLIDES

To obtain hydrogels covalently bound onto glass slides, different approaches can be used. Here, a silanization with 3-(Trimethoxysilyl)propyl methacrylate was used. Glass slides were cleaned with NaOH (2.5M for 10minutes) followed with the washing in bi. dest. water for another 10 minutes in an ultrasonic bath. Next, glass slides were rinsed with EtOH (99%). This was followed by immersion of the glass slides for 15minutes in a solution from 97vol.% EtOH, 2vol.% 3-(Trimethoxysilyl)propyl methacrylate and 1vol.% acetic acid. The container with glass slides was agitated during the immersion of the glass slide. The glass slides were dried within an air stream and additionally backed in an oven at 120°C for one hour. The 3-(Trimethoxysilyl)propyl methacrylate molecules form hydroxyl groups via hydrolysis in the solution to the silane ligand. The molecules then assembly at the glass slides surface by condensation and form a covalent bond. The free methacrylate group can now be used for the covalent crosslinking of hydrogels towards the glass slide. For pAAm hydrogels, the methacrylate group is incorporated into the radical polymerization process. For the covalently crosslinked alginates, different binding scenarios are possible. Firstly, a hydrogen bonding between hydroxyl groups of the alginate and the carbonyl group. Secondly, an Aza-Micheal reaction between the secondary amine of the adipic acid dihydrazide group and the vinyl functionality of the methacrylate group. [248], [249]

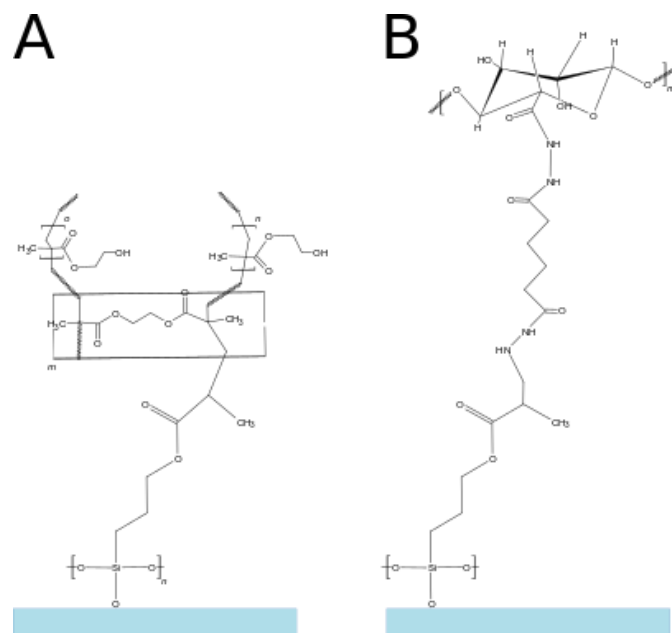


Figure 34 Scheme of possible covalent bonding between hydrogels and a glass slide. A) PAAm bound to a glass slide via radical polymerization. B) Alginate bound to the glass slide via possible aza-Michael reaction of the secondary amine of adipic dihydrazide and the vinyl group.

## 6.5 INFILTRATION OF FLUORESCENT SOLUTIONS INTO MICROSTRUCTURES HYDROGELS AND IMAGING

The process used has been described in our publication from 2019, Gutekunst *et al.*[45] Water from hydrogel samples was removed subsequently in an ethanol series starting from 50 vol.% up to 99 vol.% ethanol. The samples were washed in each concentration for at least 20 minutes. After that, the samples were immersed overnight in a solution with Fluorescein isothiocyanate – Dextran 500.000 – Conjugate (FITC- Dextran, 1.32 mg/mL, Sigma-Aldrich). After this night, the samples were imaged using confocal microscopy at 488nm in a petri dish with a glass bottom with the equipment as described above. Each z-tack was prepared by single images every 1.99 $\mu$ m. Subsequently, the z-stacks were processed using the excellence rt software (Olympus, version 1.2) using intensity voxel projection. They were resulting in measurable 3D representations. Here, tip and base of the channels were investigated. While the tip is the smallest diameter of the channel, the base is the maximum width at the origin of the tetrapod arms.

## 6.6 THE ROUTINE OF THE ALGINATE HYDROGEL PREPARATION

A 2 wt.% sodium alginate is prepared the day before and stored at 4°C overnight with the buffer MES or MOPS. Next, the AAD solution is prepared. For this, the preferred molarity, 0.094M 0.15M or 0.2M, is prepared directly with the alginate solution. Then, an EDC solution of 0.104M is prepared within the buffer solution. For the precursor mixture, the alginate-AAD solution and the EDC-buffer solution are mixed 1:1 and vortex for 10 seconds on the vortex at the highest power. Thereafter the precursor solution is transferred to a PTFE mold. The polymerization is done after 2h at room temperature under a beaker glass. After that, the samples are washed in sterile bi. dest. water at least twice. The dehydration of the samples is explained in chapter 4.4.2, Figure 32.



## 6.7 DEGRADATION OF COVALENTLY CROSSLINKED ALGINATE

The degradation of the covalent crosslinked and with RTX infiltrated samples were visually observed all 24h at the exchange of the release medium. It was checked whether the samples still are inside the aliquor. The samples were incubated at cell culture condition and agitated at 80rpm (IKA®KS 130 basic, EIMECKE). The table below shows for two independent experiments the time at which no sample was observed inside the aliquor. The infiltrated ETX is indicated by colors, it indicates the sample. For each crosslinker concentration, three technical repetitions were investigated. AAD<sub>low</sub>=AAD1= 0.094M; AAD<sub>medium</sub>= AAD2= 0.15M and AAD<sub>high</sub>= AAD3= 0.2M in 2wt.% alginate solution.

*Table 4 Days of visual control of complete hydrogel matrix degradation immersed in aliquor. The colors indicate the experiment as well as the concentration of the infiltrated ETX solution. i indicates the sample replicates.*

Time [d]	AAD1			AAD2			AAD3				
2							AAD3 Bi				
3											
4							AAD3 Aii				
5							AAD3 Aiii	AAD3 Ci	AAD3 Dii	AAD3 Diii	
6	AAD1 Ai	AAD1 Biii									
7	AAD1 Dii			AAD2 Ai	AAD2 Cii	AAD2 Ciii	AAD3 Di				
8											
9							AAD3 Bi	AAD3 Ci	AAD3 Cii	AAD3 Di	
10	AAD1 Cii			AAD2 Di	AAD2 Dii						
11	AAD1 Aiii	AAD1 Diii									
12	AAD1 Aii										
13				AAD2 Aii							
14	AAD2 Aiii	AAD2 Bi	AAD2 Ci				AAD3 Cii	AAD3 Di			
15	AAD1 Bi			AAD2 Bi			AAD3 Bi				
16	AAD1 Bi										
17	AAD1 Bii	AAD2 Ai	AAD2 Aii								
18											
19											
20	AAD1 Di	AAD1 Bii	AAD1 Ci	AAD2 Aiii	AAD2 Ci	AAD2 Di	AAD3 Ai				
	AAD1 Ciii	AAD1 Di		AAD2 Bii	AAD3 Biii	AAD2 Ci					

Infiltrated ETX:      First experiment      Second experiment

0M ETX
0.5M ETX
1.5M ETX
2M ETX

0M ETX
0.5M ETX
1.5M ETX
2M ETX

## 6.8 DELAYED SUBSTANCE RELEASE FROM ALGINATE MATRICES OBTAINED WITH PHEMA LAYER

Initial experiments for a delayed substance release were investigated additionally using covalently crosslinked alginate filled with methylene blue (Sigma Aldrich, Germany) and covered with a pHEMA

layer. The synthesis of the alginate matrices was conducted as described earlier, all three AAD concentrations were used. For the infiltration of the methylene blue, the samples were dried as explained in Figure 32 on page 96 and immersed for 24h into a methylene blue solution with a concentration of 1mg/ml. Subsequently, the samples were dried again. The dried alginate samples containing methylene blue were covered with a pHEMA layer using initial chemical vapor deposition (iCVD). For each sample, a layer of 800nm pHEMA with different was deposited. Different crosslinker concentrations of EGDMA were used (25mol.%, 50mol.%, and 75mol.%). These samples were placed into a glass container with 20 ml bi.dest. water at cell culture conditions. Samples were taken at different times and measured via UV-vis at 660nm. As expected, the first hours after the immersion shows no release since the samples were dry and needed to swell (Figure 35). Later, a clear trend for the release is visible: The lowest release rate is obtained from the samples with the highest amount of crosslinker (green), followed by a mix of medium and the lowest amount of crosslinker. However, these first data points indicate an influence of the pHEMA layer, as the slopes are the highest without the pHEMA layer. Despite this, more investigations need to be done for this approach, especially with a degradable layer that matches its degradation to the covalently crosslinked alginate. Furthermore, the substances released should be similar to those for the planned application or, in an optimal case, the drugs used for the planned clinical animal studies as these drugs will most probably interact entirely differently with the hydrogel matrices as model drugs or substances.

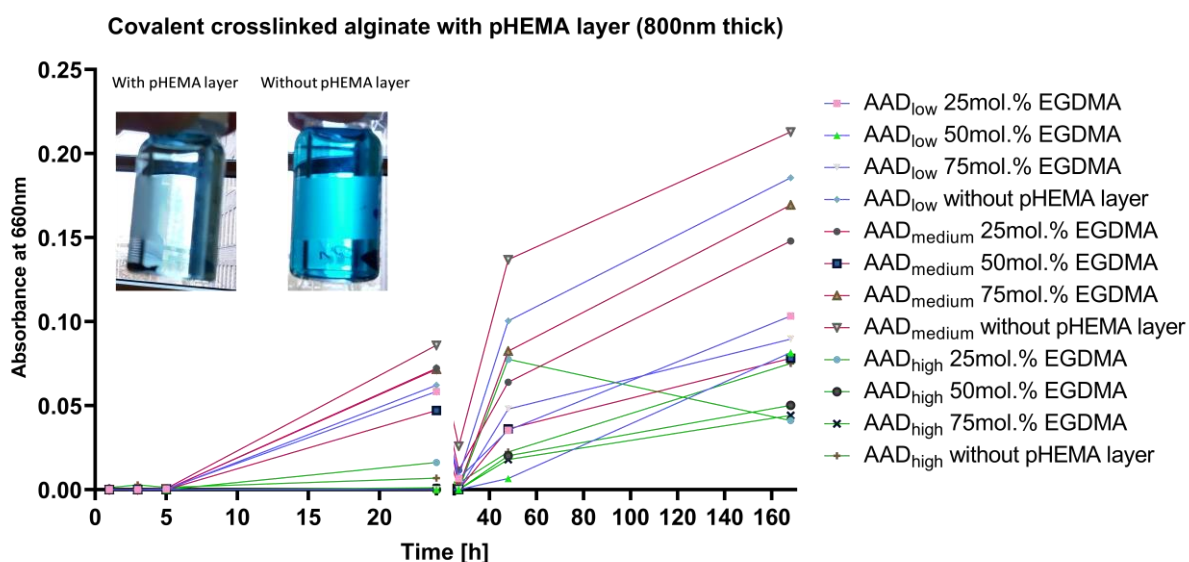


Figure 35 Delayed release of methylene blue from covalent crosslinked alginate with pHEMA layer. Blue lines indicate the experiments with the smallest amount of crosslinker inside the alginate, pink indicates the medium amount of crosslinker, and green indicates the highest amount of crosslinker.

## 6.9 ARTIFICIAL BRAIN LIQUOR FOR RELEASE EXPERIMENTS

The recipe for the artificial brain liquor (aliquor) was provided by Christina Schmitt. For each experiment, a new batch of sterilized via filtration was prepared and stored at 4°C. The chemicals below were added together and dissolved in bi. dest. water.

124mM NaCl
1,3mM MgCl <sub>2</sub>
5mM KCl
2mM CaCl <sub>2</sub>
26mM NaHCO <sub>3</sub>
10mM D-Glucose
Sterile bi. dest. water

## 6.10 CALIBRATION OF THE CANTILEVER

The calibration of the cantilever ( $\mu$ Mesh HQ:NSC 36, always the right one) used for the AFM measurements is vital due to its meaning for the measured results. The calibration provides the spring constant of the cantilever. For the measurements done, the cantilevers were calibrated via thermal noise analysis. This is a function already installed into the used AFM set-up from Olympus. Initially, the cantilever is installed into the AFM, the laser aligned to the center of the cantilever tip and the sensitivity of it was calculated. For this, the cantilever was approached towards a glass surfaced for several spectroscopy curves, and the slope of these has been calculated. From the slope, the sensitivity was determined as:

$$sensitivity \left[ \frac{nm}{V} \right] = \frac{1}{slope \left[ \frac{V}{\mu m} \right]} * 1000 \quad (28)$$

Following, the spring constant  $k$  was determined. For this and the cantilever oscillate close to the resonance frequency of the cantilever. This results in a peak from the resonance against the frequency. By determining the energy of the resonance by measuring the area under the peak, the spring constant can be determined. As described from Hutter et al. [250] Furthermore, for the application of the Hertz-model, a spherical indentation body is required. Therefore, a bead of the size from  $21.82 \mu m \pm 0.87 \mu m$  (glass, microparticles GmbH, Berlin, Germany) was glued to the tip of the

cantilever, followed by the second determination of the cantilever's sensitivity. This has to be done as each change of mass of the cantilever changes also the behavior. Each measurement of the sensitivity has to be done before every measurement when newly installed the medium, e.g., water or cell culture medium, was changed.

## LIST OF PUBLICATIONS:

---

C. Chluba, K. Siemsen, C. Bechtold, C. Zamponi, C. Selhuber-Unkel, E. Quandt, R. Lima de Miranda (2020): Microfabricated bioelectrodes on self-expandable NiTi thin film devices for implants and diagnostic instruments. *Biosensors and Bioelectronics*, 153, 112034.

doi: 10.1016/j.bios.2020.112034

C. Appiah, C. Arndt, K. Siemsen, A. Heitmann, A. Staubitz, C. Selhuber-Unkel (2019): Living Materials Herald a New Era in Soft Robotics. *Advanced Materials*, 1807747.

doi: 10.1002/adma.201807747

S. Gutekunst, K. Siemsen, S. Huth, A. Möhring, B. Hesseler, M. Timmermann, I. Paulowicz, Y. Mishra, L. Siebert, R. Adelung, C. Selhuber-Unkel (2019): 3D Hydrogels Containing Interconnected Microchannels of Subcellular Size for Capturing Human Pathogenic *Acanthamoeba Castellanii*. *ACS Biomaterials Science & Engineering*, 5 (4), 1784-1792.

doi: 10.1021/acsbmaterials.8b01009

## BIBLIOGRAPHY

---

- [1] T. J. Kirby and J. Lammerding, "Emerging views of the nucleus as a cellular mechanosensor," *Nat. Cell Biol.*, vol. 20, pp. 373–381, 2018.
- [2] K. Munk, C. Abröll, T. Kurth, T. Langer, R. Nethe-Jaenchen, G. Pohl-Apel, H. Schlatter, B. Schultze, and K. Wolf, *Taschenlehrbuch Biologie Biochemie - Zellbiologie*. Stuttgart, New York: Georg Thieme Verlag, 2008.
- [3] F. J. Calero-Cuenca, C. S. Janota, and E. R. Gomes, "Dealing with the nucleus during cell migration," *Curr. Opin. Cell Biol.*, vol. 50, pp. 35–41, 2018.
- [4] L. F. Kadem, "Nanostructured and photoswitchable biointerfaces for controlling cell adhesion," Dissertation, Christian-Albrechts University of Kiel, 2016.
- [5] K. Wolf, M. te Lindert, M. Krause, S. Alexander, J. te Riet, A. L. Willis, R. M. Hoffman, C. G. Figdor, S. J. Weiss, and P. Friedl, "Physical limits of cell migration: Control by ECM space and nuclear deformation and tuning by proteolysis and traction force," *J. Cell Biol.*, vol. 201, no. 7, pp. 1069–1084, 2013.
- [6] A. J. Earle, T. J. Kirby, G. R. Fedorchak, P. Isermann, J. Patel, S. Iruvanti, S. A. Moore, G. Bonne, L. L. Wallrath, and J. Lammerding, "Mutant lamins cause nuclear envelope rupture and DNA damage in skeletal muscle cells," *Nat. Mater.*, vol. 19, no. 4, pp. 464–473, 2020.
- [7] C. L. Stewart, K. J. Roux, and B. Burke, "Blurring the Boundary: The Nuclear Envelope Extends Its Reach," *Science.*, vol. 318, no. 5855, pp. 1408–1412, 2007.
- [8] M. Krause, F. W. Yang, M. te Lindert, P. Isermann, J. Schepens, R. J. A. Maas, C. Venkataraman, J. Lammerding, A. Madzvamuse, W. Hendriks, J. te Riet, and K. Wolf, "Cell migration through three-dimensional confining pores: speed accelerations by deformation and recoil of the nucleus," *Philos. Trans. R. Soc. B Biol. Sci.*, vol. 374, no. 1779, p. 20180225, 2019.
- [9] A. D. Stephens, E. J. Banigan, S. A. Adam, R. D. Goldman, and J. F. Marko, "Chromatin and lamin A determine two different mechanical response regimes of the cell nucleus," *Mol. Biol. Cell*, vol. 28, no. 14, pp. 1984–1996, 2017.
- [10] J. Irianto, C. R. Pfeifer, R. R. Bennett, Y. Xia, I. L. Ivanovska, A. J. Liu, R. A. Greenberg, and D. E. Discher, "Nuclear constriction segregates mobile nuclear proteins away from chromatin," *Mol. Biol. Cell*, vol. 27, no. 25, pp. 4011–4020, 2016.

- [11] G. R. Fedorchak, A. Kaminski, and J. Lammerding, "Cellular mechanosensing: Getting to the nucleus of it all," *Prog. Biophys. Mol. Biol.*, vol. 115, no. 2–3, pp. 76–92, 2014.
- [12] L. E. McNamara, R. Burchmore, M. O. Riehle, P. Herzyk, M. J. P. Biggs, C. D. W. Wilkinson, A. S. G. Curtis, and M. J. Dalby, "The role of microtopography in cellular mechanotransduction," *Biomaterials*, vol. 33, no. 10, pp. 2835–2847, 2012.
- [13] P. Friedl, K. Wolf, and J. Lammerding, "Nuclear mechanics during cell migration," *Curr. Opin. Cell Biol.*, vol. 23, no. 1, pp. 55–64, 2011.
- [14] M. Maninová, M. P. Iwanicki, and T. Vomastek, "Emerging role for nuclear rotation and orientation in cell migration," *Cell Adh. Migr.*, vol. 8, no. 1, pp. 42–48, 2014.
- [15] P. Isermann and J. Lammerding, "Nuclear Mechanics and Mechanotransduction in Health and Disease," *Curr. Biol.*, vol. 23, no. 24, pp. R1113–R1121, 2013.
- [16] S. R. Peyton, C. M. Ghajar, C. B. Khatiwala, and A. J. Putnam, "The emergence of ECM mechanics and cytoskeletal tension as important regulators of cell function," *Cell Biochem. Biophys.*, vol. 47, pp. 300–320, 2007.
- [17] R. Paul, P. Heil, J. P. Spatz, and U. S. Schwarz, "Propagation of Mechanical Stress through the Actin Cytoskeleton toward Focal Adhesions: Model and Experiment," *Biophys. J.*, vol. 94, no. 4, pp. 1470–1482, 2008.
- [18] D. A. Starr and H. N. Fridolfsson, "Interactions Between Nuclei and the Cytoskeleton Are Mediated by SUN-KASH Nuclear-Envelope Bridges," *Annu. Rev. Cell Dev. Biol.*, vol. 26, no. 1, pp. 421–444, 2010.
- [19] A. J. S. Ribeiro, A. K. Denisin, R. E. Wilson, and B. L. Pruitt, "For whom the cells pull: Hydrogel and micropost devices for measuring traction forces," *Methods*, vol. 94, pp. 51–64, 2016.
- [20] J. Zhong, Y. Yang, L. Liao, and C. Zhang, "Matrix stiffness-regulated cellular functions under different dimensionalities," *Biomater. Sci.*, vol. 8, no. 10, pp. 2734–2755, 2020.
- [21] M. Maninová and T. Vomastek, "Dorsal stress fibers, transverse actin arcs, and perinuclear actin fibers form an interconnected network that induces nuclear movement in polarizing fibroblasts," *FEBS J.*, vol. 283, no. 20, pp. 3676–3693, 2016.
- [22] I. Dupin, Y. Sakamoto, and S. Etienne-Manneville, "Cytoplasmic intermediate filaments mediate actin-driven positioning of the nucleus," *J. Cell Sci.*, vol. 124, no. 6, pp. 865–872, 2011.
- [23] S. I. Fraley, Y. Feng, R. Krishnamurthy, D.-H. Kim, A. Celedon, G. D. Longmore, and D. Wirtz, "A

- distinctive role for focal adhesion proteins in three-dimensional cell motility," *Nat. Cell Biol.*, vol. 12, no. 6, pp. 598–604, 2010.
- [24] P. Hernández-Varas, U. Berge, J. G. Lock, and S. Strömblad, "A plastic relationship between vinculin-mediated tension and adhesion complex area defines adhesion size and lifetime," *Nat. Commun.*, vol. 6, no. 7524, pp. 1–13, 2015.
- [25] K. A. Jansen, P. Atherton, and C. Ballestrem, "Mechanotransduction at the cell-matrix interface," *Semin. Cell Dev. Biol.*, vol. 71, pp. 75–83, 2017.
- [26] A. D. Doyle and K. M. Yamada, "Mechanosensing via cell-matrix adhesions in 3D microenvironments," *Exp. Cell Res.*, vol. 343, pp. 60–66, 2016.
- [27] B. Geiger and K. M. Yamada, "Molecular architecture and function of matrix adhesions," *Cold Spring Harb. Perspect. Biol.*, vol. 3, no. 5, pp. 1–21, 2011.
- [28] B. Geiger, J. P. Spatz, and A. D. Bershadsky, "Environmental sensing through focal adhesions," *Nat. Rev. Mol. Cell Biol.*, vol. 10, no. 1, pp. 21–33, 2009.
- [29] N. Q. Balaban, U. S. Schwarz, D. Riveline, P. Goichberg, G. Tzur, I. Sabanay, D. Mahalu, S. Safran, A. Bershadsky, L. Addadi, and B. Geiger, "Force and focal adhesion assembly: A close relationship studied using elastic micropatterned substrates," *Nat. Cell Biol.*, vol. 3, no. 5, pp. 466–472, 2001.
- [30] F. Rosso, A. Giordano, M. Barbarisi, and A. Barbarisi, "From Cell-ECM interactions to tissue engineering," *J. Cell. Physiol.*, vol. 199, no. 2, pp. 174–180, 2004.
- [31] Y. Kim, H. Ko, I. K. Kwon, and K. Shin, "Extracellular Matrix Revisited: Roles in Tissue Engineering," *Int. Neurorol. J.*, vol. 20, no. Suppl 1, pp. S23-29, 2016.
- [32] C. Frantz, K. M. Stewart, and V. M. Weaver, "The extracellular matrix at a glance," *J. Cell Sci.*, vol. 123, no. 24, pp. 4195–4200, 2010.
- [33] R. O. Hynes, "The Extracellular Matrix: Not Just Pretty Fibrils," *Science.*, vol. 326, no. 5957, pp. 1216–1219, 2009.
- [34] C. C. DuFort, M. J. Paszek, and V. M. Weaver, "Balancing forces: architectural control of mechanotransduction," *Nat. Rev. Mol. Cell Biol.*, vol. 12, no. 5, pp. 308–319, 2011.
- [35] W. P. Daley, S. B. Peters, and M. Larsen, "Extracellular matrix dynamics in development and regenerative medicine," *J. Cell Sci.*, vol. 121, no. 3, pp. 255–264, 2008.
- [36] P. Lu, K. Takai, V. M. Weaver, and Z. Werb, "Extracellular Matrix Degradation and Remodeling in Development and Disease," *Cold Spring Harb. Perspect. Biol.*, vol. 3, no. a005058, pp. 1–24,



- 2011.
- [37] R. J. Petrie, H. M. Harlin, L. I. T. Korsak, and K. M. Yamada, "Activating the nuclear piston mechanism of 3D migration in tumor cells," *J. Cell Biol.*, vol. 216, no. 1, pp. 93–100, 2017.
- [38] D. E. Discher, "Tissue Cells Feel and Respond to the Stiffness of Their Substrate," *Science.*, vol. 310, no. 5751, pp. 1139–1143, 2005.
- [39] G. Charras and E. Sahai, "Physical influences of the extracellular environment on cell migration," *Nat. Rev. Mol. Cell Biol.*, vol. 15, no. 12, pp. 813–824, 2014.
- [40] P.-H. Wu, D. M. Gilkes, and D. Wirtz, "The Biophysics of 3D Cell Migration," *Annu. Rev. Biophys.*, vol. 47, no. 1, pp. 549–567, 2018.
- [41] A. Fruleux and R. J. Hawkins, "Physical role for the nucleus in cell migration," *J. Phys. Condens. Matter*, vol. 28, no. 36, pp. 1–11, 2016.
- [42] A. W. Holle, N. Govindan Kutty Devi, K. Clar, A. Fan, T. Saif, R. Kemkemer, and J. P. Spatz, "Cancer Cells Invade Confined Microchannels via a Self-Directed Mesenchymal-to-Amoeboid Transition," *Nano Lett.*, vol. 19, no. 4, pp. 2280–2290, 2019.
- [43] P. M. Davidson, C. Denais, M. C. Bakshi, and J. Lammerding, "Nuclear Deformability Constitutes a Rate-Limiting Step During Cell Migration in 3-D Environments," *Cell. Mol. Bioeng.*, vol. 7, no. 3, pp. 293–306, 2014.
- [44] M. Miron-Mendoza, J. Seemann, and F. Grinnell, "The differential regulation of cell motile activity through matrix stiffness and porosity in three dimensional collagen matrices," *Biomaterials*, vol. 31, no. 25, pp. 6425–6435, 2010.
- [45] S. B. Gutekunst, K. Siemsen, S. Huth, A. Möhring, B. Hesseler, M. Timmermann, I. Paulowicz, Y. K. Mishra, L. Siebert, R. Adelung, and C. Selhuber-Unkel, "3D Hydrogels Containing Interconnected Microchannels of Subcellular Size for Capturing Human Pathogenic *Acanthamoeba Castellani*," *ACS Biomater. Sci. Eng.*, vol. 5, no. 4, pp. 1784–1792, 2019.
- [46] J. S. Harunaga and K. M. Yamada, "Cell-matrix adhesions in 3D," *Matrix Biol.*, vol. 30, no. 7–8, pp. 363–368, 2011.
- [47] S. I. Fraley, Y. Feng, D. Wirtz, and G. D. Longmore, "Reply: reducing background fluorescence reveals adhesions in 3D matrices," *Nat. Cell Biol.*, vol. 13, no. 1, pp. 5–7, 2011.
- [48] H. Hirata, H. Tatsumi, and M. Sokabe, "Zyxin emerges as a key player in the mechanotransduction at cell adhesive structures," *Commun. Integr. Biol.*, vol. 1, no. 2, pp. 192–195, 2008.

- [49] S. I. Fraley, Y. Feng, A. Giri, G. D. Longmore, and D. Wirtz, "Dimensional and temporal controls of three-dimensional cell migration by zyxin and binding partners," *Nat. Commun.*, vol. 3, no. 719, pp. 1–13, 2012.
- [50] A. Huttenlocher and A. R. Horwitz, "Integrins in cell migration," *Cold Spring Harb. Perspect. Biol.*, vol. 3, no. 9, pp. 1–16, 2011.
- [51] A. Ray, Z. M. Slama, R. K. Morford, S. A. Madden, and P. P. Provenzano, "Enhanced Directional Migration of Cancer Stem Cells in 3D Aligned Collagen Matrices," *Biophys. J.*, vol. 112, no. 5, pp. 1023–1036, 2017.
- [52] E. M. Balzer, Z. Tong, C. D. Paul, W. Hung, K. M. Stroka, A. E. Boggs, S. S. Martin, and K. Konstantopoulos, "Physical confinement alters tumor cell adhesion and migration phenotypes," *FASEB J.*, vol. 26, no. 10, pp. 4045–4056, 2012.
- [53] J. da Silva, F. Lautenschläger, E. Sivaniah, and J. R. Guck, "The cavity-to-cavity migration of leukaemic cells through 3D honey-combed hydrogels with adjustable internal dimension and stiffness," *Biomaterials*, vol. 31, no. 8, pp. 2201–2208, 2010.
- [54] P. Tayalia, E. Mazur, and D. J. Mooney, "Controlled architectural and chemotactic studies of 3D cell migration," *Biomaterials*, vol. 32, no. 10, pp. 2634–2641, 2011.
- [55] R. W. Carlsen and M. Sitti, "Bio-Hybrid Cell-Based Actuators for Microsystems," *SMALL*, vol. 10, no. 19, pp. 3831–3851, 2014.
- [56] A. J. Engler, L. Bacakova, C. Newman, A. Hategan, M. Griffin, and D. Discher, "Substrate Compliance versus Ligand Density in Cell on Gel Responses," *Biophys. J.*, vol. 86, no. 1, pp. 617–628, 2004.
- [57] D. H. Kim, K. Han, K. Gupta, K. W. Kwon, K. Y. Suh, and A. Levchenko, "Mechanosensitivity of fibroblast cell shape and movement to anisotropic substratum topography gradients," *Biomaterials*, vol. 30, no. 29, pp. 5433–5444, 2009.
- [58] S. E. Naleway, M. M. Porter, J. McKittrick, and M. A. Meyers, "Structural Design Elements in Biological Materials: Application to Bioinspiration," *Adv. Mater.*, vol. 27, no. 37, pp. 5455–5476, 2015.
- [59] J. Kim, J. Park, S. Yang, J. Baek, B. Kim, S. H. Lee, E.-S. Yoon, K. Chun, and S. Park, "Establishment of a fabrication method for a long-term actuated hybrid cell robot," *Lab Chip*, vol. 7, no. 11, p. 1504, 2007.
- [60] D. Motlagh, T. J. Hartman, T. A. Desai, and B. Russell, "Microfabricated grooves recapitulate neonatal myocyte connexin43 and N-cadherin expression and localization," *J. Biomed. Mater.*

- Res.*, vol. 67A, no. 1, pp. 148–157, 2003.
- [61] E. Entcheva and H. Bien, “Tension Development and Nuclear Eccentricity in Topographically Controlled Cardiac Syncytium,” *Biomed. Microdevices*, vol. 5, no. 2, pp. 163–168, 2003.
- [62] W. Bian and N. Bursac, “Tissue engineering of functional skeletal muscle: challenges and recent advances,” *IEEE Eng. Med. Biol. Mag.*, vol. 27, no. 5, pp. 109–13, 2008.
- [63] V. A. Webster, E. L. Hawley, O. Akkus, H. J. Chiel, and R. D. Quinn, “Effect of actuating cell source on locomotion of organic living machines with electrocompacted collagen skeleton,” *Bioinspiration and Biomimetics*, vol. 11, no. 3, 2016.
- [64] K. M. Hakkinen, J. S. Harunaga, A. D. Doyle, and K. M. Yamada, “Direct Comparisons of the Morphology, Migration, Cell Adhesions, and Actin Cytoskeleton of Fibroblasts in Four Different Three-Dimensional Extracellular Matrices,” *Tissue Eng. Part A*, vol. 17, no. 5–6, pp. 713–724, 2011.
- [65] A. D. Doyle, M. L. Kutys, M. A. Conti, K. Matsumoto, R. S. Adelstein, and K. M. Yamada, “Micro-environmental control of cell migration - myosin IIA is required for efficient migration in fibrillar environments through control of cell adhesion dynamics,” *J. Cell Sci.*, vol. 125, no. 9, pp. 2244–2256, 2012.
- [66] T. Patino, R. Mestre, and S. Sánchez, “Miniaturized soft bio-hybrid robotics: A step forward into healthcare applications,” *Lab Chip*, vol. 16, no. 19, pp. 3626–3630, 2016.
- [67] A. J. Engler, M. A. Griffin, S. Sen, C. G. Bönnemann, H. L. Sweeney, and D. E. Discher, “Myotubes differentiate optimally on substrates with tissue-like stiffness: Pathological implications for soft or stiff microenvironments,” *J. Cell Biol.*, vol. 166, no. 6, pp. 877–887, 2004.
- [68] A. J. Engler, C. Carag-Krieger, C. P. Johnson, M. Raab, H.-Y. Tang, D. W. Speicher, J. W. Sanger, J. M. Sanger, and D. E. Discher, “Embryonic cardiomyocytes beat best on a matrix with heart-like elasticity: scar-like rigidity inhibits beating,” *J. Cell Sci.*, vol. 121, no. 22, pp. 3794–3802, 2008.
- [69] L. F. Kadem, C. Lamprecht, J. Purtov, and C. Selhuber-Unkel, “Controlled Self-Assembly of Hexagonal Nanoparticle Patterns on Nanotopographies,” *Langmuir*, vol. 31, no. 34, pp. 9261–9265, 2015.
- [70] L. E. Dickinson, D. R. Rand, J. Tsao, W. Eberle, and S. Gerecht, “Endothelial cell responses to micropillar substrates of varying dimensions and stiffness,” *J. Biomed. Mater. Res. Part A*, vol. 100, no. 6, pp. 1457–1466, 2012.

- [71] M. Taale, "Fibrous biomimetic and biohybrid carbon scaffolds for 3D cell growth," Dissertation, Christian-Albrechts Universität zu Kiel, 2019.
- [72] M. Miron-Mendoza, J. Seemann, and F. Grinnell, "The differential regulation of cell motile activity through matrix stiffness and porosity in three dimensional collagen matrices," *Biomaterials*, vol. 31, no. 25, pp. 6425–6435, 2010.
- [73] V. A. Schulte, M. Diez, Y. Hu, M. Möller, and M. C. Lensen, "Combined Influence of Substrate Stiffness and Surface Topography on the Antiadhesive Properties of Acr-sP(EO- stat -PO) Hydrogels," *Biomacromolecules*, vol. 11, no. 12, pp. 3375–3383, 2010.
- [74] S. V. Graeter, J. Huang, N. Perschmann, M. López-García, H. Kessler, J. Ding, and J. P. Spatz, "Mimicking Cellular Environments by Nanostructured Soft Interfaces," *Nano Lett.*, vol. 7, no. 5, pp. 1413–1418, 2007.
- [75] C. S. Verbeke and D. J. Mooney, "Injectable, Pore-Forming Hydrogels for In Vivo Enrichment of Immature Dendritic Cells," *Adv. Healthc. Mater.*, vol. 4, no. 17, pp. 2677–2687, 2015.
- [76] V. Chan, J. H. Jeong, P. Bajaj, M. Collens, T. Saif, H. Kong, and R. Bashir, "Multi-material bio-fabrication of hydrogel cantilevers and actuators with stereolithography," *Lab Chip*, vol. 12, no. 1, pp. 88–98, 2012.
- [77] A. Pathak and S. Kumar, "Independent regulation of tumor cell migration by matrix stiffness and confinement," *Proc. Natl. Acad. Sci. U. S. A.*, vol. 109, no. 26, pp. 10334–10339, 2012.
- [78] K. H. Bouhadir, D. S. Hausman, and D. J. Mooney, "Synthesis of cross-linked poly(aldehyde guluronate) hydrogels," *Polymer (Guildf.)*, vol. 40, no. 12, pp. 3575–3584, 1999.
- [79] H. Park, K. Park, and W. S. W. Shalaby, *Biodegradable Hydrogels for Drug Delivery*. Boca Raton: CRC Press, Taylor & Francis Group, 1993.
- [80] J. M. Shapiro and M. L. Oyen, "Hydrogel Composite Materials for Tissue Engineering Scaffolds," *JOM*, vol. 65, no. 4, pp. 505–516, 2013.
- [81] N. A. Peppas, Y. Huang, M. Torres-Lugo, J. H. Ward, and J. Zhang, "Physicochemical Foundations and Structural Design of Hydrogels in Medicine and Biology," *Annu. Rev. Biomed. Eng.*, vol. 2, no. 1, pp. 9–29, 2000.
- [82] M. Galli, K. S. C. Comley, T. A. V. Shean, and M. L. Oyen, "Viscoelastic and poroelastic mechanical characterization of hydrated gels," *J. Mater. Res.*, vol. 24, no. 03, pp. 973–979, 2009.
- [83] S. Di Cio and J. E. Gautrot, "Cell sensing of physical properties at the nanoscale: Mechanisms

- and control of cell adhesion and phenotype,” *Acta Biomater.*, vol. 30, pp. 26–48, 2016.
- [84] K. Y. Lee and D. J. Mooney, “Alginate: properties and biomedical applications.,” *Prog. Polym. Sci.*, vol. 37, no. 1, pp. 106–126, 2012.
- [85] J. L. Drury and D. J. Mooney, “Hydrogels for tissue engineering: scaffold design variables and applications,” *Biomaterials*, vol. 24, no. 24, pp. 4337–4351, 2003.
- [86] J. A. Rowley, G. Madlambayan, and D. J. Mooney, “Alginate hydrogels as synthetic extracellular matrix materials,” *Biomaterials*, vol. 20, no. 1, pp. 45–53, 1999.
- [87] E. Ruvinov and S. Cohen, “Alginate biomaterial for the treatment of myocardial infarction: Progress, translational strategies, and clinical outlook,” *Adv. Drug Deliv. Rev.*, vol. 96, pp. 54–76, 2016.
- [88] A. Steinbüchel and S. K. Rhee, *Polysaccharides and Polyamides in the Food Industry : Volume 1*. Wiley-VCH, 2005.
- [89] X. Zhao, N. Huebsch, D. J. Mooney, and Z. Suo, “Stress-relaxation behavior in gels with ionic and covalent crosslinks,” *J. Appl. Phys.*, vol. 107, no. 063509, pp. 1–5, 2010.
- [90] T. Mimae, T. Hirayasu, K. B. Kimura, A. Ito, Y. Miyata, and M. Okada, “Advantage of absorbable suture material for pulmonary artery ligation,” *Gen. Thorac. Cardiovasc. Surg.*, vol. 58, pp. 511–515, 2010.
- [91] S. Rajakulendran and M. G. Hanna, “The Role of Calcium Channels in Epilepsy,” *Cold Spring Harb. Perspect. Med.*, vol. 6, no. a022723, pp. 1–21, 2016.
- [92] J. V. Raimondo, R. J. Burman, A. A. Katz, and C. J. Akerman, “Ion dynamics during seizures,” *Front. Cell. Neurosci.*, vol. 9, no. 419, pp. 1–14, 2015.
- [93] S. Wu, T. Braschler, R. Anker, F. Wildhaber, A. Bertsch, J. Brugger, and P. Renaud, “Composite hydrogel-loaded alumina membranes for nanofluidic molecular filtration,” *J. Memb. Sci.*, vol. 477, pp. 151–156, 2015.
- [94] Thermo Scientific, *Thermo Scientific: Crosslinkers Technical Handbook*. Thermo Fischer Scientific Inc., 2012.
- [95] P. Menter, “Acrylamide Polymerization—A Practical Approach,” *Bio-Rad Tech Note 1156*, 2000. [https://www.bio-rad.com/webroot/web/pdf/lsr/literature/Bulletin\\_1156.pdf](https://www.bio-rad.com/webroot/web/pdf/lsr/literature/Bulletin_1156.pdf) (accessed Jun. 01, 2020).
- [96] D. V. Shepherd, J. H. Shepherd, S. Ghose, S. J. Kew, R. E. Cameron, and S. M. Best, “The process of EDC-NHS cross-linking of reconstituted collagen fibres increases collagen fibrillar

- order and alignment," *APL Mater.*, vol. 3, no. 014902, pp. 2–9, 2015.
- [97] B. Li, J. Chen, and J. H. C. Wang, "RGD peptide-conjugated poly(dimethylsiloxane) promotes adhesion, proliferation, and collagen secretion of human fibroblasts," *J. Biomed. Mater. Res. - Part A*, vol. 79, no. 4, pp. 989–998, 2006.
- [98] J. R. Tse and A. J. Engler, "Preparation of Hydrogel Substrates with Tunable Mechanical Properties," *Curr. Protoc. Cell Biol.*, vol. 47, no. 1, pp. 1–16, 2010.
- [99] K. S. Masters, "Covalent Growth Factor Immobilization Strategies for Tissue Repair and Regeneration," *Macromol. Biosci.*, vol. 11, no. 9, pp. 1149–1163, 2011.
- [100] P. Rajagopalan, W. A. Marganski, X. Q. Brown, and J. Y. Wong, "Direct Comparison of the Spread Area, Contractility, and Migration of balb/c 3T3 Fibroblasts Adhered to Fibronectin- and RGD-Modified Substrata," *Biophys. J.*, vol. 87, no. 4, pp. 2818–2827, 2004.
- [101] K. Franze, P. A. Janmey, and J. Guck, "Mechanics in Neuronal Development and Repair," *Annu. Rev. Biomed. Eng.*, vol. 15, no. 1, pp. 227–251, 2013.
- [102] A. Toma, "Hydrocephalus in Adults," in *Principles of Neurological Surgery*, Elsevier, 2018, pp. 822-831.e1.
- [103] P. Moshayedi, G. Ng, J. C. F. Kwok, G. S. H. Yeo, C. E. Bryant, J. W. Fawcett, K. Franze, and J. Guck, "The relationship between glial cell mechanosensitivity and foreign body reactions in the central nervous system," *Biomaterials*, vol. 35, no. 13, pp. 3919–3925, 2014.
- [104] K. Holtzmann, H. O. B. Gautier, A. F. Christ, J. Guck, R. T. Káradóttir, and K. Franze, "Brain tissue stiffness is a sensitive marker for acidosis," *J. Neurosci. Methods*, vol. 271, pp. 50–54, 2016.
- [105] E. Moeendarbary, I. P. Weber, G. K. Sheridan, D. E. Koser, S. Soleman, B. Haenzi, E. J. Bradbury, J. Fawcett, and K. Franze, "The soft mechanical signature of glial scars in the central nervous system," *Nat. Commun.*, vol. 8, no. 14787, pp. 1–11, 2017.
- [106] A. Buxboim, I. L. Ivanovska, and D. E. Discher, "Matrix elasticity, cytoskeletal forces and physics of the nucleus: how deeply do cells 'feel' outside and in?," *J. Cell Sci.*, vol. 123, no. 3, pp. 297–308, 2010.
- [107] A. J. Engler, S. Sen, H. L. Sweeney, and D. E. Discher, "Matrix Elasticity Directs Stem Cell Lineage Specification," *Cell*, vol. 126, no. 4, pp. 677–689, 2006.
- [108] G. Kaklamani, D. Cheneler, L. M. Grover, M. J. Adams, and J. Bowen, "Mechanical properties of alginate hydrogels manufactured using external gelation," *J. Mech. Behav. Biomed. Mater.*,

- vol. 36, pp. 135–142, 2014.
- [109] M. L. Oyen, “Mechanical characterisation of hydrogel materials,” *Int. Mater. Rev.*, vol. 59, no. 1, pp. 44–59, 2014.
- [110] D. R. Askeland, *Materialwissenschaften: Grundlagen, Übungen, Lösungen*. Heidelberg; Berlin; Oxford: Spektrum Akademischer Verlag GmbH, 1996.
- [111] S. F. M. Duncan and A. J. Weiland, “Minimally invasive reduction and osteosynthesis of articular fractures of the distal radius,” *Injury*, vol. 32, pp. 14–24, 2001.
- [112] S. N. Khotimah, S. Viridi, Widayani, and Khairurrijal, “The dependence of the spring constant in the linear range on spring parameters,” *Phys. Educ.*, vol. 46, no. 5, pp. 540–543, 2011.
- [113] K. Hoshino, T. Nakajima, T. Matsuda, T. Sakai, and J. P. Gong, “Network elasticity of a model hydrogel as a function of swelling ratio: from shrinking to extreme swelling states,” *Soft Matter*, vol. 14, no. 47, pp. 9693–9701, 2018.
- [114] D. Xu, K. M. Liechti, and K. Ravi-Chandar, “On the modified Tabor parameter for the JKR–DMT transition in the presence of a liquid meniscus,” *J. Colloid Interface Sci.*, vol. 315, no. 2, pp. 772–785, 2007.
- [115] M. Ciavarella, J. Joe, A. Papangelo, and J. Barber, “The role of adhesion in contact mechanics,” *J. R. Soc. Interface*, vol. 16, pp. 1–22, 2018.
- [116] K. L. Johnson, *Contact Mechanics*. Cambridge: Cambridge University Press, 1985.
- [117] D. R. Askeland and P. P. Fulay, *Essentials of Materials Science and Engineering*, vol. 58, no. 12. Cambridge, 2004.
- [118] M. Christopher W., *Rheology Principles, Measurements, and Applications*. Wiley-VCH, 1994.
- [119] L. Pescosolido, L. Feruglio, R. Farra, S. Fiorentino, I. Colombo, T. Coviello, P. Matricardi, W. E. Hennink, T. Vermonden, and M. Grassi, “Mesh size distribution determination of interpenetrating polymer network hydrogels,” *Soft Matter*, vol. 8, pp. 7708–7715, 2012.
- [120] D. Jain and D. Bar-Shalom, “Alginate drug delivery systems: application in context of pharmaceutical and biomedical research,” *Drug Dev. Ind. Pharm.*, vol. 40, no. 12, pp. 1576–1584, 2014.
- [121] B. Yao, C. Ni, C. Xiong, C. Zhu, and B. Huang, “Hydrophobic modification of sodium alginate and its application in drug controlled release,” *Bioprocess Biosyst. Eng.*, vol. 33, no. 4, pp. 457–463, 2010.
- [122] S. T. Moe, G. Skjaak-Braek, A. Elgsaeter, and O. Smidsroed, “Swelling of covalently crosslinked

- alginate gels: influence of ionic solutes and nonpolar solvents," *Macromolecules*, vol. 26, no. 14, pp. 3589–3597, 1993.
- [123] P. Matricardi, C. Di Meo, T. Coviello, W. E. Hennink, and F. Alhaique, "Interpenetrating Polymer Networks polysaccharide hydrogels for drug delivery and tissue engineering.," *Adv. Drug Deliv. Rev.*, vol. 65, no. 9, pp. 1172–1187, 2013.
- [124] M. T. Chevalier, J. Gonzalez, and V. Alvarez, "Biodegradable Polymeric Microparticles as Drug Delivery Devices," in *Journal of Controlled Release*, vol. 70, no. 1–2, 2015, pp. 187–190.
- [125] J. Li and D. J. Mooney, "Designing hydrogels for controlled drug delivery," *Nat. Rev. Mater.*, vol. 1, no. 12, p. 16071, 2016.
- [126] D. J. Phillips, S. R. Pygall, V. B. Cooper, and J. C. Mann, "Overcoming sink limitations in dissolution testing: a review of traditional methods and the potential utility of biphasic systems," *J. Pharm. Pharmacol.*, vol. 64, no. 11, pp. 1549–1559, 2012.
- [127] D. Klose, C. Delplace, and J. Siepmann, "Unintended potential impact of perfect sink conditions on PLGA degradation in microparticles," *Int. J. Pharm.*, vol. 404, no. 1–2, pp. 75–82, 2011.
- [128] M. Gibaldi and S. Feldman, "Establishment of sink conditions in dissolution rate determinations. Theoretical considerations and application to nondisintegrating dosage forms," *J. Pharm. Sci.*, vol. 56, no. 10, pp. 1238–1242, 1967.
- [129] S. Petralito, I. Zanardi, A. Memoli, M. Cristina, V. Millucci, and V. Travagli, "Apparent Solubility and Dissolution Profile at Non-Sink Conditions as Quality Improvement Tools," in *Promising Pharmaceuticals*, InTech, 2012.
- [130] D. L. Bernik, D. Zubiri, M. E. Monge, and R. M. Negri, "New kinetic model of drug release from swollen gels under non-sink conditions," *Colloids Surfaces A Physicochem. Eng. Asp.*, vol. 273, no. 1–3, pp. 165–173, 2006.
- [131] J. Bevernage, J. Brouwers, M. E. Brewster, and P. Augustijns, "Evaluation of gastrointestinal drug supersaturation and precipitation: Strategies and issues," *Int. J. Pharm.*, vol. 453, no. 1, pp. 25–35, 2013.
- [132] C.-C. Lin and A. T. Metters, "Hydrogels in controlled release formulations: Network design and mathematical modeling," *Adv. Drug Deliv. Rev.*, vol. 58, no. 12–13, pp. 1379–1408, 2006.
- [133] D. Caccavo, S. Cascone, G. Lamberti, A. A. Barba, and A. Larsson, "Swellable Hydrogel-based Systems for Controlled Drug Delivery," in *Smart Drug Delivery System*, InTech, 2016.



- [134] K. S. Soppimath, T. M. Aminabhavi, A. R. Kulkarni, and W. E. Rudzinski, "Biodegradable polymeric nanoparticles as drug delivery devices," *J. Control. Release*, vol. 70, no. 1–2, pp. 1–20, 2001.
- [135] P. Gupta, K. Vermani, and S. Garg, "Hydrogels: from controlled release to pH-responsive drug delivery," *Drug Discov. Today*, vol. 7, no. 10, pp. 569–579, 2002.
- [136] P. L. Ritger and N. A. Peppas, "A simple equation for description of solute release I. Fickian and non-fickian release from non-swellable devices in the form of slabs, spheres, cylinders or discs," *J. Control. Release*, vol. 5, no. 1, pp. 23–36, 1987.
- [137] N. A. Peppas and A. R. Khare, "Preparation, structure and diffusional behavior of hydrogels in controlled release," *Adv. Drug Deliv. Rev.*, vol. 11, no. 1–2, pp. 1–35, 1993.
- [138] Y. Fu and W. J. Kao, "Drug release kinetics and transport mechanisms of non-degradable and degradable polymeric delivery systems," *Expert Opin. Drug Deliv.*, vol. 7, no. 4, pp. 429–444, 2010.
- [139] M. W. Dong, *HPLC and UHPLC for Practicing Scientists*, 2nd ed. Newark: John Wiley & Sons, Incorporated, 2019.
- [140] E. Pretsch, P. Bühlmann, and M. Badertscher, *Spektroskopische Daten zur Strukturaufklärung organischer Verbindungen*, 5th ed. Berlin, Heidelberg: Springer Berlin Heidelberg, 2010.
- [141] E. Tamariz and F. Grinnell, "Modulation of Fibroblast Morphology and Adhesion during Collagen Matrix Remodeling," *Mol. Biol. Cell*, vol. 13, no. 11, pp. 3915–3929, 2002.
- [142] I. Ohizumi, M. Tanemura, and S. Kaihoh, "A novel styryl diphenylamine derivative reverts the transformed phenotype of human fibrosarcoma HT1080 cells," *Br. J. Cancer*, vol. 72, no. 5, pp. 1219–1223, 1995.
- [143] N. Jiménez, V. J. D. Krouwer, and J. A. Post, "A new, rapid and reproducible method to obtain high quality endothelium in vitro," *Cytotechnology*, vol. 65, no. 1, pp. 1–14, 2013.
- [144] E. F. Smeets, E. J. U. von Asmuth, C. J. van der Linden, J. F. M. Leeuwenberg, and W. A. Buurman, "A comparison of substrates for human umbilical vein endothelial cell culture," *Biotech. Histochem.*, vol. 67, no. 4, pp. 241–250, 1992.
- [145] ISO 10993-5:2009, "Biological evaluation of medical devices - Part 5: Tests for cytotoxicity: in vitro methods," *ISO 10993-5:2009*, pp. 1–42, 2009.
- [146] ISO 10993-12:2004, "Biological Evaluation of Medical Devices Part 12: Sample preparation and reference materials," pp. 1–38, 2004.

- [147] I. Ellinger and A. Ellinger, "Smallest Unit of Life: Cell Biology," in *Comparative Medicine*, Vienna: Springer Vienna, 2014, pp. 19–33.
- [148] K. Munk, C. Abröll, T. Kurth, T. Langer, R. Nethe-Jaenchen, G. Pohl-Apel, H. Schlatter, B. Schultze, and K. Wolf, *Taschenlehrbuch Biologie Biochemie - Zellbiologie*. Stuttgart: Georg Thieme Verlag, 2008.
- [149] D. Mohammed, M. Versaevel, C. Bruyère, L. Alaimo, M. Luciano, E. Vercruysse, A. Procès, and S. Gabriele, "Innovative Tools for Mechanobiology: Unraveling Outside-In and Inside-Out Mechanotransduction," *Front. Bioeng. Biotechnol.*, vol. 7, no. 162, pp. 1–18, 2019.
- [150] C. G. Rolli, T. Seufferlein, R. Kemkemer, and J. P. Spatz, "Impact of Tumor Cell Cytoskeleton Organization on Invasiveness and Migration: A Microchannel-Based Approach," *PLoS One*, vol. 5, no. 1, pp. 1–8, 2010.
- [151] V. te Boekhorst, L. Preziosi, and P. Friedl, "Plasticity of Cell Migration In Vivo and In Silico," *Annu. Rev. Cell Dev. Biol.*, vol. 32, no. 1, pp. 491–526, 2016.
- [152] S. B. Khatau, R. J. Bloom, S. Bajpai, D. Razafsky, S. Zang, A. Giri, P.-H. Wu, J. Marchand, A. Celedon, C. M. Hale, S. X. Sun, D. Hodzic, and D. Wirtz, "The distinct roles of the nucleus and nucleus-cytoskeleton connections in three-dimensional cell migration," *Sci. Rep.*, vol. 2, no. 488, pp. 1–11, 2012.
- [153] B. M. Baker and C. S. Chen, "Deconstructing the third dimension – how 3D culture microenvironments alter cellular cues," *J. Cell Sci.*, vol. 125, no. 13, pp. 3015–3024, 2012.
- [154] T. Aberle, K. Franke, E. Rist, K. Benz, and B. Schlosshauer, "Cell-Type Specific Four-Component Hydrogel," *PLoS One*, vol. 9, no. 1, pp. 1–14, 2014.
- [155] Y.-H. Tsou, J. Khoneisser, P.-C. Huang, and X. Xu, "Hydrogel as a bioactive material to regulate stem cell fate," *Bioact. Mater.*, vol. 1, no. 1, pp. 39–55, 2016.
- [156] H. Li, A. Wijekoon, and N. D. Leipzig, "3D Differentiation of Neural Stem Cells in Macroporous Photopolymerizable Hydrogel Scaffolds," *PLoS One*, vol. 7, no. 11, pp. 1–11, 2012.
- [157] D. J. Abraham and J. Varga, "Scleroderma: from cell and molecular mechanisms to disease models," *Trends Immunol.*, vol. 26, no. 11, pp. 587–595, 2005.
- [158] L. E. Bertassoni, M. Cecconi, V. Manoharan, M. Nikkhah, J. Hjortnaes, A. L. Cristino, G. Barabaschi, D. Demarchi, M. R. Dokmeci, Y. Yang, and A. Khademhosseini, "Hydrogel bioprinted microchannel networks for vascularization of tissue engineering constructs," *Lab Chip*, no. 14, pp. 2202–2211, 2014.

- [159] C. M. Denais, R. M. Gilbert, P. Isermann, A. L. McGregor, M. te Lindert, B. Weigelin, P. M. Davidson, P. Friedl, K. Wolf, and J. Lammerding, "Nuclear envelope rupture and repair during cancer cell migration.," *Science*, vol. 352, no. 6283, pp. 353–8, 2016.
- [160] C. M. Denais, R. M. Gilbert, P. Isermann, A. L. McGregor, M. te Lindert, B. Weigelin, P. M. Davidson, P. Friedl, K. Wolf, and J. Lammerding, "Nuclear envelope rupture and repair during cancer cell migration," *Science*, vol. 352, no. 6283, pp. 353–358, 2016.
- [161] C. F. Guimarães, L. Gasperini, A. P. Marques, and R. L. Reis, "The stiffness of living tissues and its implications for tissue engineering," *Nat. Rev. Mater.*, vol. 5, pp. 351–370, 2020.
- [162] P. Friedl and S. Alexander, "Cancer invasion and the microenvironment: Plasticity and reciprocity," *Cell*, vol. 147, no. 5, pp. 992–1009, 2011.
- [163] P. P. Provenzano, D. R. Inman, K. W. Eliceiri, S. M. Trier, and P. J. Keely, "Contact Guidance Mediated Three-Dimensional Cell Migration is Regulated by Rho/ROCK-Dependent Matrix Reorganization," *Biophys. J.*, vol. 95, no. 11, pp. 5374–5384, 2008.
- [164] J. C. Ashworth, M. Mehr, P. G. Buxton, S. M. Best, and R. E. Cameron, "Towards Cellular Sieving: Exploring the Limits of Scaffold Accessibility for Cell Type Specific Invasion," *Adv. Biosyst.*, vol. 2, no. 8, p. 1700257, 2018.
- [165] D. Kedrin, J. van Rheenen, L. Hernandez, J. Condeelis, and J. E. Segall, "Cell Motility and Cytoskeletal Regulation in Invasion and Metastasis," *J. Mammary Gland Biol. Neoplasia*, vol. 12, pp. 143–152, 2007.
- [166] C. G. Rolli, H. Nakayama, K. Yamaguchi, J. P. Spatz, R. Kemkemer, and J. Nakanishi, "Switchable adhesive substrates: Revealing geometry dependence in collective cell behavior," *Biomaterials*, vol. 33, no. 8, pp. 2409–2418, 2012.
- [167] O. Chaudhuri, L. Gu, D. Klumpers, M. Darnell, S. A. Bencherif, J. C. Weaver, N. Huebsch, H.-P. Lee, E. Lippens, G. N. Duda, and D. J. Mooney, "Hydrogels with tunable stress relaxation regulate stem cell fate and activity," *Nat. Mater.*, vol. 15, no. 3, pp. 326–334, 2016.
- [168] J. Schindelin, I. Arganda-Carreras, E. Frise, V. Kaynig, M. Longair, T. Pietzsch, S. Preibisch, C. Rueden, S. Saalfeld, B. Schmid, J.-Y. Tinevez, D. J. White, V. Hartenstein, K. Eliceiri, P. Tomancak, and A. Cardona, "Fiji: an open-source platform for biological-image analysis," *Nat. Methods*, vol. 9, pp. 676–682, 2012.
- [169] K. N. Dahl, S. M. Kahn, K. L. Wilson, and D. E. Discher, "The nuclear envelope lamina network has elasticity and a compressibility limit suggestive of a molecular shock absorber," *J. Cell Sci.*, vol. 117, no. 20, pp. 4779–4786, 2004.

- [170] J. M. Garcia-Arcos, R. Chabrier, M. Deygas, G. Nader, L. Barbier, P. J. Sáez, A. Mathur, P. Vargas, and M. Piel, "Reconstitution of cell migration at a glance," *J. Cell Sci.*, vol. 132, no. 4, p. jcs225565, 2019.
- [171] J. Lammerding and K. Wolf, "Nuclear envelope rupture: Actin fibers are putting the squeeze on the nucleus," *J. Cell Biol.*, vol. 215, no. 1, pp. 5–8, 2016.
- [172] M. Werner, S. B. G. Blanquer, S. P. Haimi, G. Korus, J. W. C. Dunlop, G. N. Duda, D. W. Grijpma, and A. Petersen, "Surface Curvature Differentially Regulates Stem Cell Migration and Differentiation via Altered Attachment Morphology and Nuclear Deformation," *Adv. Sci.*, vol. 4, no. 2, pp. 1–11, 2017.
- [173] Y. Xia, I. L. Ivanovska, K. Zhu, L. Smith, J. Irianto, C. R. Pfeifer, C. M. Alvey, J. Ji, D. Liu, S. Cho, R. R. Bennett, A. J. Liu, R. A. Greenberg, and D. E. Discher, "Nuclear rupture at sites of high curvature compromises retention of DNA repair factors," *J. Cell Biol.*, vol. 217, no. 11, pp. 3796–3808, 2018.
- [174] L. Pieuchot, J. Marteau, A. Guignandon, T. Dos Santos, I. Brigaud, P.-F. Chauvy, T. Cloatre, A. Ponche, T. Petithory, P. Rougerie, M. Vassaux, J.-L. Milan, N. Tusamda Wakhloo, A. Spangenberg, M. Bigerelle, and K. Anselme, "Curvotaxis directs cell migration through cell-scale curvature landscapes," *Nat. Commun.*, vol. 9, no. 1, p. 3995, 2018.
- [175] R. K. Assoian, N. D. Bade, C. V. Cameron, and K. J. Stebe, "Cellular sensing of micron-scale curvature: a frontier in understanding the microenvironment," *Open Biol.*, vol. 9, no. 10, pp. 1–8, 2019.
- [176] J. Y. Park, D. H. Lee, E. J. Lee, and S.-H. Lee, "Study of cellular behaviors on concave and convex microstructures fabricated from elastic PDMS membranes," *Lab Chip*, vol. 9, no. 14, pp. 2043–2049, 2009.
- [177] G. de Vicente and M. C. Lensen, "Topographically and elastically micropatterned PEG-based hydrogels to control cell adhesion and migration," *Eur. Polym. J.*, vol. 78, pp. 290–301, 2016.
- [178] E. Hannezo and C.-P. Heisenberg, "Mechanochemical Feedback Loops in Development and Disease," *Cell*, vol. 178, no. 1, pp. 12–25, 2019.
- [179] W. W. Yan, Y. Liu, and B. M. Fu, "Effects of curvature and cell–cell interaction on cell adhesion in microvessels," *Biomech. Model. Mechanobiol.*, vol. 9, pp. 629–640, 2010.
- [180] R. J. Petrie, A. D. Doyle, and K. M. Yamada, "Random versus directionally persistent cell migration," *Nat. Rev. Mol. Cell Biol.*, vol. 10, pp. 538–549, 2009.
- [181] C. R. Bone and D. A. Starr, "Nuclear migration events throughout development," *J. Cell Sci.*,

- vol. 129, pp. 1951–1961, 2016.
- [182] L. A. Lautscham, C. Kämmerer, J. R. Lange, T. Kolb, C. Mark, A. Schilling, P. L. Strissel, R. Strick, C. Gluth, A. C. Rowat, C. Metzner, and B. Fabry, “Migration in Confined 3D Environments Is Determined by a Combination of Adhesiveness, Nuclear Volume, Contractility, and Cell Stiffness,” *Biophys. J.*, vol. 109, no. 5, pp. 900–913, 2015.
- [183] R. Bruinsma, A. Y. Grosberg, Y. Rabin, and A. Zidovska, “Chromatin Hydrodynamics,” *Biophys. J.*, vol. 106, no. 9, pp. 1871–1881, 2014.
- [184] S. Pagliara, K. Franze, C. R. McClain, G. W. Wylde, C. L. Fisher, R. J. M. Franklin, A. J. Kabla, U. F. Keyser, and K. J. Chalut, “Auxetic nuclei in embryonic stem cells exiting pluripotency,” *Nat. Mater.*, vol. 13, no. 6, pp. 638–644, 2014.
- [185] N. Belaadi, J. Aureille, and C. Guilluy, “Under Pressure: Mechanical Stress Management in the Nucleus,” *Cells*, vol. 5 (2), no. 27, pp. 1–11, 2016.
- [186] M. D. Welch, “Cell Migration, Freshly Squeezed,” *Cell*, vol. 160, no. 4, pp. 581–582, 2015.
- [187] J. Chang, E. M. Pang, K. Adebawale, K. M. Wisdom, and O. Chaudhuri, “Increased Stiffness Inhibits Invadopodia Formation and Cell Migration in 3D,” *Biophys. J.*, vol. 119, no. 4, pp. 726–736, 2020.
- [188] M. Bergert, A. Erzberger, R. A. Desai, I. M. Aspalter, A. C. Oates, G. Charras, G. Salbreux, and E. K. Paluch, “Force transmission during adhesion-independent migration,” *Nat. Cell Biol.*, vol. 17(4), pp. 524–529, 2015.
- [189] Y. K. Mishra and R. Adelung, “ZnO tetrapod materials for functional applications,” *Mater. Today*, vol. 21, no. 6, pp. 631–651, 2018.
- [190] M. Mecklenburg, A. Schuchardt, Y. K. Mishra, S. Kaps, R. Adelung, A. Lotnyk, L. Kienle, and K. Schulte, “Aerographite: Ultra Lightweight, Flexible Nanowall, Carbon Microtube Material with Outstanding Mechanical Performance,” *Adv. Mater.*, vol. 24, no. 26, pp. 3486–3490, 2012.
- [191] Y. K. Mishra, S. Kaps, A. Schuchardt, I. Paulowicz, X. Jin, D. Gedamu, S. Freitag, M. Claus, S. Wille, A. Kovalev, S. N. Gorb, and R. Adelung, “Fabrication of Macroscopically Flexible and Highly Porous 3D Semiconductor Networks from Interpenetrating Nanostructures by a Simple Flame Transport Approach,” *Part. Part. Syst. Character.*, vol. 30, no. 9, pp. 775–783, 2013.
- [192] A. Parslow, A. Cardona, and R. J. Bryson-Richardson, “Sample Drift Correction Following 4D Confocal Time-lapse Imaging,” *J. Vis. Exp.*, vol. 86, no. e51086, 2014.
- [193] F. Cordelires, “Manual Tracking.java,” 2005. <https://imagej.nih.gov/ij/plugins/track/track.html>

(accessed Aug. 06, 2020).

- [194] M. Vert, Y. Doi, K.-H. Hellwich, M. Hess, P. Hodge, P. Kubisa, M. Rinaudo, and F. Schué, "Terminology for biorelated polymers and applications (IUPAC Recommendations 2012)," *Pure Appl. Chem.*, vol. 84, no. 2, pp. 377–410, 2012.
- [195] K. Loger, A. Engel, J. Haupt, Q. Li, R. Lima de Miranda, E. Quandt, G. Lutter, and C. Selhuber-Unkel, "Cell adhesion on NiTi thin film sputter-deposited meshes," *Mater. Sci. Eng. C*, vol. 59, pp. 611–616, 2016.
- [196] K. Merrett, C. M. Griffith, Y. Deslandes, G. Pleizier, and H. Sheardown, "Adhesion of corneal epithelial cells to cell adhesion peptide modified pHEMA surfaces," *J. Biomater. Sci. Polym. Ed.*, vol. 12, no. 6, pp. 647–671, 2001.
- [197] B. W. Hanak, C. Hsieh, W. Donaldson, S. R. Browd, K. K. S. Lau, and W. Shain, "Reduced cell attachment to poly(2-hydroxyethyl methacrylate)-coated ventricular catheters in vitro," *J. Biomed. Mater. Res. Part B Appl. Biomater.*, vol. 106, no. 3, pp. 1268–1279, 2018.
- [198] J.-P. Montheard, M. Chatzopoulos, and D. Chappard, "2-Hydroxyethyl Methacrylate (HEMA): Chemical Properties and Applications in Biomedical Fields," *MACROMOL. CHEM. PHYS.*, vol. 32, no. 1, pp. 1–34, 1992.
- [199] M. Kiremitçi, A. İ. Şerbetçi, R. Çolak, and E. Pişkin, "Cell attachment to PU and PHEMA based biomaterials: Relation to structural properties," *Clin. Mater.*, vol. 8, no. 1–2, pp. 9–16, 1991.
- [200] C. E. Kadow, P. C. Georges, P. A. Janmey, and K. A. Benigo, "Polyacrylamide Hydrogels for Cell Mechanics: Steps Toward Optimization and Alternative Uses," in *Methods in Cell Biology*, vol. 83, 2007, pp. 29–46.
- [201] J. F. Lees and N. J. Bulleid, "The role of cysteine residues in the folding and association of the COOH- terminal propeptide of types I and III procollagen," *J. Biol. Chem.*, vol. 269, no. 39, pp. 24354–24360, 1994.
- [202] A. S. DiChiara, R. C. Li, P. H. Suen, A. S. Hosseini, R. J. Taylor, A. F. Weickhardt, D. Malhotra, D. R. McCaslin, and M. D. Shoulders, "A cysteine-based molecular code informs collagen C-propeptide assembly," *Nat. Commun.*, vol. 9, no. 4206, pp. 1–14, 2018.
- [203] H. Wegener, H. Paulsen, and K. Seeger, "The cysteine-rich region of type VII collagen is a cystine knot with a new topology," *J. Biol. Chem.*, vol. 289, no. 8, pp. 4861–4869, 2014.
- [204] W. S. Argraves, S. Suzuki, H. Arai, K. Thompson, M. D. Pierschbacher, and E. Ruoslahti, "Amino acid sequence of the human fibronectin receptor.," *J. Cell Biol.*, vol. 105, no. 3, pp. 1183–1190, 1987.

- [205] C. Chluba, K. Siemsen, C. Bechtold, C. Zamponi, C. Selhuber-Unkel, E. Quandt, and R. Lima de Miranda, "Microfabricated bioelectrodes on self-expandable NiTi thin film devices for implants and diagnostic instruments," *Biosens. Bioelectron.*, vol. 153, no. 112034, pp. 1–9, 2020.
- [206] J. S. Colligon, A. Dekker, A. Curry, and C. J. Kirkpatrick, "The surface modification of polymers to modulate endothelial cell growth," *J. Mater. Sci. Mater. Med.*, vol. 7, pp. 119–123, 1996.
- [207] E. W. Ades, F. J. Candal, R. A. Swerlick, V. G. George, S. Summers, D. C. Bosse, and T. J. Lawley, "HMEC-1: Establishment of an Immortalized Human Microvascular Endothelial Cell Line," *J. Invest. Dermatol.*, vol. 99, no. 6, pp. 683–690, 1992.
- [208] I. Dion, L. Bordenave, F. Lefebvre, R. Bareille, C. Baquey, J.-R. Monties, and P. Havlik, "Physico-chemistry and cytotoxicity of ceramics," *J. Mater. Sci. Mater. Med.*, vol. 5, no. 1, pp. 18–24, 1994.
- [209] Y. Lupu-Haber, O. Pinkas, S. Boehm, T. Scheper, C. Kasper, and M. Machluf, "Functionalized PLGA-doped zirconium oxide ceramics for bone tissue regeneration," *Biomed. Microdevices*, vol. 15, pp. 1055–1066, 2013.
- [210] C. Park, S. Kim, H.-E. Kim, and T.-S. Jang, "Mechanically stable tantalum coating on a nano-roughened NiTi stent for enhanced radiopacity and biocompatibility," *Surf. Coatings Technol.*, vol. 305, pp. 139–145, 2016.
- [211] J. Wang, W. Yin, X. He, Q. Wang, M. Guo, and S. Chen, "Good Biocompatibility and Sintering Properties of Zirconia Nanoparticles Synthesized via Vapor-phase Hydrolysis," *Sci. Rep.*, vol. 6, no. 35020, pp. 1–9, 2016.
- [212] S. van Helvert, C. Storm, and P. Friedl, "Mechanoreciprocity in cell migration," *Nat. Cell Biol.*, vol. 20, no. 1, pp. 8–20, 2018.
- [213] M. J. Dalby, M. O. Riehle, S. J. Yarwood, C. D. W. Wilkinson, and A. S. G. Curtis, "Nucleus alignment and cell signaling in fibroblasts: response to a micro-grooved topography," *Exp. Cell Res.*, vol. 284, no. 2, pp. 272–280, 2003.
- [214] O. Koniev and A. Wagner, "Developments and recent advancements in the field of endogenous amino acid selective bond forming reactions for bioconjugation," *Chem. Soc. Rev.*, vol. 44, no. 15, pp. 5495–5551, 2015.
- [215] S. Kelleher, A. Jongerius, A. Loebus, C. Strehmel, Z. Zhang, and M. C. Lensen, "AFM Characterization of Elastically Micropatterned Surfaces Fabricated by Fill-Molding In Capillaries (FIMIC) and Investigation of the Topographical Influence on Cell Adhesion to the

- Patterns,” *Adv. Eng. Mater.*, vol. 14, no. 3, pp. B56–B66, 2012.
- [216] M. C. Lensen, V. A. Schulte, and M. Diez, “Cell Adhesion and Spreading on an Intrinsically Anti-Adhesive PEG Biomaterial,” in *Biomaterials - Physics and Chemistry*, R. Pignatello, Ed. InTech, 2011, pp. 397–414.
- [217] A. Zellander, C. Zhao, M. Kotecha, R. Gemeinhart, M. Wardlow, J. Abiade, and M. Cho, “Characterization of pore structure in biologically functional poly(2-hydroxyethyl methacrylate) - Poly(ethylene glycol) diacrylate (PHEMA-PEGDA),” *PLoS One*, vol. 9, no. 5, pp. 1–8, 2014.
- [218] Y. Inoue, T. Nakanishi, and K. Ishihara, “Elastic Repulsion from Polymer Brush Layers Exhibiting High Protein Repellency,” *Langmuir*, vol. 29, no. 34, pp. 10752–10758, 2013.
- [219] D. S. Achilias and P. I. Siafaka, “Polymerization Kinetics of Poly(2-Hydroxyethyl Methacrylate) Hydrogels and Nanocomposite Materials,” *Processes*, vol. 5, no. 21, pp. 1–19, 2017.
- [220] K. L. Chaichana, L. Pinheiro, and H. Brem, “Delivery of local therapeutics to the brain: working toward advancing treatment for malignant gliomas,” *Ther. Deliv.*, vol. 6, no. 3, pp. 353–369, 2015.
- [221] H. H. Tønnesen and J. Karlsen, “Alginate in Drug Delivery Systems,” *Drug Dev. Ind. Pharm.*, vol. 28, no. 6, pp. 621–630, 2002.
- [222] L. S. Taylor and G. G. Z. Zhang, “Physical chemistry of supersaturated solutions and implications for oral absorption,” *Adv. Drug Deliv. Rev.*, vol. 101, pp. 122–142, 2016.
- [223] I. Rivolta, A. Panariti, B. Lettiero, S. Sesana, P. Gasco, M. R. Gasco, M. Masserini, and G. Miserocchi, “Cellular uptake of coumarin-6 as a model drug loaded in solid lipid nanoparticles,” *J. Physiol. Pharmacol.*, vol. 62, no. 1, pp. 45–53, 2011.
- [224] W. Dang and W. M. Saltzman, “Dextran Retention in the Rat Brain Following Release from a Polymer Implant,” *Biotechnol. Prog.*, vol. 8, no. 6, pp. 527–532, 1992.
- [225] A. N. Ford Versypt, D. W. Pack, and R. D. Braatz, “Mathematical modeling of drug delivery from autocatalytically degradable PLGA microspheres - A review,” *J. Control. Release*, vol. 165, no. 1, pp. 29–37, 2013.
- [226] S. Choudhary, J. M. Reck, A. J. Carr, and S. R. Bhatia, “Hydrophobically modified alginate for extended release of pharmaceuticals,” *Polym. Adv. Technol.*, vol. 29, no. 1, pp. 198–204, 2018.
- [227] K. Y. Lee, K. H. Bouhadir, and D. J. Mooney, “Controlled degradation of hydrogels using multi-functional cross-linking molecules,” *Biomaterials*, vol. 25, no. 13, pp. 2461–2466, 2004.



- [228] P. E. Penovich and L. James Willmore, "Use of a new antiepileptic drug or an old one as first drug for treatment of absence epilepsy," *Epilepsia*, vol. 50, no. SUPPL. 8, pp. 37–41, 2009.
- [229] W. C. Huang, T. J. Lee, C. S. Hsiao, S. Y. Chen, and D. M. Liu, "Characterization and drug release behavior of chip-like amphiphilic chitosan-silica hybrid hydrogel for electrically modulated release of ethosuximide: An in vitro study," *J. Mater. Chem.*, vol. 21, no. 40, pp. 16077–16085, 2011.
- [230] S. K. Kessler and E. McGinnis, "A Practical Guide to Treatment of Childhood Absence Epilepsy," *Pediatr. Drugs*, vol. 21, no. 1, pp. 15–24, 2019.
- [231] F. Zhou, Z. Song, Y. Wen, H. Xu, L. Zhu, and R. Feng, "Transdermal delivery of curcumin-loaded supramolecular hydrogels for dermatitis treatment," *J. Mater. Sci. Mater. Med.*, vol. 30, no. 11, pp. 1–11, 2019.
- [232] S. H. Park, D. Y. Kim, P. Panta, J. Y. Heo, H. Y. Lee, J. H. Kim, B. H. Min, and M. S. Kim, "An intratumoral injectable, electrostatic, cross-linkable curcumin depot and synergistic enhancement of anticancer activity," *NPG Asia Mater.*, vol. 9, no. e397, pp. 1–14, 2017.
- [233] M. K. Hazra, S. Roy, and B. Bagchi, "Hydrophobic hydration driven self-assembly of curcumin in water: Similarities to nucleation and growth under large metastability, and an analysis of water dynamics at heterogeneous surfaces," *J. Chem. Phys.*, vol. 141, no. 18C501, pp. 1–8, 2014.
- [234] S. Huth, S. Sindt, and C. Selhuber-Unkel, "Automated analysis of soft hydrogel microindentation: Impact of various indentation parameters on the measurement of Young's modulus," *PLoS One*, vol. 14, no. 8, pp. 1–17, 2019.
- [235] P. Calvert, "Hydrogels for soft machines," *Adv. Mater.*, vol. 21, no. 7, pp. 743–756, 2009.
- [236] J. Bevernage, J. Brouwers, P. Annaert, and P. Augustijns, "Drug precipitation-permeation interplay: Supersaturation in an absorptive environment," *Eur. J. Pharm. Biopharm.*, vol. 82, no. 2, pp. 424–428, 2012.
- [237] K. Y. Lee, E. Alsberg, and D. J. Mooney, "Degradable and injectable poly(aldehyde guluronate) hydrogels for bone tissue engineering," *J. Biomed. Mater. Res.*, vol. 56, no. 2, pp. 228–233, 2001.
- [238] L. Wang, J. Shansky, C. Borselli, D. Mooney, and H. Vandenburgh, "Design and Fabrication of a Biodegradable, Covalently Crosslinked Shape-Memory Alginate Scaffold for Cell and Growth Factor Delivery," *Tissue Eng. Part A*, vol. 18, no. 19–20, pp. 2000–2007, 2012.
- [239] C. V. Liew, L. W. Chan, A. L. Ching, and P. W. S. Heng, "Evaluation of sodium alginate as drug

- release modifier in matrix tablets," *Int. J. Pharm.*, vol. 309, no. 1–2, pp. 25–37, 2006.
- [240] J. Tu, S. Bolla, J. Barr, J. Miedema, X. Li, and B. Jasti, "Alginate microparticles prepared by spray-coagulation method: Preparation, drug loading and release characterization," *Int. J. Pharm.*, vol. 303, no. 1–2, pp. 171–181, 2005.
- [241] L. W. Chan, A. L. Ching, C. V. Liew, and P. W. S. Heng, "Mechanistic Study on Hydration and Drug Release Behavior of Sodium Alginate Compacts," *Drug Dev. Ind. Pharm.*, vol. 33, no. 6, pp. 667–676, 2007.
- [242] T. Miao, S. L. Fenn, P. N. Charron, and R. A. Oldinski, "Self-Healing and Thermoresponsive Dual-Cross-Linked Alginate Hydrogels Based on Supramolecular Inclusion Complexes," *Biomacromolecules*, vol. 16, no. 12, pp. 3740–3750, 2015.
- [243] G. Balasundaram, M. Sato, and T. J. Webster, "Using hydroxyapatite nanoparticles and decreased crystallinity to promote osteoblast adhesion similar to functionalizing with RGD," *Biomaterials*, vol. 27, no. 14, pp. 2798–2805, 2006.
- [244] C. Herranz-Diez, Q. Li, C. Lamprecht, C. Mas-Moruno, S. Neubauer, H. Kessler, J. M. Manero, J. Guillem-Martí, and C. Selhuber-Unkel, "Bioactive compounds immobilized on Ti and TiNbHf: AFM-based investigations of biofunctionalization efficiency and cell adhesion," *Colloids Surfaces B Biointerfaces*, vol. 136, pp. 704–711, 2015.
- [245] O. Pop-Georgievski, D. Kubies, J. Zemek, N. Neykova, R. Demianchuk, E. M. Chánová, M. Šlouf, M. Houska, and F. Rypáček, "Self-assembled anchor layers/polysaccharide coatings on titanium surfaces: a study of functionalization and stability," *Beilstein J. Nanotechnol.*, vol. 6, pp. 617–631, 2015.
- [246] T. D. Sargeant, M. S. Rao, C.-Y. Koh, and S. I. Stupp, "Covalent functionalization of NiTi surfaces with bioactive peptide amphiphile nanofibers," *Biomaterials*, vol. 29, no. 8, pp. 1085–1098, 2008.
- [247] S. A. Raina, G. G. Z. Zhang, D. E. Alonzo, J. Wu, D. Zhu, N. D. Catron, Y. Gao, and L. S. Taylor, "Enhancements and limits in drug membrane transport using supersaturated solutions of poorly water soluble drugs," *J. Pharm. Sci.*, vol. 103, no. 9, pp. 2736–2748, 2014.
- [248] D. Love, K. Kim, D. W. Domaille, O. Williams, J. Stansbury, C. Musgrave, and C. Bowman, "Catalyst-free, aza-Michael polymerization of hydrazides: Polymerizability, kinetics, and mechanistic origin of an  $\alpha$ -effect," *Polym. Chem.*, vol. 10, no. 42, pp. 5790–5804, 2019.
- [249] John, M. Janeta, M. Rajczakowska, J. Ejfler, D. Łydzba, and S. Szafert, "Synthesis and microstructural properties of the scaffold based on a 3-(trimethoxysilyl)propyl methacrylate-

POSS hybrid towards potential tissue engineering applications,” *RSC Adv.*, vol. 6, no. 70, pp. 66037–66047, 2016.

[250] J. L. Hutter and J. Bechhoefer, “Calibration of atomic-force microscope tips,” *Rev. Sci. Instrum.*, vol. 64, no. 7, pp. 1868–1873, 1993.

## ACKNOWLEDGMENTS/ DANKSAGUNG

---

An diesem Punkt möchte ich mich bei den vielen Menschen bedanken, die diese Arbeit ermöglicht und zu einer wunderbaren Zeit gemacht haben.

Da wäre zuerst Christine Selhuber-Unkel: Bei dir möchte ich mich für die Möglichkeit bedanken in deiner Arbeitsgruppe meine Dissertation anfertigen und mit ganz wunderbaren Personen zusammenarbeiten zu dürfen.

Diese wunderbaren Personen sind die vorhergegangenen und derzeitigen Kollegen der Arbeitsgruppe Biokompatible Nanomaterialien. Mir war es eine Freude mit euch zusammen zu arbeiten, zu Kochen und das eine oder andere geistige Getränk einnehmen zu können. Hier möchte ich ganz besonders Ellen Riemer hervorheben und mich für die lustigen Mittagessen bedanken. Danke an: Christine Arndt, Angelika Duttman, Sören Gutekunst, Britta Hesseler, Steven Huth, Laith Kadem, Tina Kerby, Mishal Khan, Manuela Lieb, Nils Lukat, Hendrikje Neumann, Julia Revery, Sunil Rajput, Sandra Sindt, Shane Scott, Tobias Spratte, Mohammadreza Taale, Tobias Tellkamp und Michael Timmermann.

Während meiner Dissertation hatte ich die Möglichkeit verschiedene Studenten in ihren Abschlussarbeiten, Bachelor- und Masterarbeiten, und in ihren Hiwi-Arbeiten zu betreuen die auch zum Teil zu meiner Arbeit beigetragen haben. Dazu möchte ich mich bedanken bei: Laura Schumacher, Roshani Yasanthika Madurawala, Julia Sierck, Huu Chánh Trinh, Saman Stölting, Justus Proksch, Sophie Klemm, Raunak Lohar, Abhijith Beeram und Karoline Teichmann. Insbesondere dem wunderbaren A-team aus unserem Büro möchte ich meinen Dank aussprechen.

Ich möchte auch der DFG Danken, die durch die Förderung des GRK2154 meine Arbeit möglich gemacht hat. Zudem möchte ich dem gesamten Team des GRK2154 meinen Dank für die Zusammenarbeit und die großen Diskussionsrunden während der Retreats bedanken. Dazu möchte ich besonders die erste Generation herausheben und das Zusammensitzen während besagter Retreats: Vielen Dank für die Projekte, die wir miteinander erarbeiten konnten.

Für die Hilfe mit dem t-ZnO im 3D Projekt bin ich Prof. Dr. Rainer Adelung und Florian Rasch Dankbar. Für die Zusammenarbeit im Curcumin Projekt bin ich Kristina Schmitt und Dr. rer. nat. Kirsten Hattermann dankbar. Bedanken möchte ich mich auch für die Wunderbare Zusammenarbeit am ETX Projekt: Anna Buschhoff und Eva Peschke für die tollen Diskussionen, ich hoffe das geht so weiter. Sowie vielen lieben Dank Hanna Götsche und Prof. Dr. Regina Scherließ für die Unterstützung mit den HPLC Untersuchungen der Release Studien.

Ich möchte mich bei PhD Jan Lammerding bedanken, für die Möglichkeit während meines Forschungsaufenthaltes an der Cornell University in seinem willkommen heißenden und hilfsbereiten Team arbeiten zu können.

Ich möchte mich für die gelungene Kooperation bei dem Team Acquandas bedanken.

Weiterhin möchte ich mich für die gelungenen Kooperationen bei Prof. Dr. Anne Staubitz, Clement Appiah und Anne Heitmann bedanken.

Ich möchte mich für das Korrekturlesen meiner Arbeit bedanken bei: Alexander Vahl, Sandra Sindt, Laith Kadem, Mohammadreza Taale, Maike Wegener, Shane Scott, Lena Nolte, und Lea Jessen und Sunil Rajput.

Nur mit Arbeit und ohne unterstützende Freunde wären die letzten Jahre nur halb so schön gewesen. Danke, dass ihr für mich da ward und seid und wir viele lustige Stunden bei Brettspielen, gemeinsam kochen, beim Sport und auch einfach so verbracht haben.

Ich möchte hier meiner Familie danken: Meinen Eltern Rolf und Christiane, meinem Großvater und besonders meinem Bruder Torge.

**Danke für Eure Unterstützung!**